

**AZOLIUM IONS: A VERSATILE FRAMEWORK FOR  
CHEMISTRY ON EARLY EARTH**

A Dissertation  
Presented to  
The Academic Faculty

by

Ryan M Clairmont

In Partial Fulfillment  
of the Requirements for the Degree  
Doctor of Philosophy in Chemical Engineering in the  
School of Chemical & Biomolecular Engineering

Georgia Institute of Technology  
May 2016

**COPYRIGHT © RYAN M CLAIRMONT 2016**

**AZOLIUM IONS: A VERSATILE FRAMEWORK FOR  
CHEMISTRY ON EARLY EARTH**

Approved by:

Dr. Andreas S. Bommarius, Advisor  
School of Chemical Engineering  
*Georgia Institute of Technology*

Dr. Charles L. Liotta, Advisor  
School of Chemistry  
*Georgia Institute of Technology*

Dr. Martha Grover  
School of Chemical Engineering  
*Georgia Institute of Technology*

Dr. Joseph Schork  
School of Chemical Engineering  
*Georgia Institute of Technology*

Dr. Arthur Weber  
External Advisor  
*SETI Institute*

Date Approved: March 30, 2016

[To my parents]

## ACKNOWLEDGEMENTS

There are too many people to thank for helping me finish my graduate degree. My experience has truly been impacted by all the students, advisors, administrators, friends, and family who I've had the great opportunity to meet along the way. I want to begin with my husband, who has provided amazing support throughout this experience. In my heart, he will always be my greatest success story from grad school. My experience has also been shaped by the many advisors and mentors who helped guide me along with way. Christine Conwell, Andy Bommarius, and Art Weber really helped support me mentally throughout the arduous journey of graduate school. I have also gained a sharper scientific mind from the often difficult, but always well-meaning efforts of Charlie Liotta and Ram Krishnamurthy. I would like to thank all current and former members of the Bommarius lab, especially Jon "T" Rubin, Jon Park, and John "Mick" Robbins. I have been lucky to develop many friendships during my time in grad school and to have seen the efforts from many different researchers. Every grad student has an individual experience that they take from their school, and seeing this diversity has greatly broadened my perspective of graduate school. Finally I want to end by thanking my parents and brother. My family may not have understood why I wanted to pursue graduate school, or what I hoped to gain from it, but now nearing completion I can say the experience was worth the effort, but I am happy to be done!

# TABLE OF CONTENTS

	Page
ACKNOWLEDGEMENTS	iv
TABLE OF CONTENTS	v
LIST OF FIGURES	viii
LIST OF SYMBOLS AND ABBREVIATIONS	xi
SUMMARY	xii
1 INTRODUCTION	1
1.1 Azolium Background	1
1.2 Azolium Structure-Function Relationship	4
1.3 Azolium Catalysis Using Formaldehyde	4
1.4 Evolutionary Models	6
1.5 Plausibility of Metabolic Cycles	6
1.6 Scope of Investigation	7
1.7 References	8
2 AN ITERATIVE CATALYTIC CYCLE USING IMIDAZOLIUM IONS AS A MODEL FOR CHEMICAL EVOLUTION	10
2.1 Introduction	10
2.2 Methods	12
2.2.1 Materials	12
2.2.2 DHA+Aniline Reaction	13
2.2.3 C18 Isolated Imidazolium Catalysis	13
2.2.4 Process Initiation, Cycle 0	13

2.2.5 Dilution Reactions, Cycle 1	13
2.2.6 Cycling Reactions, Cycles 2+3	14
2.2.7 Analytical Separation (LCMS)	14
2.2.8 Process Separation (SPE)	15
2.3 Results	15
2.3.1 Characterizing Imidazolium Compounds	15
2.3.2 Catalysis using DHA + Aniline Reaction Imidazolium Ions	18
2.3.3 Characterizing the Cyclic Process	21
2.4 Discussion	25
2.5 Conclusions	27
2.6 References	28
<b>3 MODELING KINETICS OF IMIDAZOLIUM GROWTH IN THE MODEL SYSTEM</b>	<b>30</b>
3.1 Introduction	30
3.2 Autocatalytic kinetics as a non-physical descriptor	32
3.2.1 Polymerization kinetics	32
3.2.2 Amyloid kinetics	32
3.3 Autocatalytic Reaction Simulations	35
3.4 Discussion	38
3.5 Methods	39
3.5.1 Kinetics and Simulation Parameters	39
3.6 References	39
<b>4 INVESTIGATING CATALYSIS USING MODIFIED IMIDAZOLIUM IONS IN AQUEOUS SOLUTION</b>	<b>41</b>

4.1 Introduction	41
4.2 Methods	43
4.2.1 Materials	43
4.2.2 Synthesis of 1-dodecyl 3-methyl Benzimidazolium Bromide (BzIm)	43
4.2.3 Glyoxylic Acid pH study	43
4.2.4 Isolation of C3-Adduct	43
4.2.5 3C-adduct Reaction with GA*	44
4.3 Results	44
4.4 Discussion	57
4.5 Conclusions	57
4.6 References	58
5 FUTURE DIRECTIONS	59
5.1 Continuing Project from Section 2	59
5.2 Continuing Project from Section 3	62
5.3 Continuing Project from Section 4	63
APPENDIX A	65
SUPPORTING INFORMATION	65
APPENDIX B	82
CASE STUDY PLASTIGON PROGRAM	82
APPENDIX C	89
CASE STUDY UNIVERSAL LUXURY GROUP	89

## LIST OF FIGURES

	Page
Figure 1.1: General azolium structure	1
Figure 1.2: Summary of Breslow's work on thiamine catalyzed benzoin mechanism	3
Figure 1.3: Mechanisms for the Formose Reaction and Formoin Reaction	5
Figure 1.4: Publication trends for azolium and imidazolium search terms	7
Figure 2.1: Two reaction chemical cycle for imidazolium synthesis	11
Figure 2.2: Pathway for carbene catalyzed benzoin reaction using thiamine	12
Figure 2.3: Imidazolium catalysts identified in the DHA + Aniline Reaction	16
Figure 2.4: Proposed DHA + Aniline Reaction mechanism	17
Figure 2.5: EIC spectra of imidazolium ions before and after reaction	19
Figure 2.6: Catalytic mechanism showing formation of "Breslow Intermediates"	19
Figure 2.7: NMR catalytic activity of isolated imidazolium ions	20
Figure 2.8: Process flow diagram illustrating synthesis of imidazolium ions	21
Figure 2.9: Cycle 1 dilution reactions	23
Figure 2.10: Tracking imidazolium ions over multiple process cycles	25
Figure 3.1: 1-Dimensional growth model that could apply to polymer and amyloids	34
Figure 3.2: Four simulations provide examples of stoichiometry, mechanism, kinetics	36
Figure 4.1: Benzimidazolium structure developed by Iwamoto	41
Figure 4.2: Possible catalytic pathways using glyoxylic acid as the aldehyde	42
Figure 4.3: MS analysis of reaction between GA and BzIm	45
Figure 4.4: pH profile and mechanism for addition of GA and BzIm to yield adduct	46
Figure 4.5: NMR spectrum comparing BzIm to 3C-adduct	47
Figure 4.6: NMR spectra of 3C-adduct reaction with GA*	48

Figure 4.7: NMR spectra of thiamine reaction with GA at RT and 50C	49
Figure 4.8: NMR spectrum of BzIm reaction with GA at 50C	50
Figure 4.9: Deuterium exchange study of 3C-adduct	51
Figure 4.10: NMR spectra kinetics of 3C-adduct reaction with GA*	52
Figure 4.11: Reaction time course monitoring 3C-adduct reaction with GA*	54
Figure 4.12: MS of 3C-adduct after 24 days reaction	55
Figure 4.13: TOF MS of 3C-adduct reaction compared to predicted isotope pattern	56
Figure 4.14: TOF MS of 3C-adduct reaction compared to predicted isotope pattern	56
Figure 5.1: Comparison of imidazolium reaction products using different amines	59
Figure 5.2: EIC or predicted reaction products using 3AP with MSMS fragmentation	60
Figure 5.3: EIC kinetics of mixed reaction using 3AP and aniline	61
Figure 5.4: Kinetics plot initial rate comparison between 3AP and aniline	62
Figure 5.5: Comparing BzIm reactions using GA vs paraformaldehyde	64
Figure A.1: Proton NMR of 1,3-diphenylimidazolium catalyst	66
Figure A.2: Zoom aromatic region with peak integrations	66
Figure A.3: MS direct injection of 1,3-diphenylimidazolium catalyst	67
Figure A.4: Proton NMR of 1,3-diphenyl 2-hydroxymethylimidazolium adduct	67
Figure A.5: MS direct injection of 1,3-dipheyl 2-hydroxymethylimidazolium adduct	67
Figure A.6: MSMS of 1,3-diphenyl 2-hydroxymethylimidazolium adduct	68
Figure A.7: DHA+Aniline Reaction diagram	69
Figure A.8: DHA+Aniline Reaction products vs. imidazolium standards EIC	69
Figure A.9: Kinetic time course of EIC = 251 m/z showing two isomers	70
Figure A.10: MSMS Fragmentation of two isomer peaks	71
Figure A.11: DHA+Aniline Reaction showing EIC and predicted structures	72
Figure A.12: Product adducts from imidazolium modification by formaldehyde	73

Figure A.13: Isolated imidazolium ions before and after reaction with formaldehyde	73
Figure A.14: MSMS 311 m/z ion	74
Figure A.15: MSMS 281 m/z ion	74
Figure A.16: MSMS 251 m/z ion	74
Figure A.17: MSMS 265 m/z ion	74
Figure A.18: MSMS 386 m/z ion and 356 m/z ion indicating multiple isomers	75
Figure A.19: Effect of Separation Stage S1	76
Figure A.20: MS analysis of Process Separation Method on DHA+Aniline Reaction	77
Figure A.21: LCMS EIC of recovered imidazolium ions from process initiation	78
Figure A.22: Process flow diagram displaying volumetric dilution quantities	79
Figure A.23: MS of purified initiator catalysts for both dilution experiments	79
Figure A.24: MSMS of initiator catalyst 326 m/z ion	80
Figure A.25: Physical appearance of dissolved 326 m/z ion	80
Figure A.26: Proton NMR of initiator catalyst 326 m/z ion	81
Figure A.27: Process flow diagram showing iterative process	81

## LIST OF SYMBOLS AND ABBREVIATIONS

BzIm	Benzimidazolium
DHA	Dihydroxyacetone
DMF	Dimethylformamide
DMSO	Dimethylsulfoxide
EIC	Extracted Ion Chromatograph
GA	Glyoxylic acid
IUPAC	International Union of Pure and Applied Chemistry
LC	Liquid Chromatography
MS	Mass Spectrometry
NHC	N-Heterocyclic Carbene
NMR	Nuclear Magnetic Resonance
SPE	Solid phase extraction
TEA	Triethylamine
3AP	3-Aminopyridine
3C-adduct	3 Carbon Adduct

## SUMMARY

The work broadly covers azolium catalysis of the small molecules formaldehyde and glyoxylic acid. It is broken into two distinct projects: the first focusing on developing a process for imidazolium synthesis as a model for chemical evolution of small molecule catalysts as developed in chapter 2. This model was based upon a catalytic cycle that was proposed to show autocatalytic kinetics. However, autocatalysis could not be identified using a kinetic signature. In chapter 3, the IUPAC definition of autocatalysis is used to develop an argument against the term autocatalytic kinetics, and instead linking an autocatalytic reaction to stoichiometry. The second project expands upon the conditions of the first, examining several azolium catalysts as well as different substrates and solvents. This broad matrix of experiments is developed in chapter 4. The main projects are supplemented by a chapter proposing future experimental directions, and an appendix including supplemental information and alternative projects conducted during the course of research.

# INTRODUCTION

## 1.1 Azolium Background

Azolium ions describe a broad class of aromatic, five-membered ring heterocycles containing at least one nitrogen atom. The ring must also include one other heteroatom (O – oxazolium, N – imidazolium, S – thiazolium) separated by a methine bridge (Figure 1.1). The five-membered ring can be variously substituted producing a high degree of structural diversity. These molecules display various functions that are dependent on molecular structure including catalysis (Enders, 2007), metal coordination (Fremont, 2009), and tunable solvents (McCrary, 2012).

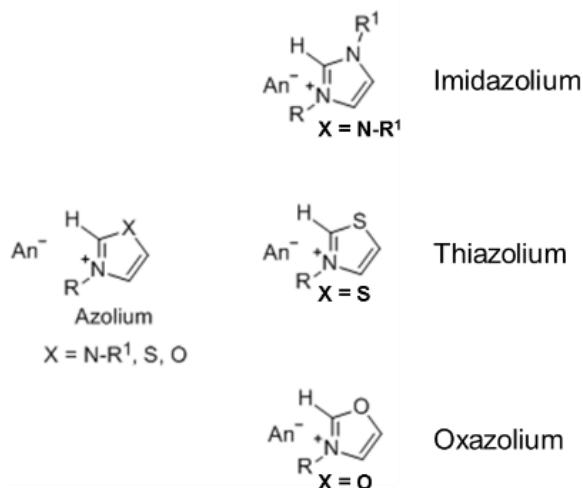
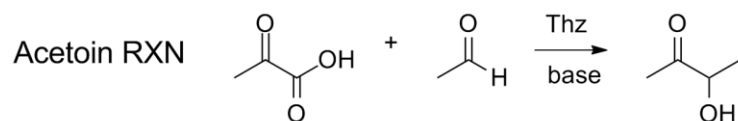
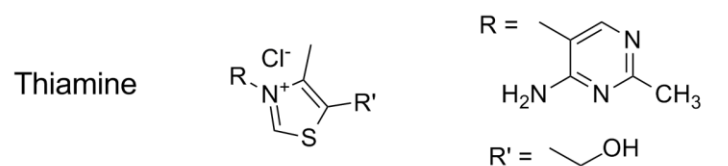


**Figure 1.1** General azolium structure shown on left. Specific types of azolium ions are shown on the right.

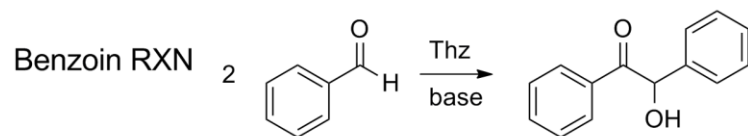
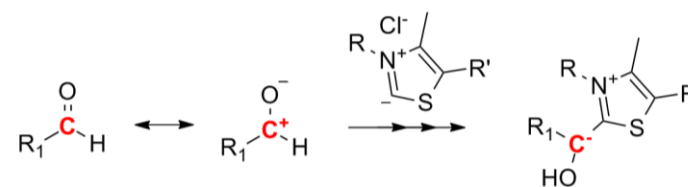
The mechanism for azolium catalysis was uncovered by Breslow who performed studies using several thiazolium ions, including the coenzyme thiamine (Breslow, 1958). Breslow found that thiamine or thiazolium structural analogs were capable of catalyzing

the acetoin and benzoin reactions (next page, Figure 1.2). Both of these reactions proceed via an umpolung inversion of the carbonyl carbon, changing the polarity from a partial positive electrophile to a partial negative nucleophile. Breslow proposed that thiazolium ions could be deprotonated at the methine carbon to yield a zwitterion, which was the true reaction catalyst. The zwitterionic form would then act as a nucleophile attacking a carbonyl group. After bonding to the carbon atom, which was initially electropositive, the thiazolium produced an electron delocalization effect that stabilized subsequent loss of a proton (benzoin reaction) or carbon dioxide (acetoin reaction). Further reaction of the resulting carbanion with a second carbonyl group would produce an alpha-dihydroxy intermediate. Reformation of the carbonyl would lead to cleavage of the alpha-hydroxy ketone product and regenerate the zwitterion catalyst.

At the time, Breslow attributed catalysis to the formation of a nucleophilic zwitterion; however, later research by Arduengo demonstrated that a neutral carbene species could be isolated as the product of imidazolium deprotonation (Arduengo, 1991). A carbene is a carbon atom which only has two covalent bonds. Atomic valence is satisfied by the presence of two non-bonding electrons that are either paired (singlet state) or unpaired (triplet state). For a review of carbene synthesis, properties, and electronics, consult Fremont et al. For a review of carbene catalysis, consult Enders et al. The isolation and characterization of a stable carbene generated from an imidazolium ion had a major impact on the field of N-heterocyclic carbenes (NHCs). Previously, carbenes were speculated to only exist as transient species in heterocycles, but the work by Arduengo appeared to indicate that carbene formation could be stabilized by the azolium structure (1991).



UMPOLUNG INVERSION



RXN MECHANISM

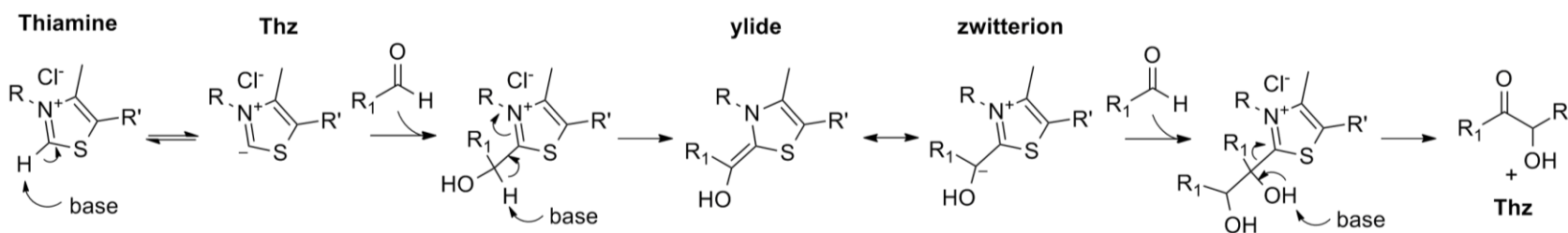


**Figure 1.2** A summary of Breslow's work detailing the structure of thiamine, the reactions investigated, the proposed mechanism, and the polarity inversion of the aldehyde carbon. The umpolung inversion involves the red highlighted carbon, which initially holds a partial positive charge. After reaction with the catalyst, this carbon inverts to instead hold a partial negative charge. The reaction mechanism displays how formation of this intermediate, and its equilibrium between two forms: a neutral ylide and charged zwitterion. Addition of a second equivalent of aldehyde yields the final reaction product, the  $\alpha$ -hydroxy ketone.

## 1.2 Azolium Structure-Function Relationship

Azolium structures have two dimensions that independently affect chemical properties: (1) the ring heteroatom and (2) ring substitution. The ring heteroatom affects the methine bridge carbon, in the following order  $N < S < O$  (Duclos, 1974). As the order increases, the methine bridge carbon becomes more susceptible to nucleophilic attack that would inactivate the catalyst. Thus imidazolium ions are the most stable class of azolium structures. Additionally, the methine bridge carbon becomes more acidic (equilibrium favors carbene formation) following the same order. Azolium ring substitutions can be generally classified as electron withdrawing or donating. Electron withdrawing substitutions have a similar affect as the heteroatom since they make the ring more prone towards nucleophilic attack. These substitutions follow the same behavior in affecting carbene equilibrium; a trend that follows the experimental yields determined by Teles using variously substituted imidazolium ions (1996).

## 1.3 Azolium Catalysis Using Formaldehyde

Castells was the first researcher to propose that an azolium ion could be used to couple formaldehyde into short chain carbohydrates (1980). This proposal was based off the notion that carbohydrates are composed of a  $\text{CH}_2\text{O}$  polymer. So if formaldehyde could be activated in an analogous mechanism to the benzoin reaction, then the resulting reaction would produce a method for yielding linear carbohydrate products.

Castells was especially interested in the ability of this reaction to produce linear carbohydrates. The Formose Reaction had long been investigated as a path for the autocondensation of formaldehyde to carbohydrates; however it was known to produce both branched and unbranched products (Cleaves, 2008). Both reactions are base promoted; however, the Formose Reaction relies on keto-enol tautomerization to produce a carbon nucleophile.

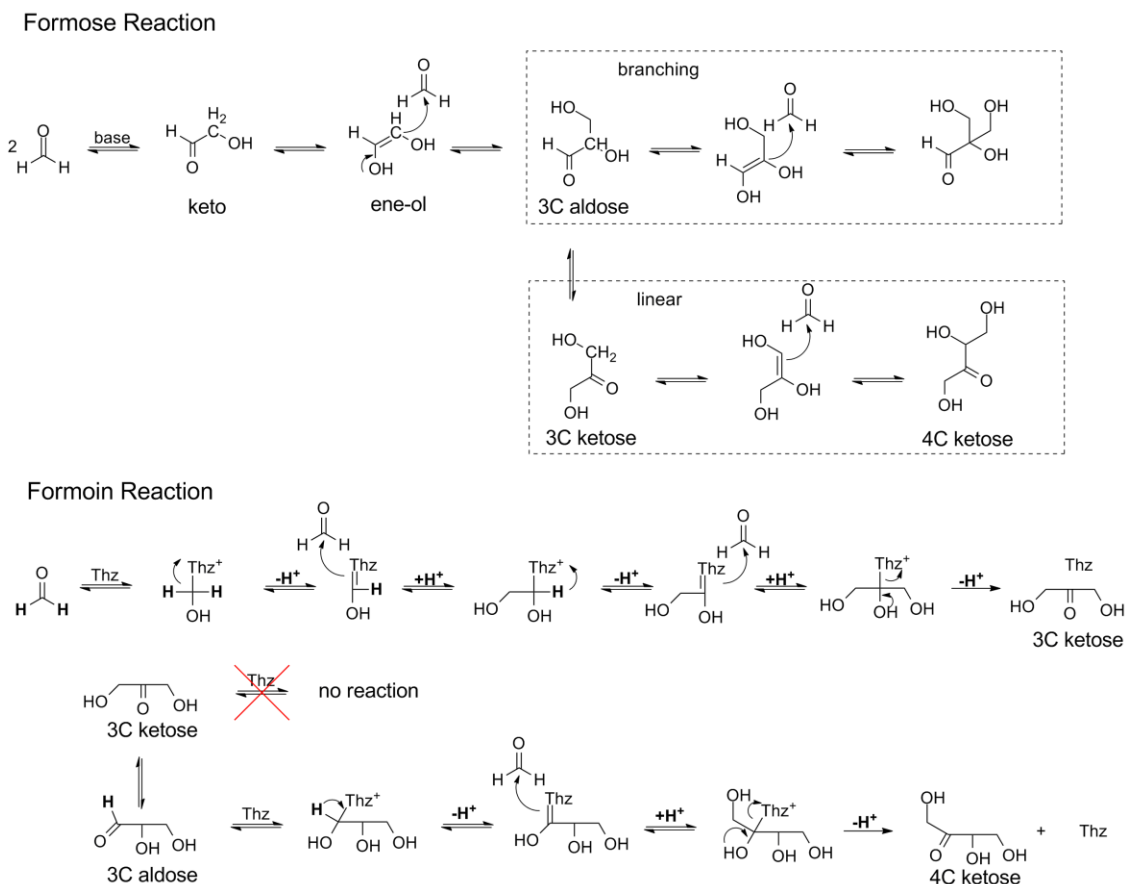


**Figure 1.3** displays mechanisms for the Formose Reaction and Formoin Reaction. The Formose Reaction can lead to the formation of branched products as highlighted in the top dotted box. The Formoin reaction relies on a different mechanism and in theory should only produce linear carbohydrate products since formaldehyde equivalents can only add to the aldehyde carbon.

Thus branched products are possible as shown in Figure 1.3. In the Formoin Reaction, only aldoses can be targeted by the catalyst, leading to better selectivity and control.

Catalytic activity of variously substituted thiazolium and imidazolium ions has been characterized using formaldehyde as the aldehyde substrate (Teles, 1996). His findings confirmed trends from earlier researchers based on deuterium exchange experiments. Thiazolium ions led to fast conversion, and required no electron withdrawing substitutions to demonstrate catalysis. Imidazolium ions displayed slower kinetics, and required electron withdrawing substitutions (such as aromatic groups) to produce significant conversion. Reaction timescale also appeared to affect selectivity.

More active catalysts displayed improved selectivity toward the proposed catalytic product, while less active catalysts yielded poor selectivity, indicating the possibility of off-pathway side reactions.

#### **1.4 Evolutionary Models**

Evolution is the process by which a population changes over time. Characteristics within the population either persist through selective pressures or they are lost. The process of evolution is integral to living organisms, and is believed to have played a major role in the emergence of life on early Earth (Oparin, 1980). At its core evolution relies on two features: diversity and selection. Chemical diversity is derived in modern biology from lengthy polymers called deoxyribonucleic acid (DNA). Due to their complexity, it is viewed as extremely unlikely that DNA would have spontaneously formed on early Earth (Pross, 2004). Instead scientists have proposed, that simpler structures with similar binding or chemical function may have formed first (Hud, 2013). Even still evolutionary polymers require first a mechanism for generating their monomer components, then linking those monomers together to form a polymer.

#### **1.5 Plausibility of Metabolic Cycles**

Using the same hypothesis that earlier chemistry can be “mapped” onto modern biology, some scientists have focused on metabolic reactions instead of replication. Examples include the glyoxylate scenario (Eschenmoser, 2007; Butch, 2013), and Reductive citric acid cycle (Morwitz, 2000). Metabolic reactions do not necessitate the formation of long polymers, and many of the proposed cycles provide a pathway for the accumulation of important building blocks such as carbohydrates, amino acids, and nucleosides.

However, there is still a large degree of skepticism these reactions could produce evolving systems (Orgel, 2008). One of Orgel’s main arguments is the lack of

chemically plausible systems which would have operated on early Earth. His perspective cites the Formose reaction as, “the only known non-enzymatic reaction sequence...similar to a metabolic cycle.” This work challenges Orgel’s assertion, and further claims that such metabolic reactions could have been catalyzed by simpler molecules than RNA or proteins. Such early catalysts could be modeled after natural coenzymes, which play an integral role in metabolic reactions.

### 1.6 Scope of Investigation

In recent decades, research in azolium ions has focused mainly on imidazolium ions (Figure 1.4). The preference towards imidazolium ions could be due to their stability towards hydrolysis and low disassociation equilibrium (Duclos, 1974); however, a specific rationale for this trend can only be speculated. Though many of the ideas within this work are generalizable toward all azolium ions, experiments mainly focused on imidazolium synthesis and catalysis due to their stability, since catalyst persistence was deemed an important aspect of the evolutionary model. Thiamine was sometimes used to compare reactions to a more “evolved” azolium catalyst.

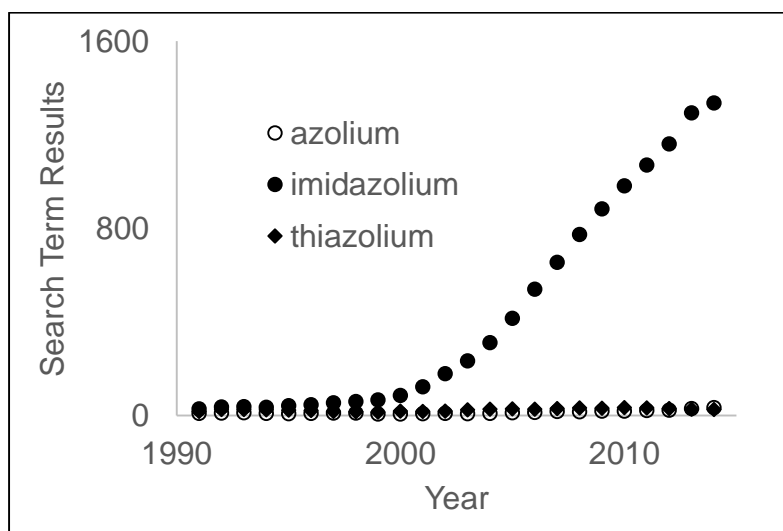


**Figure 1.4** Plot of search results showing a steep increase in publication of work related to imidazolium ions. Data points calculated as a three year moving average of the term using Web of Science.

## 1.7 References

- Arduengo III, A. J., Harlow, R. L., & Kline, M. (1991). A stable crystalline carbene. *Journal of the American Chemical Society*, *113*(1), 361-363.
- Breslow, R. (1958). On the mechanism of thiamine action. IV. 1 Evidence from studies on model systems. *Journal of the American Chemical Society*, *80*(14), 3719-3726.
- Butch, C., Cope, E. D., Pollet, P., Gelbaum, L., Krishnamurthy, R., & Liotta, C. L. (2013). Production of tartrates by cyanide-mediated dimerization of glyoxylate: a potential abiotic pathway to the citric acid cycle. *J Am Chem Soc*, *135*(36), 13440-13445.
- Castells, J., Geijo, F., & López-Calahorra, F. (1980). The “formoin reaction”: a promising entry to carbohydrates from formaldehyde. *Tetrahedron Letters*, *21*(47), 4517-4520.
- Cleaves, H. J. (2008). The prebiotic geochemistry of formaldehyde. *Precambrian Research*, *164*(3), 111-118.
- Duclos, J. M., & Haake, P. (1974). Ring opening of thiamine analogs. Role of ring opening in physiological function. *Biochemistry*, *13*(26), 5358-5362.
- Enders, D., Niemeier, O., & Henseler, A. (2007). Organocatalysis by N-heterocyclic carbenes. *Chemical Reviews*, *107*(12), 5606-5655.
- Eschenmoser, A. (2007). The search for the chemistry of life's origin. *Tetrahedron*, *63*(52), 12821-12844.
- de Frémont, P., Marion, N., & Nolan, S. P. (2009). Carbenes: synthesis, properties, and organometallic chemistry. *Coordination chemistry reviews*, *253*(7), 862-892.
- Henrique Teles, J., Melder, J. P., Ebel, K., Schneider, R., Gehrler, E., Harder, W., & Raabe, G. (1996). The Chemistry of Stable Carbenes. Part 2. Benzoin-type condensations of formaldehyde catalyzed by stable carbenes. *Helvetica chimica acta*, *79*(1), 61-83.
- Hud, N. V., Cafferty, B. J., Krishnamurthy, R., & Williams, L. D. (2013). The origin of RNA and “my grandfather’s axe”. *Chemistry & biology*, *20*(4), 466-474.
- McCrary, P. D., Beasley, P. A., Kelley, S. P., Schneider, S., Boatz, J. A., Hawkins, T. W., & Anderson, S. L. (2012). Tuning azolium azolate ionic liquids to promote surface interactions with titanium nanoparticles leading to increased passivation and colloidal stability. *Physical Chemistry Chemical Physics*, *14*(38), 13194-13198.

- Morowitz, H. J., Kostelnik, J. D., Yang, J., & Cody, G. D. (2000). The origin of intermediary metabolism. *Proceedings of the National Academy of Sciences*, 97(14), 7704-7708.
- Oparin, A. I., & Gladilin, K. L. (1980). Evolution of self-assembly of probionts. *BioSystems*, 12(3), 133-145.
- Orgel, L. E. (2008). The implausibility of metabolic cycles on the prebiotic Earth. *PLoS Biol*, 6(1), e18.
- Pross, A. (2004). Causation and the origin of life. Metabolism or replication first?. *Origins of Life and Evolution of the Biosphere*, 34(3), 307-321.

# AN ITERATIVE CATALYTIC CYCLE USING IMIDAZOLIUM IONS AS A MODEL FOR CHEMICAL EVOLUTION

## 2.1 Introduction

Hypotheses for the processes governing chemical evolution rely on the need for scientists to recognize the limits of historical data, as elaborated by Pross (2004). Instead a concerted focus must be made to understand what is at the core of fundamental aspects of evolution (Pross, 2011). In this work, a feedback process is considered to be at the core of any evolutionary system. Feedback processes play an important role in adaptation and learning, and they can be implemented at varying levels to produce diversity, function, and selection (Hinterding, 1997). Over time, the combination of these properties leads to changes at the population level that can be viewed as analogous to biological evolution. In this work, two reactions were coupled: a sugar-forming reaction analogous to the Formose Reaction and an imidazolium catalyst-forming reaction (Figure 2.1). Together these reactions produce a catalytic cycle that displays aspects of both metabolism and non-genomic replication, providing a simple evolutionary model using only small molecules. Development of model systems using simple chemical building blocks remains paramount to further defining the parallels between theory and chemical evolution. Formaldehyde and other simple aldehydes have been used with great success in abiotic syntheses of biological intermediates such as sugars (Mizuno, 1970; Sagi, 2012) and amino acids (Cleaves, 2008); however, these isolated reactions do not provide good models for evolutionary systems. For example, the Formose Reaction converts formaldehyde to various sugars, and kinetics show that the rate of formaldehyde consumption positively correlates to the concentration of sugars producing the signature

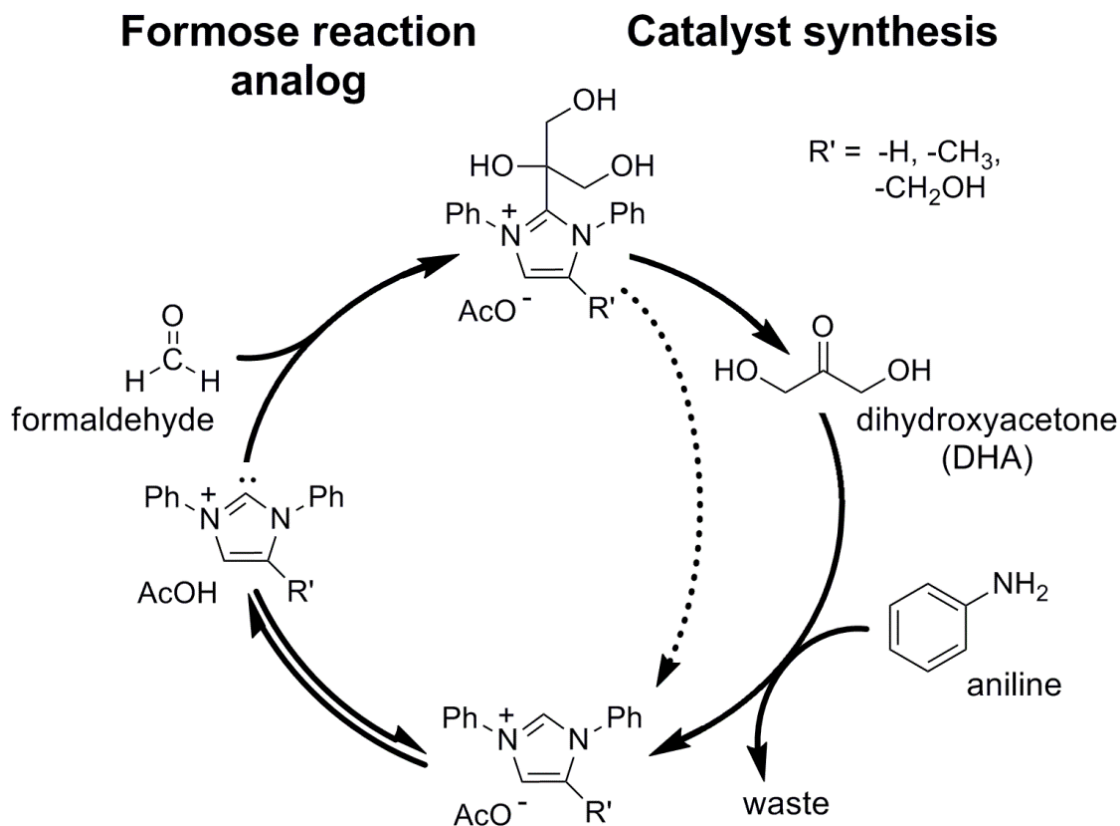


**Figure 2.1** A two-reaction Chemical network is shown to convert formaldehyde and aniline into imidazolium catalysts. The 1<sup>st</sup> reaction is an imidazolium-catalyzed Formose Reaction analog converting formaldehyde to sugars, such as dihydroxyacetone. The 2<sup>nd</sup> reaction synthesizes new catalyst from the product sugars of the 1<sup>st</sup> reaction, formaldehyde, and aniline. This chemical cycle depicts a hypothetical scenario where the reactions occur simultaneously. In this work, the individual reactions were performed separately, within an iterative process, due to formation of interfering products during catalyst synthesis.

“S-curve” concentration profile suggestive of autocatalysis. However, the sugars produced are not always stable under reaction conditions unless in the presence of certain minerals (Lambert, 2010; Kim, 2011). The reaction displays autocatalytic kinetics, but it does not display the kinetic stability that would be necessary for an evolutionary model. Additionally there exists no modern metabolic analog for the Formose Reaction. Instead biology adopted use of heterocyclic catalysts.

The emergence of heterocyclic catalysts on early Earth has generated only minor interest, even though the coenzyme thiamine plays a significant role in biology

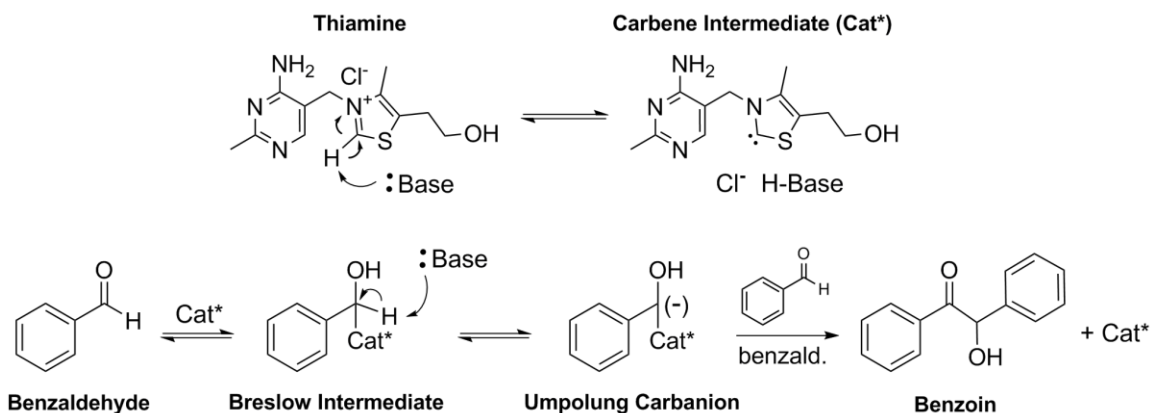


**Figure 2.2** Pathway for carbene-catalyzed benzoin reaction using thiamine. The mechanism converts a carbon-hydrogen bond to a carbon-carbon bond through a polarity reversal of the aldehyde carbon

(Bunik, 2013; Enders, 2007). Thiamine, or one of its phosphate derivatives, has been shown to catalyze a wide number of carbon-carbon bond forming reactions through the generation of a transient carbene intermediate. This mechanism was first proposed by Breslow (1958) and has since spawned a large area of research in N-heterocyclic carbenes. The benzoin reaction provides a model application of carbenes as umpolung catalysts, a reaction process that involves three steps: (i) thiamine deprotonation under basic conditions to form a carbene intermediate, (ii) reversible addition of the carbene (Cat\*) to benzaldehyde generating a Breslow intermediate (a catalyst-aldehyde adduct), and (iii) removal of the alpha proton yielding a stabilized carbanion that reacts with a second equivalent of benzaldehyde to produce benzoin (Figure 2.2)

## 2.2 Methods

### 2.2.1 Materials

All reagents, unless otherwise noted, were purchased from Sigma-Aldrich and used without additional purification. Abbreviations: dimethylformamide (DMF), dihydroxyacetone (DHA), dimethylsulfoxide (DMSO), liquid chromatography mass spectrometry (LCMS), solid phase extraction (SPE).

### 2.2.2 DHA+Aniline Reaction

In a 6 dram glass vial containing 4 mL DMF, 45 mg (0.5 mmol) DHA, 15 mg (0.5 mmol) paraformaldehyde, 94 mg (1 mmol) aniline, and 60 mg (1 mmol) acetic acid were added. The mixture was heated at 80 C with stirring, and reaction was complete after 5 h as monitored by LCMS (see section 2.2.7 “Analytical Separation”).

### 2.2.3 C18 Isolated Imidazolium Catalysis

A 1 mL sample from the DHA + Aniline Reaction was purified (see section 2.2.7 “Analytical Separation”) and evaporated to dryness. Then the residue was dissolved in 0.6 mL d6-DMSO for 1 H NMR. The sample was transferred to a 1 dram glass vial and an additional 0.5 mL d6-DMSO was added. The bottom of the vial was covered in 3 Å molecular sieves, and 22 mg (0.8 mmol) paraformaldehyde was added. The reaction was heated at 80 C for 30 min. *Note* d6-DMSO was used as both a reaction and NMR solvent to improve signal resolution. DMSO and DMF are suitable solvents for the catalytic reaction and can be used interchangeably.

### 2.2.4 Process Initiation, Cycle 0

In a 6 dram glass vial containing 4 ML DMF, 360 mg (4 mmol) DHA, 120 mg (4 mmol) paraformaldehyde, 750 mg (8 mmol) aniline, and 480 mg (8 mmol) acetic acid were added. The reaction was heated at 80 °C with stirring for 4h.

### 2.2.5 Dilution Reactions, Cycle 1

Product catalysts from Cycle 0 were isolated using flash chromatography. A sample of 0.4 mL was purified (see section 2.2.8 “Process Separation”) and evaporated to dryness. In a 6 dram vial, the residue was reconstituted in 4 mL DMF resulting in a tenfold dilution (10x). A second 0.5 mL product sample was purified (see section 2.2.8

“Process Separation”) and evaporated to dryness. In a 6 dram vial, the residue was reconstituted in 1 mL DMF resulting in a twofold dilution (2x). A control solution containing no reaction product catalyst was also prepared in a 6 dram vial containing 1 mL DMF. To the two reconstituted mixtures and control were added, respectively, 120, 30, and 30 mg paraformaldehyde (1 M formaldehyde) and the mixtures heated at 80 °C for 40 min. Reaction samples were taken for analysis after 5 and 40 min. Next, to the three reaction mixtures were added, respectively, 30, 8, 8 mg paraformaldehyde (0.26 M formaldehyde); 190, 47, 47 mg aniline (0.5 M); and 120, 3, 30 mg acetic acid (0.5 M). Heating at 80 °C was continued for an additional 4 h. Additional reaction samples were taken at 10, 30 min, 1, 2, and 4 h. All samples were diluted 1:10,000 before LCMS analysis (see section 2.2.7 “Analytical Separation”).

### **2.2.6 Cycling Reactions, Cycles 2+3**

Product imidazolium ions from cycle N-1 were isolated using SPE. A volume of 0.5 mL was purified and evaporated to dryness. The imidazolium ions were then reconstituted in 1 mL DMF resulting in a twofold dilution. To this was added 30 mg paraformaldehyde (1 M formaldehyde), and the mixture heated at 80 °C for 40 min. Subsequently, 8 mg paraformaldehyde (0.26M formaldehyde), 47 mg (0.5 M) aniline, and 30 mg (0.5 M) acetic acid were added. Heating at 80 °C was continued for an additional 4 h.

### **2.2.7 Analytical Separation (LCMS)**

Imidazolium ions were monitored in ESI positive mode using a capillary LC coupled to a Bruker Ion Trap MS. A gradient method was developed for reverse phase separation with the following starting conditions: 50 % 0.01 M ammonium acetate in

LCMS grade water (buffer A) and 50 % LC grade acetonitrile (solvent B). After 25 min, the gradient was changed to 15 % buffer A and 85 % solvent B.

### **2.2.8 Process Separation (SPE)**

A 5 g Supelco C18 column was used to isolate imidazolium catalysts by flash chromatography. A portion of the DHA + Aniline reaction was diluted with DI water to a volume of 10 mL. Two drops of saturated sodium bicarbonate solution were added to neutralize the solution. The C18 column was prepared by washing with two column volumes of DI water. Sample was introduced to the column with flow through exiting at \*1 drop per second. After the sample loading reached the frit, 7 mL of DI water were added and run at the same flow rate. All solvent was run through the column and the pressure increased to dry the column for 30 min. Then 12 mL acetone was introduced to the column and run at the same flow rate. After the solvent had reached the frit, 12 mL methanol was added to the column and run at the same flow rate. Next, 12 mL 0.1 M ammonium acetate in methanol was added; this final fraction was collected and reserved. The final elution was concentrated to a residue using a rotary evaporator and any residual solvent removed by flushing the vessel with Ar for 30 min. If isolated products were not immediately used, the residue was stored at room temperature in a dry state.

## **2.3 Results**

### **2.3.1 Characterizing Imidazolium Compounds**

Reaction of DHA, aniline, formaldehyde ( $\text{H}_2\text{CO}$ ), and acetic acid ( $\text{AcOH}$ ) produced several N,N-diphenylimidazolium compounds that can act as catalysts in sugar formation. To identify these species, 125 mM DHA (1 eq), aniline (2 eq),  $\text{H}_2\text{CO}$  (as paraformaldehyde) (1 eq), and  $\text{AcOH}$  (2 eq) were reacted in DMF for 5 h at 80 C.

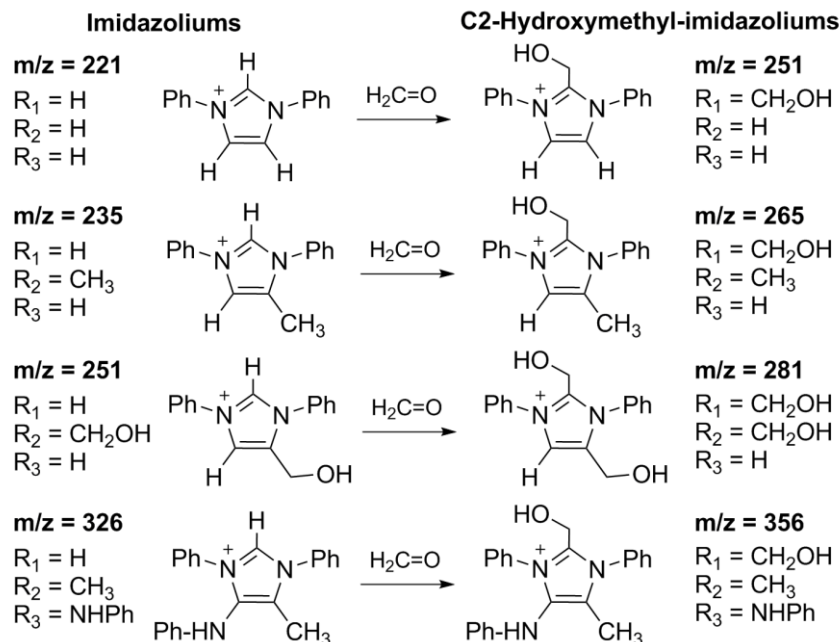
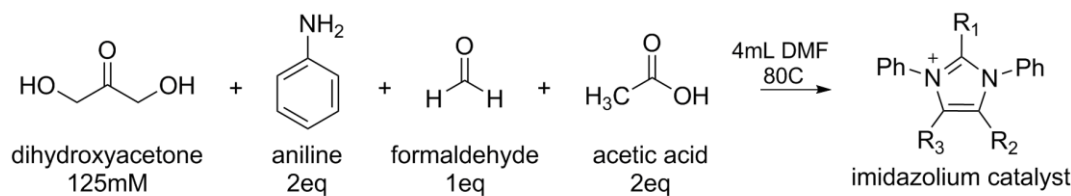


**Figure 2.3** Imidazolium catalysts identified in the DHA + Aniline Reaction. Multiple substitution patterns at the C2, C4, and C5 positions were generated in the multi-component reaction, along with undesired side products (not shown).

Reactions were analyzed using LCMS, and products identified by their m/z value (Figure 2.3). Two standards, 1,3-diphenylimidazolium (m/z = 221) and 1,3-diphenyl 2-hydroxymethylimidazolium (m/z = 251), were synthesized for comparison with reaction products using the Analytical Separation method (Appendix A). Both standards were identified, along with other imidazolium products, using a combination of MSMS fragmentation and LC elution characteristics such as retention and peak tailing (Appendix A). At least four unique (not accounting for modification at the C2 position) imidazolium structures were identified. A mechanistic pathway was proposed to rationalize the different imidazolium substitution patterns generated in these reactions starting from DHA (Figure 2.4 next page).

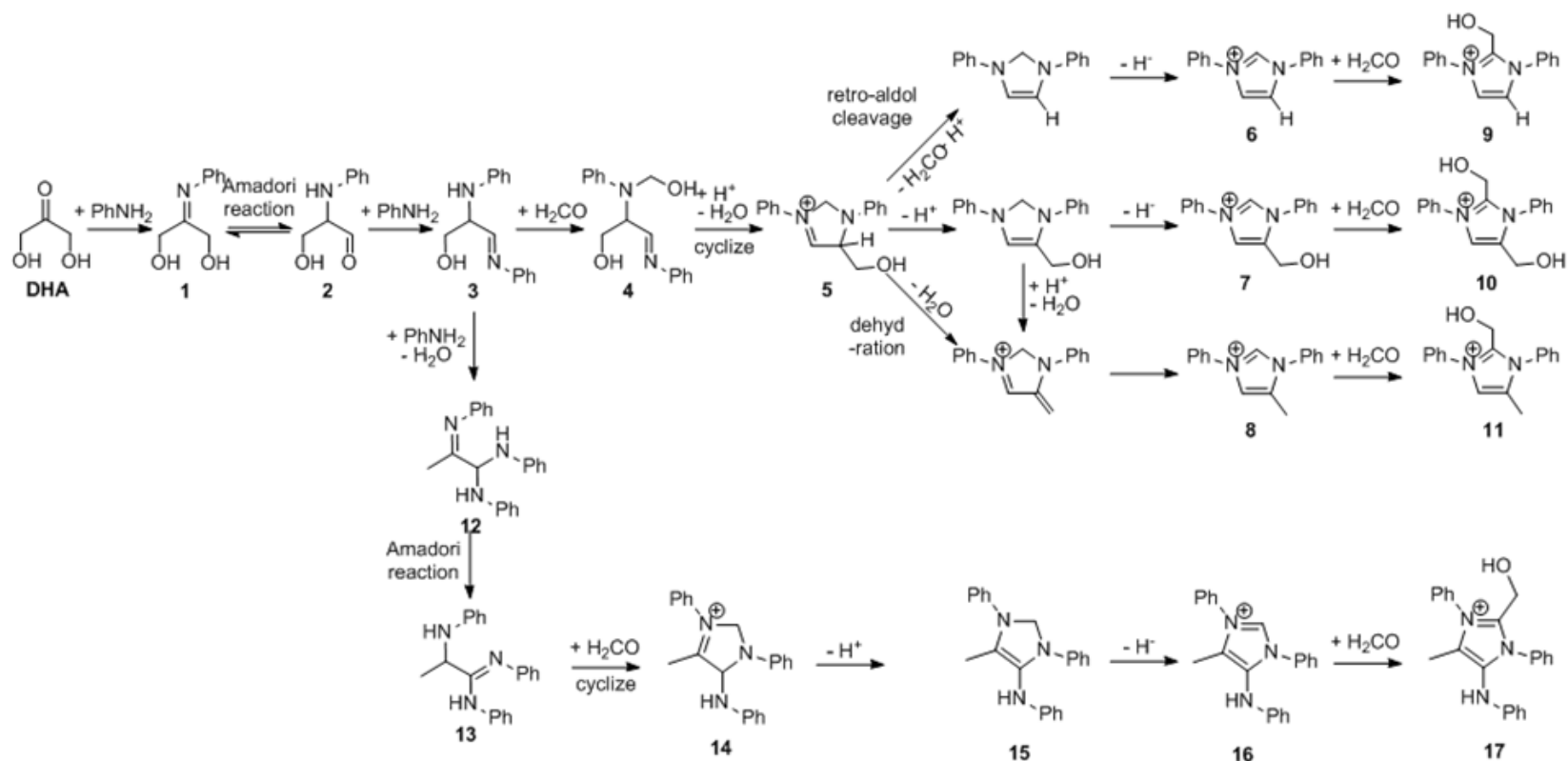


**Figure 2.4** In the first step, aniline and DHA react to form an unstable imine **1**. Via Amadori rearrangement a substituted alpha amino aldehyde **2** is formed, which adds a second equivalent of aniline to form a di-substituted alpha amino imine **3**. Reaction of this compound with CH<sub>2</sub>O followed by dehydration yields a cyclic precursor **5** to multiple imidazolium products. At the C4(5) position a – H, –CH<sub>2</sub>OH, –CH<sub>3</sub>, or –NPh group may be present depending on competing reactions. Elimination of formaldehyde by retro-aldol cleavage followed by oxidation produces 1,3-diphenylimidazolium **6**. Deprotonation followed by oxidation produces the 1,3-diphenyl 4(5)-hydroxymethylimidazolium **7**. Dehydration followed by rearrangement produces 1,3-diphenyl 4(5)-methylimidazolium **8**. Additionally, the C2 position is an active nucleophile and can form an adduct with formaldehyde to produce compounds **9**, **10**, and **11**. Similar substitution patterns of imidazoles were identified in investigations of Maillard reactions.

### 2.3.2 Catalysis using DHA + Aniline Reaction Imidazolium Ions

The DHA + Aniline Reaction not only produced imidazolium ions but a wide variety of other products, and to demonstrate that the imidazolium ions were active catalysts, they first needed to be purified. A method was developed using flash chromatography to isolate the imidazolium ions with high selectivity >99 % and minimal losses <10 % (Appendix A). Applying the Process Separation method to a 1 mL sample from a DHA + Aniline Reaction, the resulting residue was reconstituted in 0.6 mL d<sub>6</sub>-DMSO (d<sub>6</sub>-DMSO was used to improve signal resolution for NMR analysis). The dissolved imidazolium ions were then characterized before and after reaction with formaldehyde using LCMS and <sup>1</sup>H NMR.

Reaction of the SPE-isolated imidazolium ions with formaldehyde indicated all of the structures had some level of catalytic activity based on the identification of Breslow intermediates in the mass spectrometer (Figure 2.5). Imidazolium-catalyzed reactions with aldehydes go through Breslow intermediates which are adducts attached at the C2 position of the imidazolium

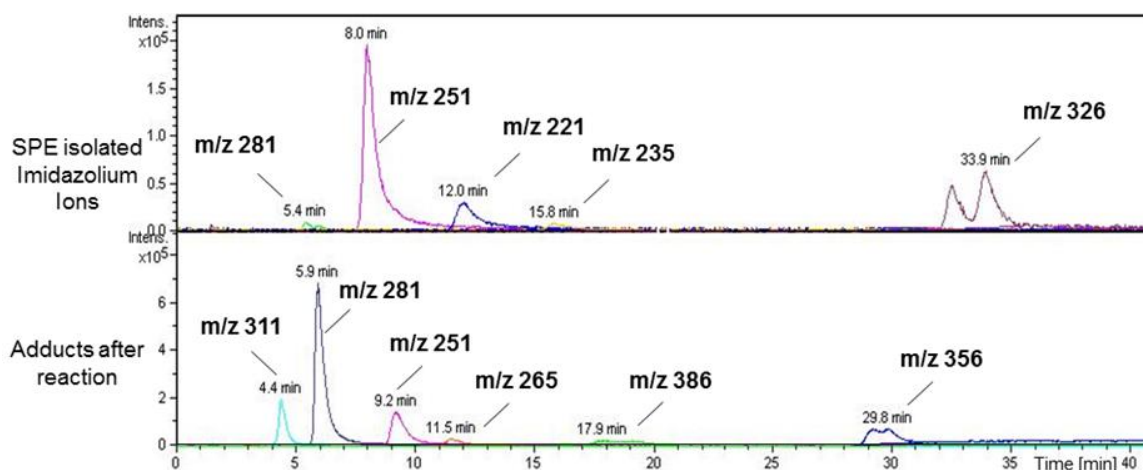


**Figure 2.5** EIC spectra of imidazolium ions before and after reaction with formaldehyde. Post reaction, the ions display a shift in retention time and m/z that corresponds to the formation of Breslow intermediates.

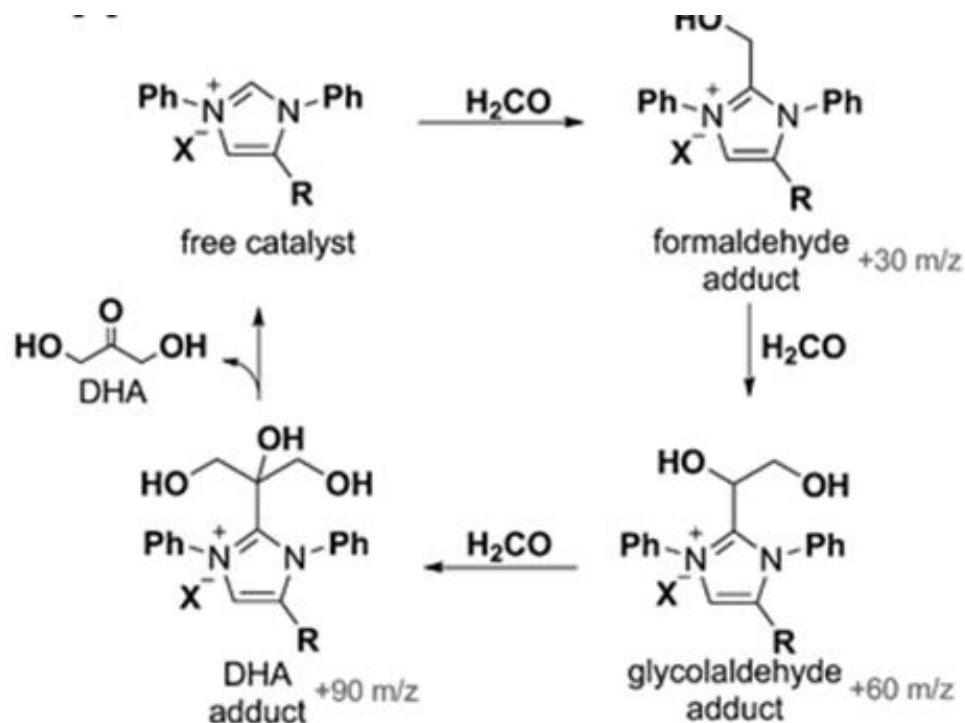


**Figure 2.6** Catalytic mechanism showing formation of catalyst aldehyde adducts, “Breslow intermediates”. After initial reaction with free catalyst, there are two protons on the formaldehyde adduct that can be removed to form a carbon nucleophile. Reaction of the formaldehyde adduct with the second equivalent of H<sub>2</sub>CO yields a glycolaldehyde adduct. A third equivalent of H<sub>2</sub>CO yields the DHA adduct. Each H<sub>2</sub>CO equivalent increases the imidazolium +30 m/z. Three additions of H<sub>2</sub>CO yield the product ketose DHA, which is theoretically unreactive. However, sugar rearrangements forming aldose isomers can continue to add equivalents of H<sub>2</sub>CO, and other sugars have been detected using similar reaction conditions (Castells et al. 1980; Teles et al. 1996).

(Figure 2.6). These intermediates of the catalytic reaction displayed a shift in retention time and increase in m/z that was consistent with addition of formaldehyde equivalents. MSMS fragmentation was also used to confirm the structures, though unique identification of certain isomers was difficult without improved baseline separation (Appendix A).

In addition to LCMS, <sup>1</sup>H NMR was used to demonstrate generation of sugars from the collective reaction of purified imidazolium ions and formaldehyde. The product spectrum showed complete consumption of paraformaldehyde, an acetal polymer that

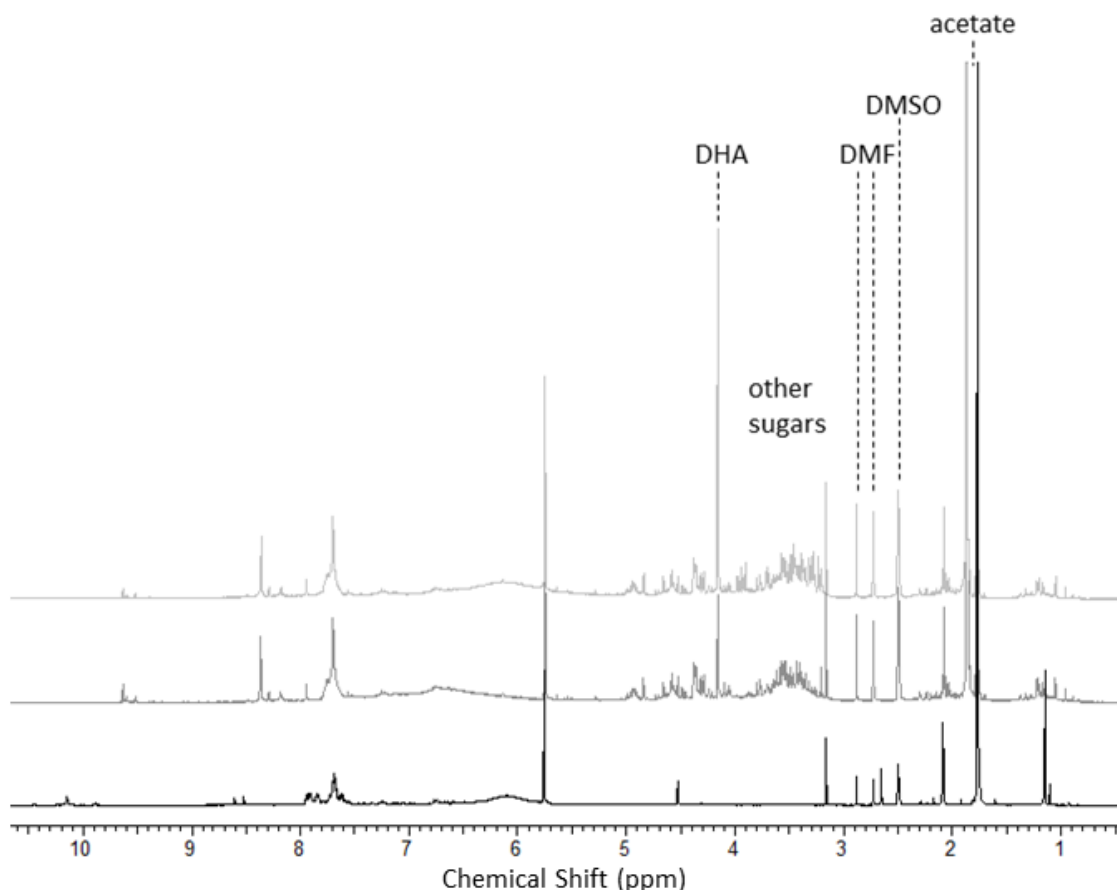


**Figure 2.7** Catalytic activity of imidazolium ions isolated from the DHA + Aniline Reaction. The bottom trace (black) displays the purified residue reconstituted in d6-DMSO. Some DMF remains, but aromatic signals between 7.5 and 10.5 ppm are indicative of imidazolium species. The middle trace (gray) displays reaction of the purified imidazolium ions with 0.75 mmol paraformaldehyde for 30 min at 80 C. New peaks appeared in the gray trace, between 3 and 5 ppm, which were indicative of sugar formation. The top trace (light gray) displays the reaction mixture spiked with dihydroxyacetone (DHA), which resulted in the increase of the peak at 4.15 ppm. A zero time NMR spectrum was not taken because paraformaldehyde is initially insoluble in the reaction mixture; all traces are referenced to the solvent at 2.5 ppm

occurs as a broad peak between 4.8 and 5.2 ppm, and DHA was positively identified by spiking a standard (Figure 2.7). A group of unresolved peaks between 3.3 and 3.8 ppm appear in the region expected for sugars and likely correspond to longer carbohydrate chains. Other signals such as residual DMF solvent and acetate also appear, but their impact on catalysis was regarded as negligible. The use of imidazolium ions isolated from a DHA + Aniline Reaction as catalysts for the production of sugars signaled that

this reaction-purification sequence could be repeated. The resulting process would generate imidazolium catalysts using only formaldehyde as a carbon source.

### 2.3.3 Characterizing the Cyclic Process

A process was developed based on the original reaction network to convert formaldehyde and aniline to imidazolium catalysts. The process was divided into three stages: two batch reactions (R1 & R2) and one chromatographic separation (S1). Stage R1, the Formose reaction analog, converts formaldehyde to a mixture of sugars ( $C_nH_{2n}O_n$ ) via an imidazolium-catalyzed polarity reversal. Stage R2, imidazolium catalyst synthesis, takes the product mixture from R1, then adds aniline, formaldehyde, and acetic acid to convert the sugars to new imidazolium catalysts. Stage S1 purifies the new imidazolium catalysts and recycles them back into the process (Fig. 2.8). Stage R1 is the catalytic conversion of formaldehyde to various sugars in DMF. Stage R2 is the multicomponent reaction of the sugar mixture with aniline, formaldehyde, and acetic acid. The product mixture from R2 is highly complex and must be purified, before additional process cycles. In stage S1, flash chromatography is used to purify imidazolium catalysts from other R2 products. These imidazolium catalysts are

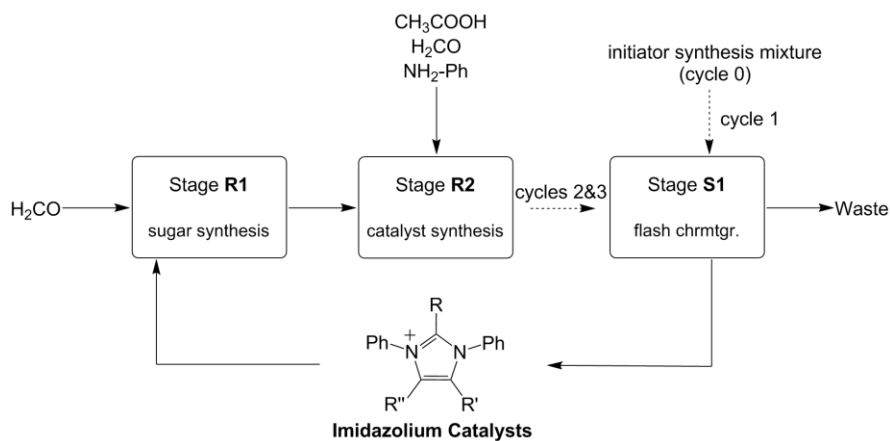


**Figure 2.8** Process Flow Diagram illustrating the three-stage synthesis of imidazolium catalysts from formaldehyde (H<sub>2</sub>CO), aniline (NH<sub>2</sub>-Ph), and acetic acid (CH<sub>3</sub>COOH).

recycled back into stage R1 forming a product feedback loop.

To characterize the process, three experiments were conducted: (1) effect of purification in Stage S1 on subsequent reaction stages, (2) effect of catalyst concentration on subsequent reaction stages, and (3) effect of multiple process cycles. In each of these experiments, the production of new imidazolium catalysts in Stages R1 and R2 was monitored as an indirect measurement of catalytic activity. In Stage R1, there should be no production of imidazolium ions giving a baseline for comparison. At the start of R2, there should be an increase in imidazolium synthesis. Stage R2 imidazolium kinetics are linked to the yield of sugars produced in stage R1, thus tracking the production of imidazolium ions in R2 provides a means of comparing different process conditions. In the following figures, the term peak area is used to represent the sum of peak integrations obtained from extracted ion chromatographs for imidazolium ions within the designated categories. New catalysts had  $m/z$  values of {221, 235, 251, 265, 281, 311}, while primer catalysts had  $m/z$  values of {326, 356, 386, 416}.

*Experiment 1:* the effect of Stage S1 was examined by comparing unpurified catalyst from the initiator mixture against purified catalyst. In the unpurified reaction, a 0.5 mL sample from the initiator mixture (cycle 0) was diluted by adding 0.5 mL of DMF to a final volume of 1 mL. In the purified reaction, a 0.5 mL sample from the initiator mixture (cycle 0) was purified to a dry residue using SPE (see “Process Separation Method” section) and then reconstituted in 1 mL DMF. These reactions were prepared to have the same catalyst concentration; however, their process kinetics in Stages R1 and R2 were different. The purified catalyst behaved as expected, showing an increase that occurred after the start of R2 ( $T = 40$  min). The unpurified catalyst did not display a significant

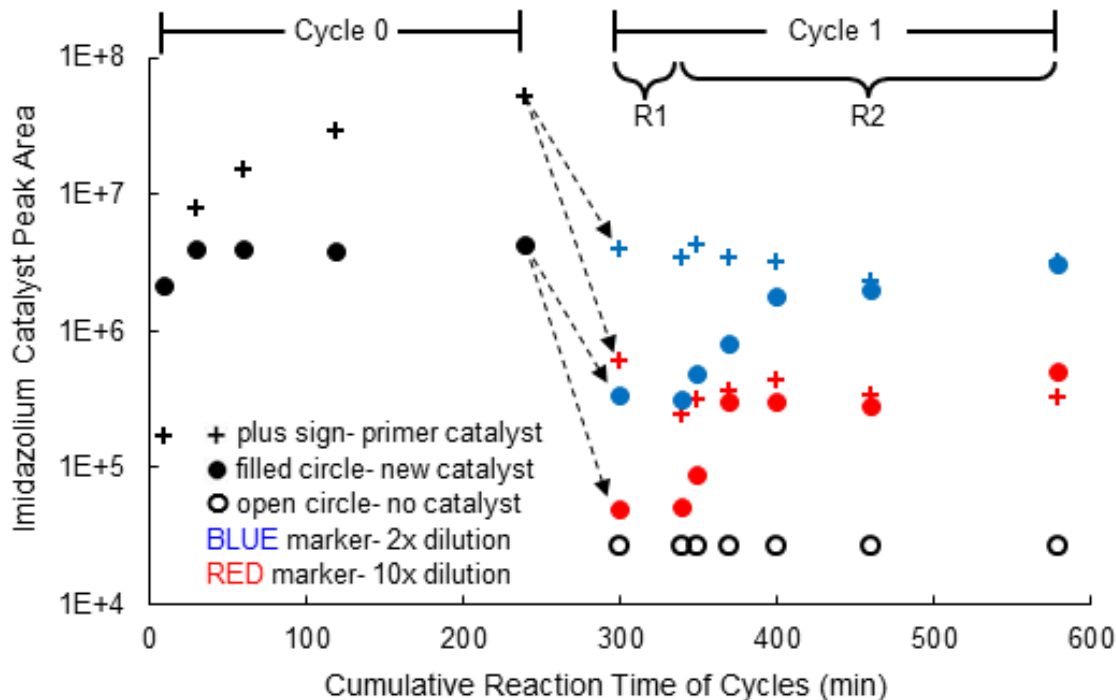


**Figure 2.9** Cycle 1 dilution reactions. Product imidazolium ions from cycle 0 were purified and reconstituted in fresh DMF solvent to achieve either a 2 x or 10 x volumetric dilutions. A control containing only fresh DMF was also prepared. Both dilution reactions display an increase in new catalyst beginning at R2, while the control and primer catalyst signals remain flat.

increase (Appendix A), which reflected the expectation that imidazolium catalysts are sensitive to the reaction environment. For reaction to occur, the imidazolium must first be deprotonated to form an active carbene species which then adds to the aldehyde carbon. Without purification, the initial step or subsequent carbanion formation was impeded by other products or unreacted starting materials quenching reaction.

*Experiment 2:* the effect of catalyst concentration was examined using different dilution ratios of purified catalyst from Stage S1 (Figure 2.9). Catalysts from the Cycle 0 were purified and then reconstituted in a new volume of solvent to achieve either a twofold dilution (blue markers) or a tenfold dilution (red markers) based on the initial volume. These two reactions were compared against a control containing no catalyst (open circles). Both of the reactions that contained initiator catalyst behaved as expected,

showing no significant increase in new catalyst during Stage R1 followed by an increase after the start of Stage R2, indicating that sugars were formed in the preliminary reaction stage. For the control reaction, catalyst was not produced and only background signal is detected, indicating formaldehyde does not form carbon–carbon bonds (either as sugars or imidazolium ions directly) under these conditions, in the absence of catalyst.

Designations, “primer” and “new” catalyst, are used to segment kinetic behavior, so that the initiator catalyst signal did not overwhelm signal of newly synthesized catalysts. Primer catalyst made up the major component of the initiator mixture (cycle 0) and was not produced in subsequent process stages. New catalyst was a minor component of cycle 0 and was produced in subsequent cycles. These differences occur because of the complexity of the DHA + Aniline Reaction mechanism. Stoichiometry and reactant concentrations can result in different imidazolium structures, allowing differentiation of initiator catalyst from catalyst produced in the process.

*Experiment 3:* the effect of multiple process cycles was examined by continuing the twofold dilution procedure through a 2nd and 3rd iteration to show continued production of new catalyst (Figure 2.10). Each cycle after cycle 0 displayed the same trends: “new” catalysts decreased after dilution, but subsequently increased over the course of Stage R2. By contrast “primer” catalysts decreased and then remained approximately constant. After only two cycles of dilution and reaction, the production of “new” imidazolium catalyst was able to overtake the “primer” catalyst as the major component in solution. This inversion indicated that formaldehyde could be used as a feedstock to produce functional imidazolium catalysts based on the hypothesized chemical cycle.

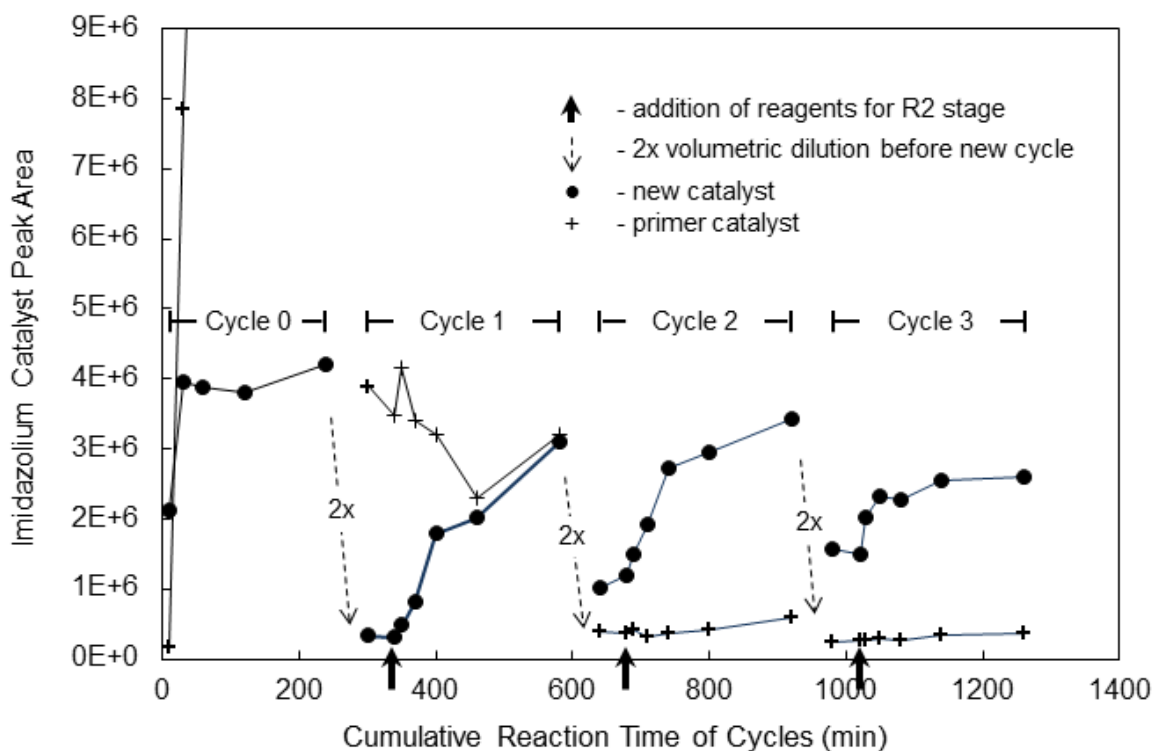


**Figure 2.10** Process Flow Diagram illustrating the three-stage synthesis of imidazolium catalysts from formaldehyde ( $\text{H}_2\text{CO}$ ), aniline ( $\text{NH}_2\text{-Ph}$ ), and acetic acid ( $\text{CH}_3\text{COOH}$ ).

## 2.4 Discussion

Developing a working process incorporating formaldehyde into an imidazolium organocatalyst required the sequential coupling of two reactions with a separation process. The first reaction, self-condensation of formaldehyde by imidazolium-catalyzed umpolung reaction, was inspired by the coenzyme thiamine. Thiamine has many functions in biology that involve the manipulation of sugars or sugar intermediates. Castells first demonstrated its use as a catalyst for the Formose Reaction, something he termed the Formoin Reaction (1958). While the prebiotic utility of the Formoin Reaction was speculated by Castells, his work was not extended until Teles investigated a variety of Nheterocyclic carbene-producing azolium ions to show that variously substituted imidazoliums, thiazoliums, and triazoliums could catalyze the reaction of formaldehyde to sugars (1996). Our task was to select an azolium catalyst structure that could be formed from sugar precursors and catalyze production of those same sugar precursors.

N,N-diphenylimidazolium ions were chosen for two major reasons: (i) they are capable of catalyzing sugar synthesis from formaldehyde (Teles, 1996) and (ii) they are more stable towards hydrolysis than thiazolium ions (Duclos, 1974). The formation of imidazoles and imidazolium ions in reactions of sugars with ammonia or amino acids has been documented, though there remains disagreement on an exact reaction mechanism (Kort, 1971; Velisek, 1989). However, use of an aromatic amine, such as aniline, for imidazolium synthesis had not been examined prior to this work. Since aromatic substitutions to the azolium ring activate catalysis, aniline was chosen as the simplest aromatic amine. On the early Earth, it is likely a mixture of amines would have been present—both aromatic and aliphatic—further increasing the diversity of possible catalyst substitutions.

Production of complex and diverse product mixtures recalls the importance of purifying imidazolium catalysts to achieve a working process. While the separation procedure used in this work is not prebiotic, it can hardly be argued that nature did not develop techniques for purification and compartmentalization. Certain chemistries are inaccessible under aqueous conditions, but the formation of microenvironments using micelles or localized binding could possibly surmount this issue. In this system, solid–liquid interfaces were used to take advantage of the imidazolium ions charged, hydrophobic structures. The imidazolium ions were strongly bound to the hydrophobic solid phase and remained bound even during exposure to pure organic solvents due to low solubility of the charged ions. Such selective binding and partitioning affinities may have proved advantageous on early Earth and could explain the persistence of small molecule catalysts like coenzymes in biology.

Binding of small molecule catalysts to biopolymers is used in biology to achieve many important transformations. At least 28 enzymes have been identified that are dependent on the coenzyme thiamine or one of its phosphate derivatives for reactions involving carbon metabolism (Bunik, 2013). An even greater number of enzymes are

known that are nicotinamide adenine dinucleotide (NAD) dependent. Thus binding of catalysts to early biopolymers may have acted as a selection process and provided mutual benefit. The polymer could have stabilized the catalyst and protected its activity from possibly harsh environmental conditions. In turn early catalysts may have helped synthesize polymer building blocks or aided polymerization reactions. This beneficial association could help explain a prevailing issue within the prebiotic community, the requirement for suitably long polymers to display structure and catalytic activity. Instead, it is likely that the emergence of polymers with binding affinity toward small molecule catalysts could have required smaller polymers.

As designed, the imidazolium iterative process would not have functioned in an aqueous environment, but with the help of other molecules this system has very large potential. Ease of synthesis, binding properties, and stability makes for a powerful combination that warrants further investigation. Developing cyclic catalytic processes and systems is an important step in building models for chemical evolution, and in the future we will seek to produce more prebiotic analogs of the model system presented.

## **2.5 Conclusions**

Accessing certain chemistries may have necessitated the purification and/or compartmentalization of molecules from complex mixtures. In this work, imidazolium ions, which could form nucleophilic carbene catalysts, were produced by means of a multi-component synthesis. However, without purification of the imidazolium ions, no significant catalytic reaction was possible. Demonstrating that small molecule catalysts could be produced with various structures shows that structural diversity can be incorporated into many different frameworks. Imidazolium catalysts, due to similarities in structure and activity to the coenzyme thiamine, may have played a major role in

chemical evolution. The process investigated in this work demonstrates a mechanism for these catalysts to have selected and evolved different substitution patterns.

## 2.6 References

- Breslow, R. (1958). On the mechanism of thiamine action. IV. 1 Evidence from studies on model systems. *Journal of the American Chemical Society*, 80(14), 3719-3726.
- Bunik, V. I., Tylicki, A., & Lukashev, N. V. (2013). Thiamin diphosphate-dependent enzymes: from enzymology to metabolic regulation, drug design and disease models. *FEBS Journal*, 280(24), 6412-6442.
- Castells, J., Geijo, F., & López-Calahorra, F. (1980). The “formoin reaction”: a promising entry to carbohydrates from formaldehyde. *Tetrahedron Letters*, 21(47), 4517-4520.
- Cleaves, H. J. (2008). The prebiotic geochemistry of formaldehyde. *Precambrian Research*, 164(3), 111-118.
- Duclos, J. M., & Haake, P. (1974). Ring opening of thiamine analogs. Role of ring opening in physiological function. *Biochemistry*, 13(26), 5358-5362.
- Enders, D., Niemeier, O., & Henseler, A. (2007). Organocatalysis by N-heterocyclic carbenes. *Chemical Reviews*, 107(12), 5606-5655.
- Henrique Teles, J., Melder, J. P., Ebel, K., Schneider, R., Gehrler, E., Harder, W., & Raabe, G. (1996). The Chemistry of Stable Carbenes. Part 2. Benzoin-type condensations of formaldehyde catalyzed by stable carbenes. *Helvetica chimica acta*, 79(1), 61-83.
- Hinterding, R., Michalewicz, Z., & Eiben, A. E. (1997, April). Adaptation in evolutionary computation: A survey. In *Evolutionary Computation, 1997., IEEE International Conference on* (pp. 65-69). IEEE.
- Kim HJ, Ricardo A, Illangkoon HI, Kim MJ, Carrigan MA, Frye F, Benner SA (2011) Synthesis of carbohydrates in mineral-guided prebiotic cycles. *J Am Chem Soc* 133:9457–9468. doi:10.1021/ja201769f
- Kort, M. J. (1970). Reactions of free sugars with aqueous ammonia. *Advances in carbohydrate chemistry and biochemistry*, 25, 311-349.
- Lambert, J. B., Gurusamy-Thangavelu, S. A., & Ma, K. (2010). The silicate-mediated formose reaction: bottom-up synthesis of sugar silicates. *Science*, 327(5968), 984-986.

- Mizuno T, Mori N, Shiomi N, Nakatsyji H (1970) Studies on synthesis and utilization of formose. Part 1. Sugar formation by the formaldehyde condensation in the presence of inorganic or organic bases. *Nippon Nogli Kagaku Kaishi, J Agr Chem Soc Jpn* 44:324–331
- Pross, A. (2004). Causation and the origin of life. Metabolism or replication first?. *Origins of Life and Evolution of the Biosphere*, 34(3), 307-321.
- Pross, A. (2011). Toward a general theory of evolution: extending Darwinian theory to inanimate matter. *J. Syst. Chem*, 2(1), 1-1.
- Sagi, V. N., Punna, V., Hu, F., Meher, G., & Krishnamurthy, R. (2012). Exploratory experiments on the chemistry of the “glyoxylate scenario”: formation of ketosugars from dihydroxyfumarate. *Journal of the American Chemical Society*, 134(7), 3577-3589.
- Velíšek, J., Davidek, T., Daviek, J., Trška, P., Kvasnička, F., & Velcova, K. (1989). New imidazoles formed in nonenzymatic browning reactions. *Journal of food science*, 54(6), 1544-1546.

# MODELING KINETICS OF IMIDAZOLIUM GROWTH IN THE MODEL SYSTEM

## 3.1 Introduction

Autocatalysis is a common motif in biology, and developing systems which display autocatalytic growth is viewed to be an important goal of origins of life research. These systems would have had an advantage in competition for resources and chemical persistence. The imidazolium chemical cycle developed in Section 2 was hypothesized to yield autocatalytic growth; however, a kinetic rate enhancement could not be observed due to the temporal and physical separation of the two reactions.

IUPAC defines an autocatalytic reaction as, “[one] in which a product (or a reaction intermediate) also functions as a catalyst. In such a reaction the observed rate...is often found to increase with time from its initial value (2016).” Using this definition, the term autocatalysis or autocatalytic should not be used to describe kinetic behavior. All reactions displaying such a stoichiometry display kinetic modularity such that the rate is a function of catalyst concentration. However, adoption of the term autocatalysis in fields where product stoichiometry is difficult to calculate has led to the term being associated with kinetic enhancement, product feedback, and positive cooperativity. This chapter argues that the definition of autocatalysis not be broadened as a kinetic descriptor. Instead kinetic behavior should be described based on developing a mechanistic understanding to rationalize observed behavior.

The issue of using kinetic observations as the definition for autocatalysis was first noted by Blackmond, comparing autocatalytic vs. autoinductive reactions (2009). She

showed that both could display product-enhanced reaction kinetics, yet only one yielded production of new catalyst. Blackmond termed reactions which produced exponential growth without new catalyst formation as autoinductive and not autocatalytic, a distinction that is in line with the IUPAC definition. However, Blackmond did not completely address the issue of autocatalysis being broadly used as a kinetic descriptor.

Many terms have been used by scientists to describe the observation of kinetic enhancement, and currently there exists no standard term to describe the phenomenon. IUPAC redirects positive feedback and kinetic feedback to the term composite reaction, a broad term that seems to describe any multi-step reaction.

Further complicating the association between autocatalysis and kinetics has been adoption of the term in several fields including polymer chemistry, amyloids (misfolded proteins relevant in neurodegenerative diseases), and nucleation. In each of these fields, product heterogeneity results in difficulties calculating stoichiometry. Instead, the consumption of reactant is tracked as an indirect measure of product formation. The confusion regarding nomenclature was recognized in a review by Morris et al., who cite autocatalytic kinetics, positive cooperativity, positive feedback, and autocatalysis as all being used to describe sigmoidal kinetic behavior (2009).

This chapter proposes that the definition for an autocatalytic reaction stand as unique and no longer be broadly applied to describe kinetic behavior. All reactions which feature a stoichiometry that produces new catalyst have the potential to yield exponential kinetic growth. This phenomenon is inherent in reaction stoichiometry, and so it is all that is needed to claim autocatalysis. The observation of kinetic enhancement should then be rationalized through more in-depth mechanistic understanding.

Several examples are given to highlight the use of “autocatalytic kinetics” in polymerization, protein aggregation, and nucleation. These are followed by simulations of four reaction mechanisms which fit the IUPAC definition for autocatalysis. Each is meant to highlight the importance of the separation of kinetic behavior from stoichiometry. Observed kinetics should be categorized based on a mechanistic understanding. This methodology would serve to disassociate the term autocatalysis from kinetics.

### 3.2 Autocatalytic kinetics as a non-physical descriptor

#### 3.2.1 Polymerization kinetics

Radical photopolymerization has been modeled using equation 1 (Hsieh, 1990). Here  $\alpha$  represents the product concentration and  $(1 - \alpha)$  the reactant concentration.

$$\text{Eq.1 } d\alpha/dt = (k_1 + k_2\alpha^m)(1-\alpha)^n = k_1(1-\alpha)^n + k_2\alpha^m(1-\alpha)^n$$

While this equation can be used to fit reaction data, it does not shed any light on the underlying reaction mechanism. In fact the authors state as much:

“The present approach bears no assumption on the actual reactions involved in the cure process and is only phenomenological. However, due exactly to its phenomenological nature, the method is general and should be capable of presenting the thermokinetics of thermosetting systems in a self-consistent manner.” – Hsieh et al, 1990

This equation, and the term ‘autocatalytic’ have been subsequently adopted by authors citing this paper (Cho, 2005; Harikrishna, 2013), further adding to the association between autocatalysis and kinetics, without providing a mechanistic rationale. While empirical observation could imply the existence of an autocatalytic reaction, it does not prove it to a suitable standard.

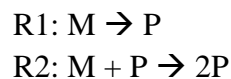
#### 3.2.2 Amyloid kinetics

Understanding the growth and elongation of amyloids (structured fibers composed of misfolded proteins) is a major field due to its applications in neurodegenerative diseases (for reviews, see Price et al. and Chiti et al). A large number of numerical models have been developed to simulate exponential product growth (Morris, 2009). However, empirical kinetic models are only as good as the information a scientist can obtain. As argued for the polymerization growth model, an empirical model can fit data without providing a true mechanistic understanding as to what is physically occurring.

Sabate et al derived a similar equation (Eq. 2) to the polymerization “autocatalytic kinetics” (2003). Here  $f$  represents the fraction of fiber (amyloid) in the system, and the terms  $a$  and  $k$  are constants. The equation is composed of two terms to represent two rates of fiber formation. The first term is not dependent on product formation, while the second term is dependent on both product and reactant concentration.

$$\text{Eq. 2 } df/dt = k(1-f) + kaf(1-f)$$

Rewriting equations 1 & 2 as a reaction mechanism is straightforward. Reactant is represented by the term  $M$  (‘monomer’), and product is represented by  $P$  (‘product’). Now it is easily seen that the second reaction obeys the definition for an autocatalytic reaction.



However, the equations derived from this mechanism contain an assumption to simplify the physical system. It is assumed that both monomer condensation to product (R1) and monomer addition to product (R2) form the exact same products. While this

1 dimensional growth as a model for kinetic processes in polymerization, amyloids, and crystallization	
Model Representation	Stoichiometry
<p>Site formation (production of new growth site)</p>	$3P \rightarrow GS$ 1 <sup>st</sup> order kinetics
<p>Precursor addition (no site change)</p>	$P + GS \rightarrow GS$ catalysis
<p>Decrease in growth sites</p>	$2GS \rightarrow GS$ Inactivation/inhibition
<p>Increase in growth sites</p>	$GS \rightarrow 2GS$ autocatalysis
<p>Precursor (P)      Growth Site (GS)</p>	

**Figure 3.1** This figure displays a 1 dimensional growth model that could be broadly applied to both polymer and amyloid growth. The model contains a cartoon representation for the physical process along with a reaction stoichiometry interpretation.

assumption may not affect the data fits, it limits the physical interpretation of these systems. As an example for 1-dimensional growth, information such as the number of polymer strands or the average strand length could not be determined using this mechanism.

Both polymerization and amyloids can be understood at a fundamental level as composed of four processes: (1) production of new growth sites, (2) no change in growth sites, and (3) decrease in growth sites (4) increase in growth sites. These processes are represented using a simple cartoon that allows a stoichiometry interpretation. For simplification, this model assumes growth is a 1-dimensional phenomenon. More complex growth models could be developed, but the general ideas should translate no matter what dimensionality is considered.

Using this representation, some precursor interacts with additional precursor by physical or chemical process to yield a growth site. Growth sites can add new precursor at a faster rate, without consuming the growth site, thus they act as catalysts.

Additionally growth sites can interact with each other to reduce their total number. If this interaction is reversible, then it is considered inhibition; if it is irreversible, then it is considered inactivation. Growth sites can also fragment to yield 2 growth sites. This fragmentation process produces a net increase in total growth sites, thus adhering to the stoichiometric definition for autocatalysis.

The examples from polymerization and amyloid formation ignore the effects of product heterogeneity, and essentially assume autocatalysis without providing a mechanistic rationale. Both models conflate elongation/growth with the formation of a new growth site. This poses a question, “can product refer to elongation of a polymer chain or must it refer production of new chains”? In the former case, the stoichiometry that makes autocatalysis unique is not satisfied; however, the IUPAC definition for autocatalytic reaction could be argued to be satisfied. The differences would support adoption of new nomenclature, such as autoinduction, to describe these systems.

### **3.3 Autocatalytic Reaction Simulations**

Proceeding from examples of applications of the term ‘autocatalysis’ to simulations of kinetic behavior. Reactions displaying stoichiometry that shows production of new catalyst are autocatalytic by IUPAC definition. In general these reactions can be defined as composed of one or more elementary reaction steps that produce a product, which also acts as a reactant.



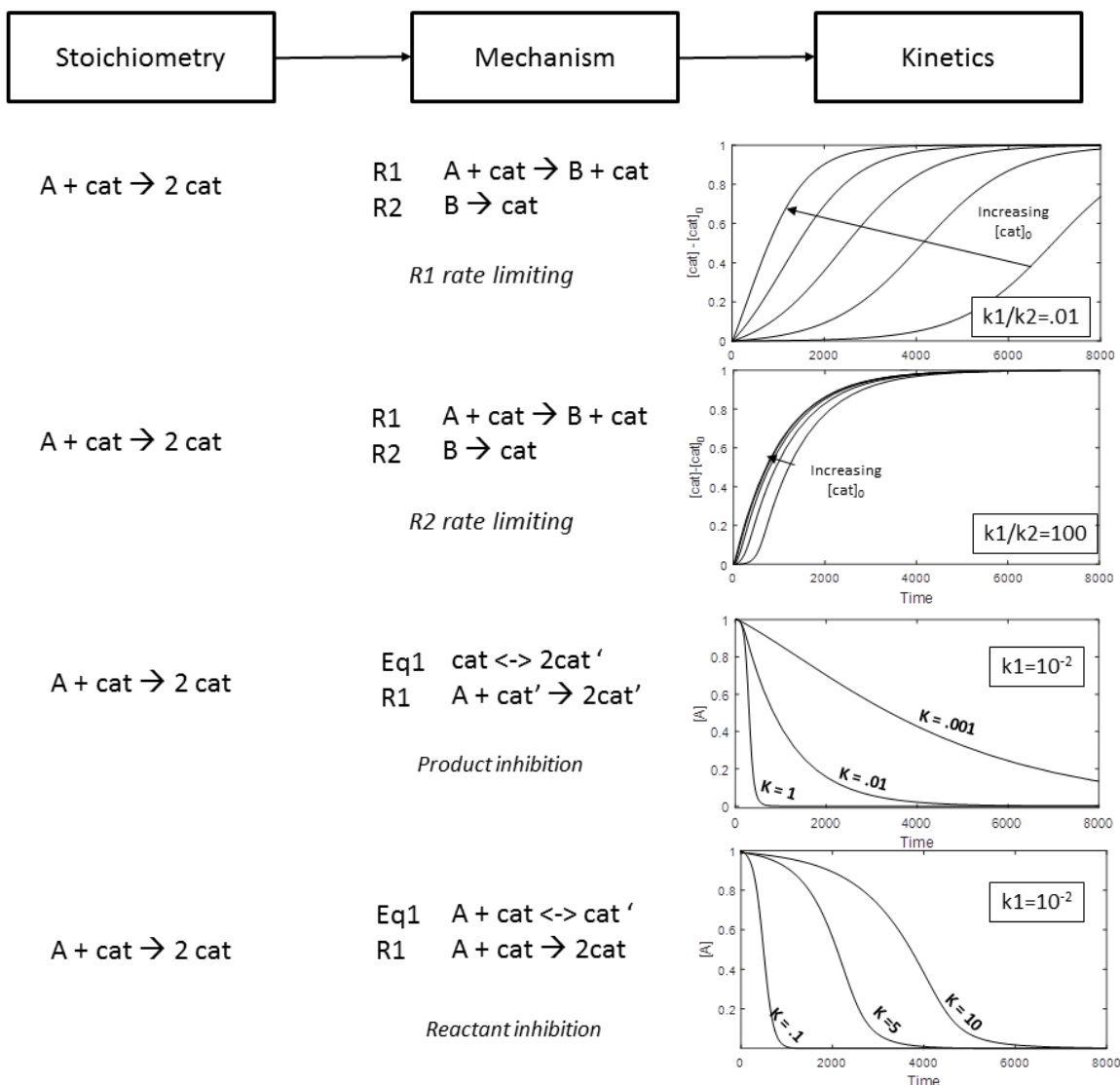


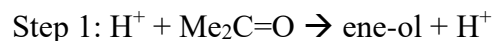
**Figure 3.2** These four simulations develop the process of going from stoichiometry to mechanism to observed kinetic behavior. All of them describe an autocatalytic reaction; however, their kinetics should not be generally described as autocatalytic. The first two examples both have the same mechanism. Differences in kinetic behavior arise from which reaction rate is limiting. When the catalytic reaction is rate limiting ( $k_1/k_2 = .01$ ) a long induction time is observed at low catalyst concentrations. This long induction isn't observed when the catalytic reaction isn't rate limiting. Both simulations varied  $[\text{cat}]_0$  between 0.001-0.625. The last two examples have different mechanisms, but both exhibit some form of inhibition. Inhibition leads to a decrease in reaction rate, the exact opposite connotation as autocatalysis. For all simulations  $A$  was held constant at 1.0.

Four scenarios in Figure 3.2 are shown that all display a stoichiometry consistent with autocatalysis. In all of these cases the kinetic profiles are highly modular, depending on variables such as equilibrium, rate constants, and concentration. However,

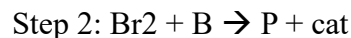
their kinetic behavior is not better understood through the label autocatalytic. This is our issue with the broad use of autocatalysis as a kinetic description.

The first two scenarios display the formation of an intermediate (B) which segments the two reactions that together display the stoichiometry for autocatalysis. However, due to their segmentation unique reaction behavior is seen depending on which reaction rate is limiting. A classic example of this behavior is the halogenation of acetone (Bell, 1964), a widely studied reaction showing kinetic enhancement.

This reaction can be generally understood as occurring in two steps: (1) acid catalyzed ene-ol formation from the ketone and (2) stoichiometric addition of the molecular halogen with the ene-ol intermediate forming a partially halogenated ketone and HX acid. These two steps are rewritten below using Bromine as the halogen:



Formation of hydrobromic acid as these steps repeat leads to increasing amounts of acid catalyst that would promote further enolization. If acid molecules are rewritten as cat, the mechanism is easily recognized:



Over time, the ene-ol intermediates will eventually react away if enough bromine is present to form a product (P) and an excess of the acid catalyst.

The third scenario displays product inhibition, whereby the catalytic reaction yields a product that would reduce the rate of reaction. An example of this scenario is replication of DNA or RNA in the absence of an enzyme, an issue called the strand

inhibition problem (Grossman, 2008; Fernando, 2007). Equilibrium interactions highly favor the formation of the template duplex, rather than the template associated to individual monomers.

While the fourth scenario has not been discussed to the author's knowledge, reactant inhibition or competition for catalytic sites are well known issues (Lee, 1986). This scenario highlights that the phenomenon could be associated with an autocatalytic reaction. In such cases, the consumption of reactant would lead to an increase in reaction rate, in addition to the formation of new product catalyst. Both of these effects impact kinetics, so using the term autocatalytic kinetics only provides an incomplete understanding of the reaction. A better description would be to say the reaction mechanism is composed of two kinetically relevant steps: inhibition equilibrium dependent on substrate concentration, and an autocatalytic reaction.

### **3.4 Discussion**

Whether autocatalysis is used by researchers to describe a kinetic observation, reaction stoichiometry, or both is dependent upon the scientific community. Currently, IUPAC asserts that an autocatalytic reaction displays a stoichiometry that could result in kinetic enhancement. Blackmond has supported this definition, and has added the term autoinduction to clarify reactions which do not meet the stoichiometry principle but feature a rate increase over time. The present chapter supports both of these distinctions and asserts the need for a more nuanced usage of the term autocatalytic. Autocatalysis should not be used to describe reaction kinetics. Autocatalysis is a phenomenological occurrence, which arises from the unique stoichiometry these reactions display. Thus it

is the responsibility of researchers to highlight the autocatalytic reaction or series of reactions rather than rely on empirical models.

Kinetic descriptions should arise from a mechanistic rationale. The term ‘*autocatalytic kinetics*’ is meaningless to the point that it should be substituted with the term ‘*empirically exponential kinetics*’. Kinetic descriptions that arise from a mechanistic understanding would produce a more universal nomenclature for researchers to draw from. Terms such as product cooperativity, inhibition, parallel reactions, and rate determining step provide a justification and rationale to the kinetics.

### 3.5 Methods

#### 3.5.1 Kinetics and Simulation Parameters

Individual reactions were modeled as elementary kinetic steps to produce concentration data for the overall reaction using Matlab built in ordinary differential equation (ODE) solver: ode23s.

### 3.6 References

- Bell, R. P. (1964). Kinetics of bromination of acetone in aqueous solution. *Journal of the chemical society*, (MAR), 902.
- Blackmond, D. G. (2009). An examination of the role of autocatalytic cycles in the chemistry of proposed primordial reactions. *Angewandte Chemie International Edition*, 48(2), 386-390.
- Chiti, F., & Dobson, C. M. (2006). Protein misfolding, functional amyloid, and human disease. *Annu. Rev. Biochem.*, 75, 333-366.
- Cho, J. D., Ju, H. T., & Hong, J. W. (2005). Photocuring kinetics of UV-initiated free-radical photopolymerizations with and without silica nanoparticles. *Journal of Polymer Science Part A: Polymer Chemistry*, 43(3), 658-670.

- Fernando, C., Von Kiedrowski, G., & Szathmary, E. (2007). A stochastic model of nonezymatic nucleic acid replication: "Elongators" sequester replicators. *Journal of Molecular Evolution*, 64(5), 572-585
- Grossmann, T. N., Strohbach, A., & Seitz, O. (2008). Achieving Turnover in DNA-Templated Reactions. *ChemBioChem*, 9(14), 2185-2192.
- Harikrishna, R., Ponrathnam, S., Rajan, C. R., & Tambe, S. S. (2013). Photopolymerization of bis-aromatic and alicyclic based solid urethane acrylate macromonomer in the presence of large excess of reactive diluent. *Journal of thermal analysis and calorimetry*, 112(2), 805-813.
- Hsieh, T. H., & Su, A. C. (1990). Cure kinetics of an epoxy-novolac molding compound. *Journal of Applied Polymer Science*, 41(5-6), 1271-1280.
- <http://goldbook.iupac.org> (2006-) created by M. Nic, J. Jirat, B. Kosata; updates compiled by A. Jenkins. ISBN 0-9678550-9-8. doi:10.1351/goldbook.A00525.
- Lee, L. G., & Whitesides, G. M. (1986). Preparation of optically active 1, 2-diols and alpha-hydroxy ketones using glycerol dehydrogenase as catalyst. Limits to enzyme-catalyzed synthesis due to noncompetitive and mixed inhibition by product. *The Journal of Organic Chemistry*, 51(1), 25-36.
- Morris, A. M., Watzky, M. A., & Finke, R. G. (2009). Protein aggregation kinetics, mechanism, and curve-fitting: a review of the literature. *Biochimica et Biophysica Acta (BBA)-Proteins and Proteomics*, 1794(3), 375-397.
- Price, D. L., Borchelt, D. R., & Sisodia, S. S. (1993). Alzheimer disease and the prion disorders amyloid beta-protein and prion protein amyloidoses. *Proceedings of the National Academy of Sciences*, 90(14), 6381-6384.
- Sabaté, R., Gallardo, M., & Estelrich, J. (2003). An autocatalytic reaction as a model for the kinetics of the aggregation of  $\beta$ -amyloid. *Peptide Science*, 71(2), 190-195.

# INVESTIGATING CATALYSIS USING MODIFIED IMIDAZOLIUM IONS IN AQUEOUS SOLUTION

## 4.1 Introduction

The protic nature of aqueous solutions necessitates the protection or stabilization of intermediates involving a transient nucleophile. In this work, transient nucleophile refers to a reaction intermediate carrying a negative or partial negative charge that could be quenched in the presence of protons. N-heterocyclic carbene (NHC) catalysts represent one such class of transient nucleophiles. These species are formed by the reversible deprotonation of an azolium ion (removal of a proton).

Using NHC catalysts to promote the formation of carbohydrates from formaldehyde has been investigated extensively in non-aqueous solvents (Teles, 1996; Castells, 1980). The goal of this work was to apply an NHC catalyst developed by Iwamoto *et al* for the aqueous reaction of aromatic aldehydes to glyoxylate (Figure 4.1). This exploratory reaction would provide a more plausible model for aldehyde coupling on early Earth, compared to the conditions used in Chapter 2.

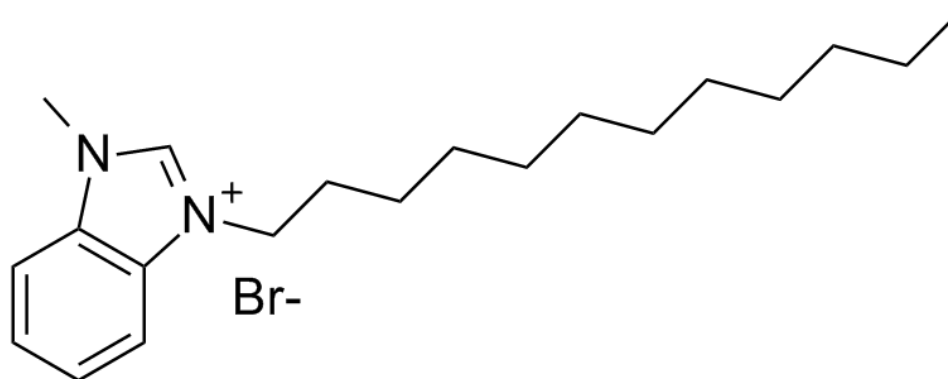


**Figure 4.1** One of several Benzimidazolium catalysts developed by Iwamoto that showed good conversion aromatic aldehyde substrates. This specific structure was adopted for use in reactions containing glyoxylate (Iwamoto, 2006).

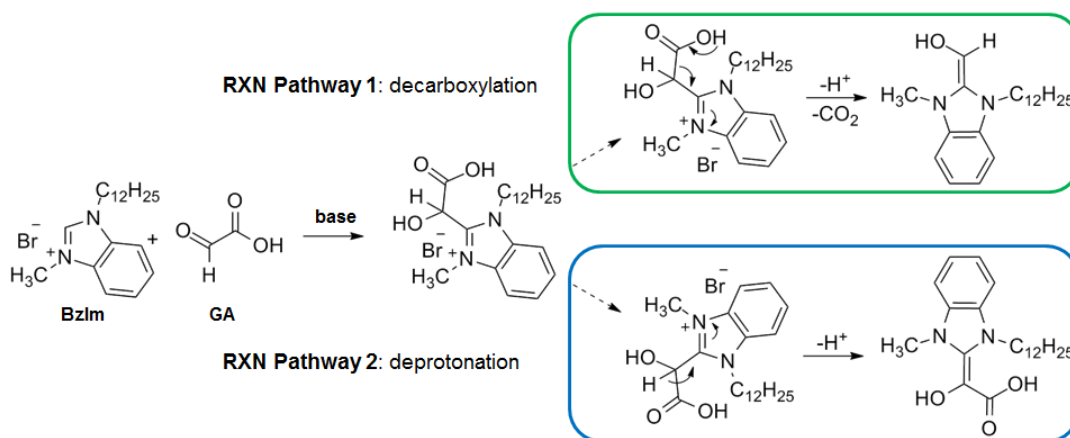


**Figure 4.2** Two different pathways are possible when using glyoxylic acid as a substrate. Both decarboxylation (acetoin rxn) and deprotonation (benzoin rxn) are known pathways for azolium activation of carbonyl compounds.

Instead of using formaldehyde to produce sugars, glyoxylate was used as an alternative aldehyde substrate. The glyoxylate scenario holds that glyoxylate may have provided a more controlled pathway to producing sugars and sugar acids on the early Earth compared to formaldehyde (Eschenmoser, 2007). Exploration of this reaction began with the hypothesis that two reaction pathways were possible for generation of a carbon nucleophile: deprotonation and decarboxylation. Carbonyl compounds react with imidazolium ions under basic conditions to form adducts at the C-2 bridge carbon (Figure 4.2). The imidazolium ion has an electron withdrawing effect, which stabilizes formation of a carbanion either through loss of carbon dioxide or a proton. Work by Butch et al. found evidence of a transient intermediate in the presence of cyanide at high pH (Butch, 2013). This intermediate could not be isolated and would have formed by a deprotonation followed by addition of a second equivalent of glyoxylate. The similarities between NHC and cyanide catalysis spurred this investigation to see if NHC catalysts would yield similar products without high pH conditions.

## 4.2 Methods

### 4.2.1 Materials

All reagents, unless otherwise noted, were purchased from Sigma-Aldrich and used without additional purification. Abbreviations: 1-dodecyl 3-methylbenzimidazolium bromide (BzIm), glyoxylic acid (GA), triethylamine (TEA), 1-dodecyl 2-(1,2-dihydroxypropionic acid) 3-methyl benzimidazolium (3C-adduct), <sup>13</sup>C labeled glyoxylic acid (GA\*), mass spectrometry (MS).

### 4.2.2 Synthesis of 1-dodecyl 3-methyl Benzimidazolium Bromide (BzIm)

In a round bottom flask combine: 1057.28 mg 1-methylbenzimidazole, 7.682 mL 1-bromododecane, and 20 mL toluene. The mixture was attached to a reflux condenser and heated with stirring until reflux was achieved. After 20 h under reflux the heating was discontinued and the contents allowed to rest for 24 h. Product was isolated by filtrating and washed with t-butyl ether. After drying the crude solid was ground to a fine powder, washed a second time with t-butyl ether, and filtered again. After drying 2.87 g product was recovered, at 93% yield.

### 4.2.3 Glyoxylic Acid pH study

A standard solution of 1M of GA was treated with a sodium hydroxide solution to attain the pH values of 3, 3.5, 4, 4.5, 5, 7, and 12 as measured by pH probe. Samples of 1 mL from each pH value were removed to which 76.2 mg (0.2 mmol) BzIm catalyst and 25.2  $\mu$ L (0.18 mmol) TEA were added. Vials were allowed to react for 24 h at room temperature with stirring and products analyzed by MS direct injection.

### 4.2.4 Isolation of C3-Adduct

The C3-Adduct was isolated from several reactions containing GA and BzIm. After 24 h the reaction was acidified with 6 M hydrochloric acid. Solid was collected by vacuum filtration and washed with acidic water followed by acetone. The solid was allowed to then dry overnight under vacuum yielding a yellow product.

#### **4.2.5 3C-adduct Reaction with GA\***

In a 2 dram glass vial, 31.8 mg (.075 mmol) 3C-adduct was added to 13.82 mg (.182 mmol) GA\*. Instead of using a pH meter, 30 uL of 5 M NaOH was added to neutralize the glyoxylic acid. DI water was then added to bring the total volume to 1 mL. The final solution was prepared by the addition of 14 mg TEA and allowed to react over one week with stirring.

### **4.3 Results**

Initial investigations of BzIm catalyzed reaction of GA demonstrated carbon-carbon bond formation; however, unlike the pathway discovered by Butch et al., decarboxylation was the main path for activation of the GA substrate. This pathway was uncovered by detection of a catalytic intermediate using direct injection MS. Under acidic conditions (GA not neutralized with sodium hydroxide) there was no evidence of reaction. However, under basic conditions (GA neutralized with 1 eq sodium hydroxide), several new signals were seen using direct injection MS. A small signal was seen that corresponded to the starting BzIm catalyst (301 m/z), but a larger signal was noted for a compound with even larger molecular weight (405 m/z). This signal corresponded to addition of 2 eq GA with loss of CO<sub>2</sub>. A sodium adduct was also noted (Figure 4.3).

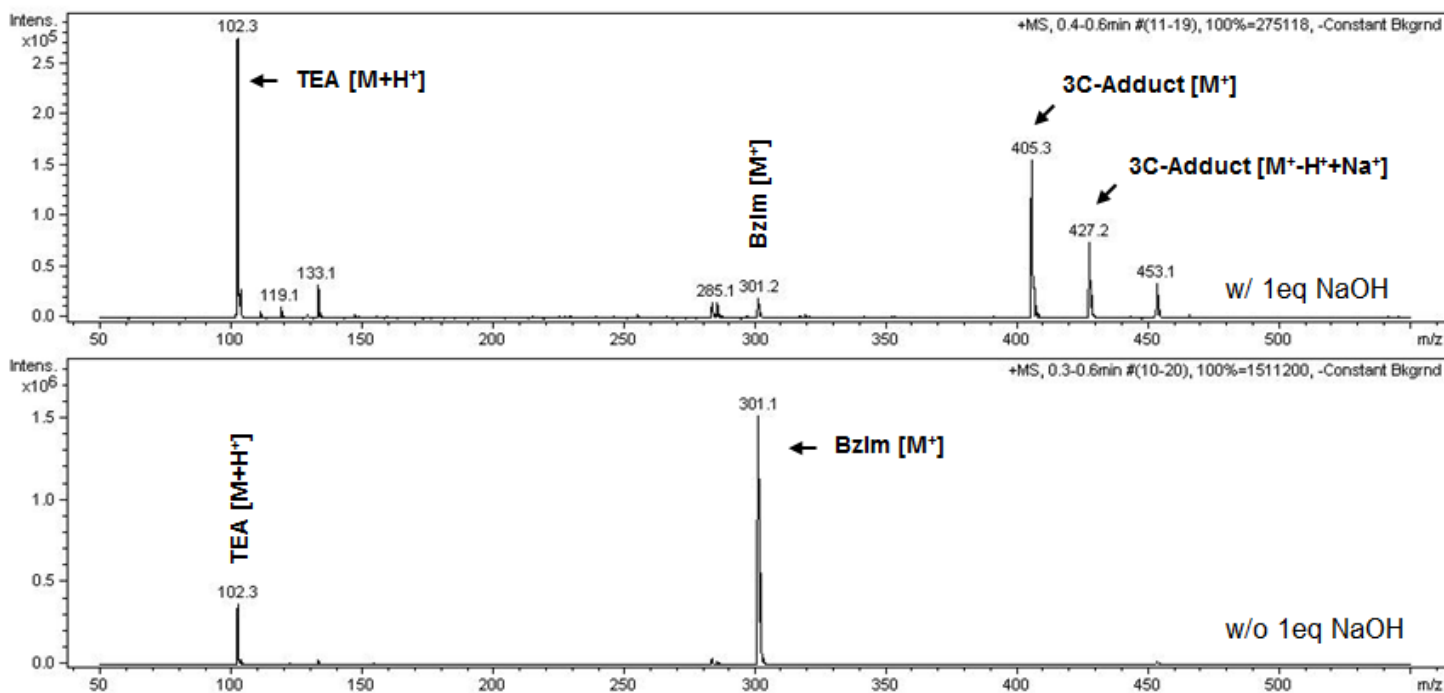
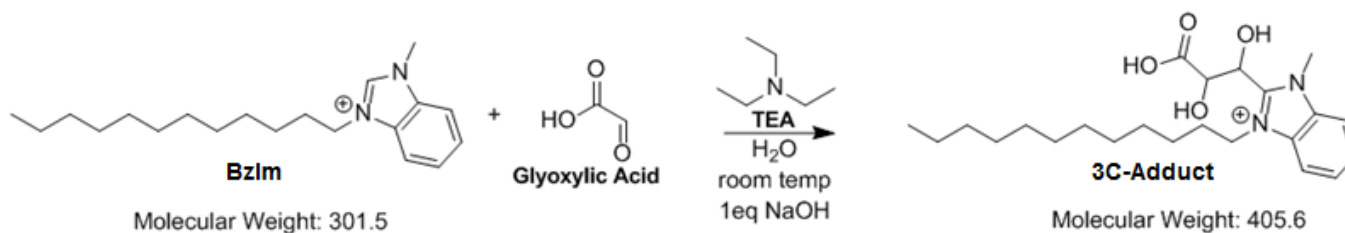


**Figure 4.3** The reaction shown at the top of the figure was confirmed using direct injection MS. Under basic conditions (top spectrum) starting BzIm is almost completely converted to a product with mass of 405 m/z. Under acidic conditions (bottom spectrum) no change in the catalyst signal was noted.

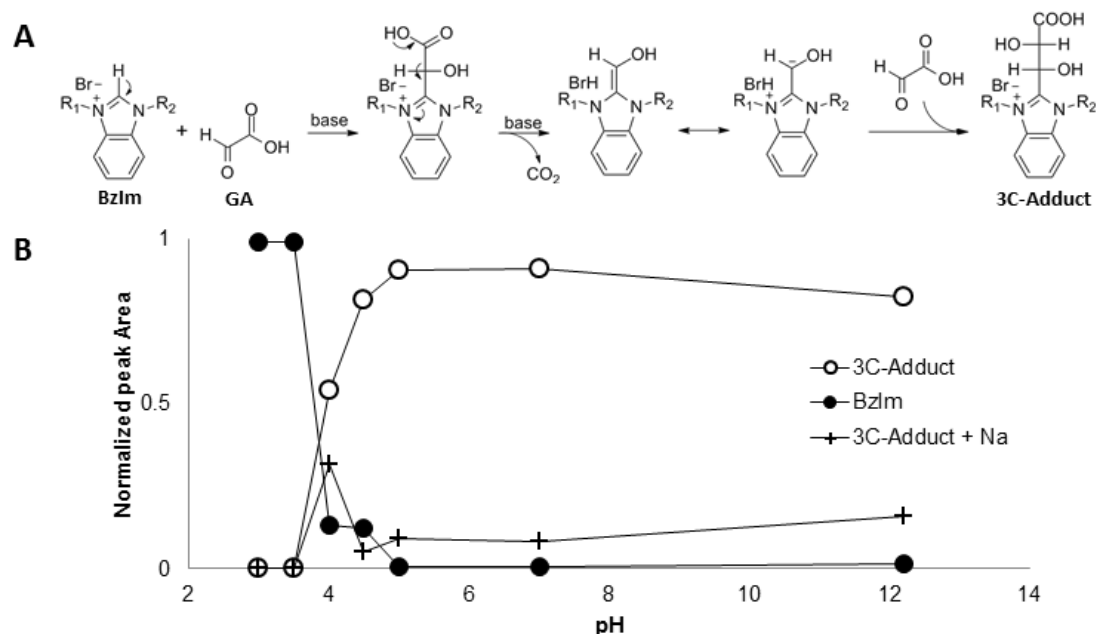


**Figure 4.4** **A** displays the mechanism for addition of GA and BzIm to yield the 3C-adduct under aqueous conditions. **B** shows MS direct injection ESI<sup>+</sup> monitoring GA + BzIm reaction products after 24h. The pH value shown is the initial pH of the 1 M GA solution and does not account for changes from TEA or BzIm addition. A clear transition was noted near pH 4, confirming that proton loss is driving this reaction.

To further understand the nature of this reaction, a pH profile was created to determine a transition pH value. For the pH profile, a 1M solution of GA was adjusted using sodium hydroxide solution to the desired pH by pH probe. This solution was added to 0.1 eq BzIm and 0.1 eq TEA quickly added (note that the figure pH is the initial measured pH, not the pH after addition of all reagents). The pH profile displays a transition near pH 4 (Figure 4.4). Below this pH, a signal corresponding to free catalyst was observed while, above this pH, free catalyst is almost undetectable. A mechanism for the formation of these products was based on the addition of GA to BzIm forming a catalyst-aldehyde adduct. This species could decarboxylate to yield a new carbanion center that could add a second equivalent of GA. The result would be a 3C-adduct with 2 stereocenters capable of forming both a true mass species and a sodium ion adduct.

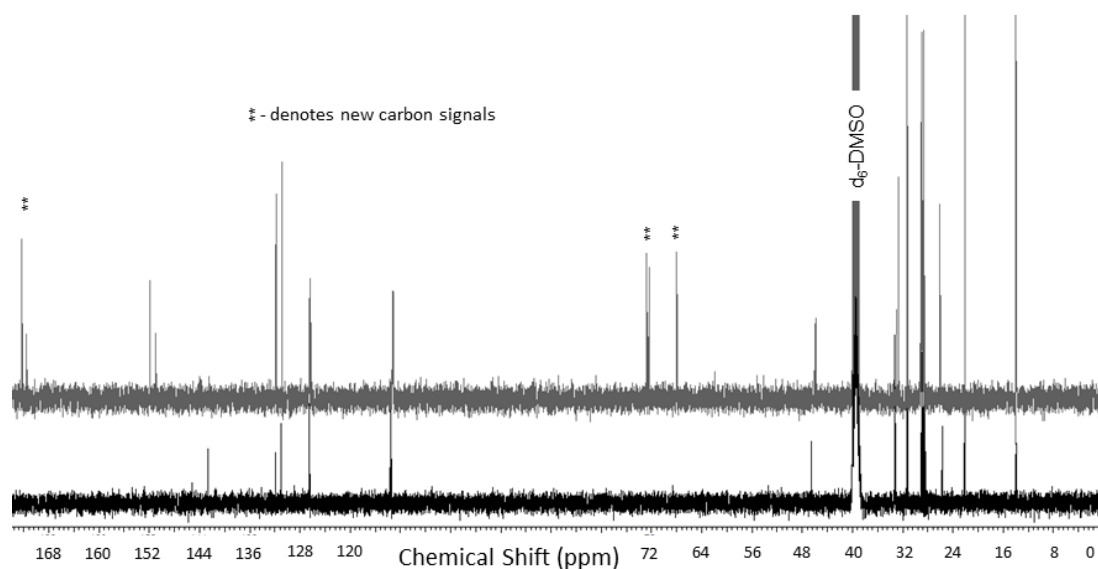


**Figure 4.5**  $^{13}\text{C}$ -NMR spectrum showing starting BzIm (bottom) and the isolated product of reaction with GA (top). Both spectra were collected in  $\text{d}_6$ -DMSO, which was also used to align the spectra. New carbon signals are denoted by 3 asterisks that would correspond to the 3 new carbons incorporated on the benzimidazolium structure. These signals display two individual peaks because there are two diastereomer structures.

The structure of the 3C-adduct was confirmed by isolating the molecule, and characterizing it using proton and carbon NMR. Under acidic conditions, a gray precipitate was observed to come out of solution upon addition of concentrated HCl. This solid was collected, washed, and dried under vacuum overnight to yield a yellow solid. Comparing the isolated solid to BzIm catalyst showed three new signals, as expected, in addition to the doubling of some signals because of the two diastereomer carbons (Figure 4.5).

After confirming the structure of the 3C-adduct, its reactivity towards further additions of glyoxylate was characterized using  $^{13}\text{C}$  labeled GA ( $\text{GA}^*$ ). All of the reactions studied thus far were monitored after 1 day of reaction, since that was all the time needed to form the 3C-adduct. However, none of them showed complete reaction of the starting glyoxylate. The decision to use  $\text{GA}^*$  was made to improve detection of trace products, such as sugars, that were expected to form by deprotonation of the 3C-adduct.

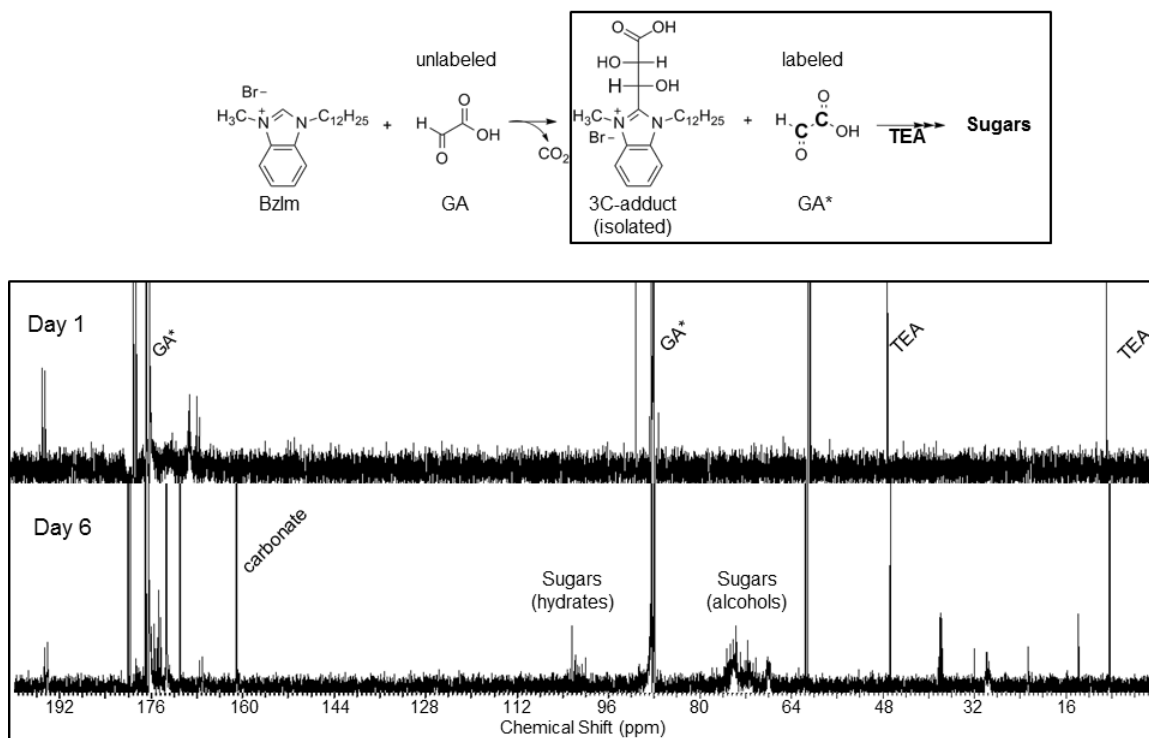


**Figure 4.6** The top scheme displays the formation of the 3C-adduct, which was isolated to perform the boxed reaction. Carbon NMR spectra of the boxed reaction between 3C-adduct and GA\* are shown below. After 6 days a broad set of peaks were noted between 64-80 ppm that could correspond to sugars, along with a carbonate signal indicating reaction progress, though starting material was still present.

A solution containing 182  $\mu\text{mol}$  GA\* was combined with 0.5 eq 3C-adduct, 0.8 eq strong base, and 0.8 eq TEA to search for products that would indicate catalyst turnover. After 1 day there was no evidence of sugars or significant decarboxylation that would indicate reaction. However, a pair of large peaks was noted near 62 ppm that corresponded to labeled glycolate. Glycolate was likely an impurity in the standard, as the peak did not change significantly over the course of reaction. After six days a new set of unresolved peaks between 64-80 ppm were noted, along with a carbonate peak near 160 ppm. These observations indicated reaction of GA\* was occurring. However, reaction was very slow, and a large amount of starting material remained (Figure 4.6).

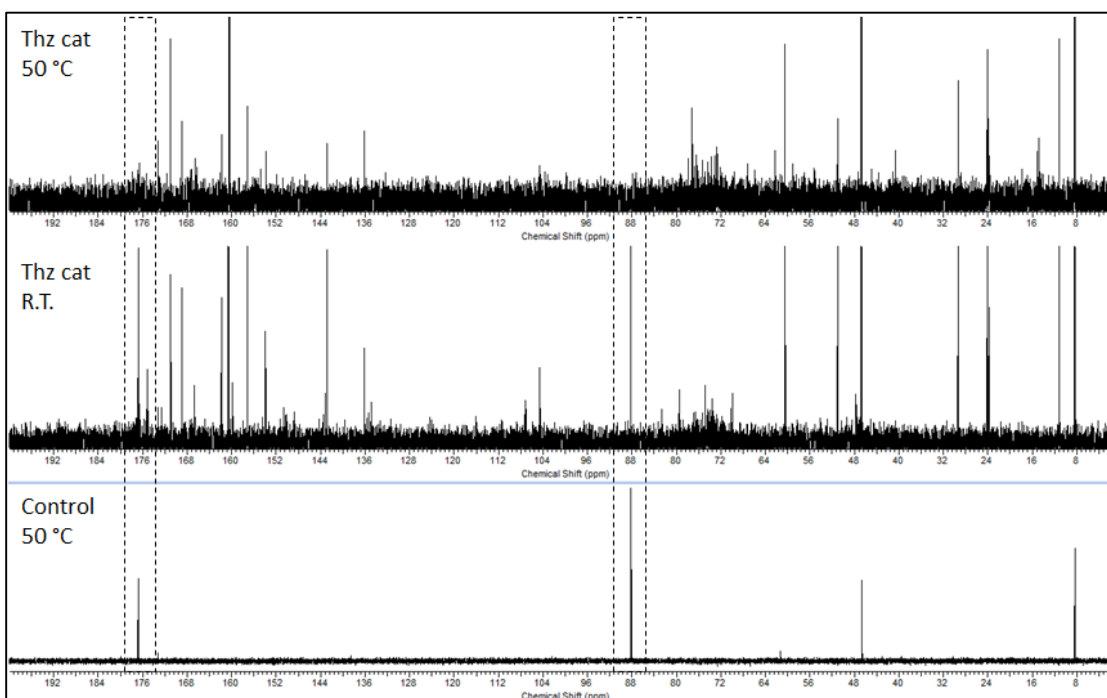


**Figure 4.7** Reaction of the GA with thiamine was monitored at room temperature and at 50 °C. A control performed under the same conditions without catalyst (bottom panel) showed that no degradation products of GA were formed as a result of heating. At room temperature (middle panel), GA conversion was incomplete after 1 day, but there was evidence of reaction products in the region 68-80 ppm. At elevated temperature (top panel) GA is completely consumed and peaks viewed in the middle panel appear to have increased in intensity. GA signals are identified by the dashed boxes.

The slow reactivity of the 3C-adduct was explored by expanding the reaction parameter space, altering catalyst, substrate, and reaction temperature to better understand the impact of each of these variables. To begin, the question of whether an azolium catalyst could promote reaction using GA as the substrate was examined. Thiamine (Thz) was used instead of BzIm as an example of a more active azolium catalyst that would still react via a similar mechanism. Three reactions were prepared using the same 1 M GA solution at pH 5: (i) a control reaction containing 0.1 eq TEA, (ii) a reaction with 0.1 eq thiamine catalyst and 0.1 eq TEA, (iii) a second reaction with 0.1 eq thiamine, and 0.1 eq TEA. Both reactions (i) and (ii) were heated at 50 °C for 24 h, while reaction (iii) was kept at room temperature (Figure 4.7).

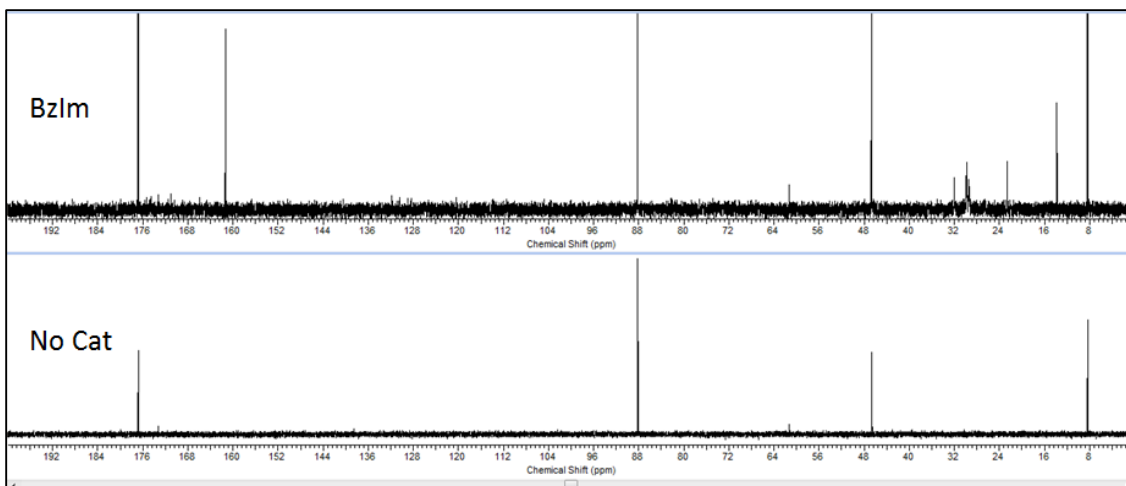


**Figure 4.8** Reaction of GA at 50 °C monitored using BzIm catalyst. After 1 day reaction, there was still remaining GA.

Using thiamine as the catalyst appeared to result in catalyst turnover as evidenced by the production of a carboxylate peak near 160 ppm, and the appearance of a group of peaks in the region between 64-80 ppm. Complete disappearance of the GA substrate using the thiazolium catalyst at elevated temperature indicated that azolium catalysts could be used in reactions with glyoxylate, and that temperature could be used to promote the reaction kinetics without promoting side reactions that would compete for GA.

The impact of temperature on reaction kinetics was further tested by conducting a reaction using BzIm catalyst at 50 °C for 24 h (Figure 4.8). This reaction used the same conditions as reactions using thiamine. Even at elevated temperature, the reaction displayed incomplete conversion, though a carbonate peak was noted at 160 ppm.

Both the heating and the alternative catalyst experiments, led to the conclusion that a better understanding of the chemical properties of the 3C-adduct was needed to achieve reaction and subsequent catalyst turnover. Based on our hypothesized mechanism, deprotonation of the 3C-adduct was necessary to achieve addition of further equivalents of GA. To examine the acidity of the 3C-adduct a deuterium exchange

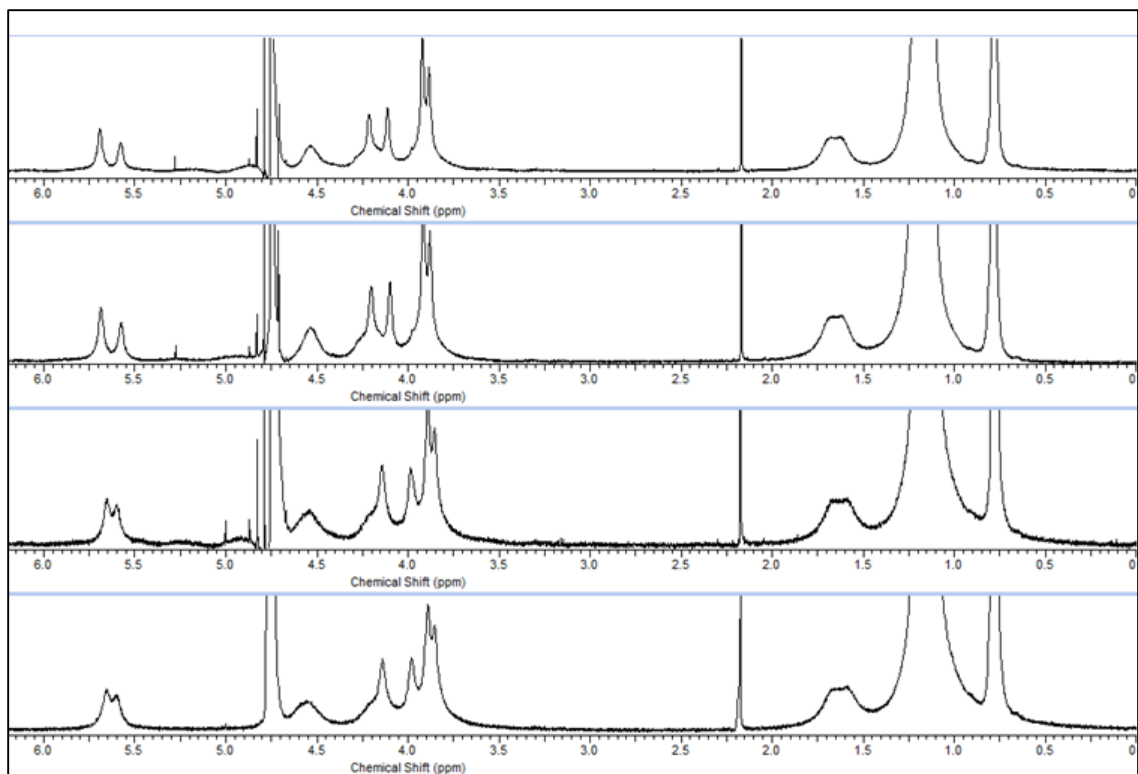


**Figure 4.9** Deuterium exchange of the 3C-adduct monitored by <sup>1</sup>H NMR in D<sub>2</sub>O. From top to bottom: no added base, +10uL 0.1% NaOD solution, +10uL 1% NaOD solution, after 24 h exchange. Over the course of this experiment, signals for the adduct proton in the alpha position (5.5-5.8 ppm) shift and merge, but never completely disappear.

experiment was performed. A series of NMR spectra were taken at increasing concentrations of sodium deuteroxide to search for loss of signal that would indicate exchange/acidity. Demonstrating proton exchange would validate that BzIm could be used as a catalyst for reaction with GA. Additionally determining the transition pH would provide a rationale for slow kinetics, if the alpha proton were found to exchange at a pH value higher than used in reactions. Observations from this experiment are shown in Figure 4.9.

Results from the deuterium exchange experiment indicated that if exchange were occurring, the process was slow and might only be observed at high concentration of base. The peaks between 5.5-5.8 ppm shift and merge, but a clear signal loss was not

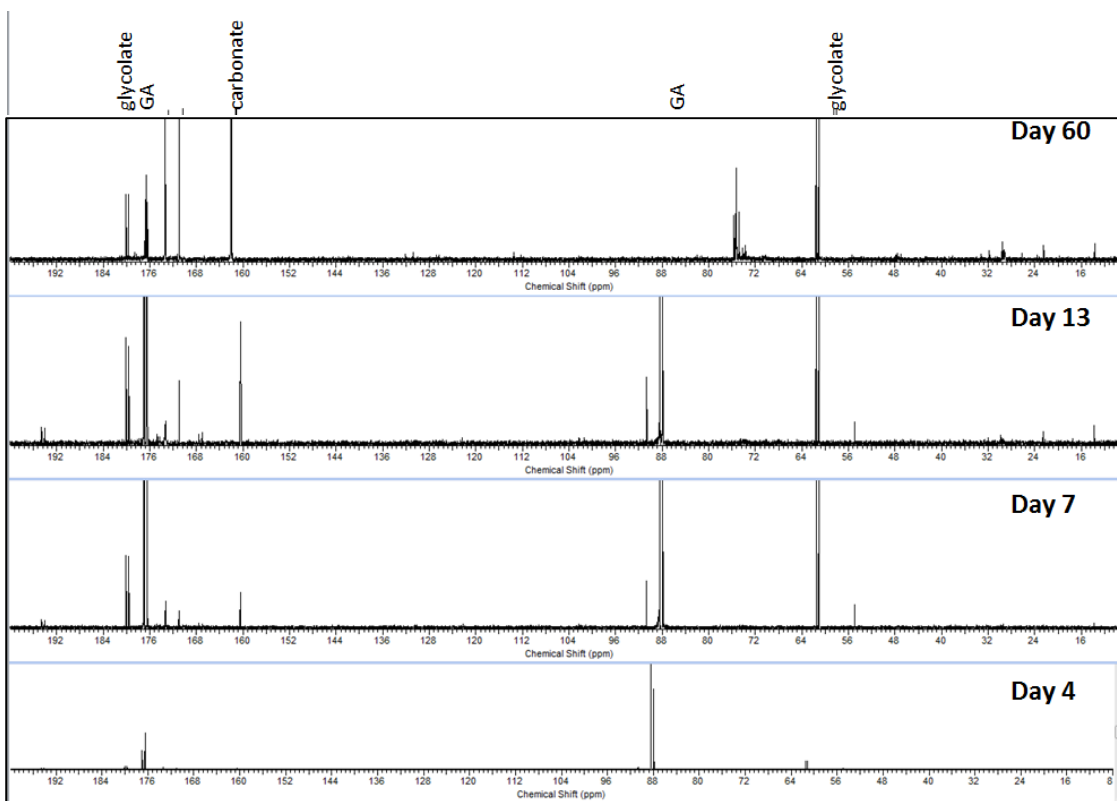


**Figure 4.10** Reaction time course monitoring the progress of reaction with 3C-adduct and Ga\*. Several important peaks are labeled above the spectra. Two peaks corresponding to carboxylate side products were noted in between the GA and carbonate signals.

observed. These peaks correspond to the diastereomers protons, alpha to the imidazolium. Change in these peaks provided an indication that reaction of the 3C-adduct was possible, but only at high pH value.

A new reaction was prepared to monitor the reaction of 3C-adduct and GA\* over a long time period. For this reaction, the starting pH was 8-9, and the pH value was measured using pH paper before sample analysis. Between days 4-13 the pH value was measured to be approximately 7. During this time period a carbonate peak appears around 160 ppm (Figure 4.10). After taking the NMR on day 13, 10uL 5 M NaOH was added to the reaction mixture, in case further production of carbonic acid halt reaction. Addition of strong base pushed the reaction to pH 14. After a period of 60 days the

products were analyzed. Over this long period the pH value had decreased to between 9 and 10. The carbonate peak had also greatly increased, and a group of peaks had appeared in the region 72-80 ppm. These results suggested carbohydrate formation, though the high pH likely led to the generation of side products as well. Two new peaks in the carboxylate reaction between carbonate and GA increased in intensity between day 13 and 60.

To remove any possible effects of pH changes, a new reaction was prepared in buffer. A solution was prepared in 2 mL borate buffer with 0.5 mmol GA\*, 0.2 eq 3C-adduct, and 0.2 eq diisopropyl ethylamine instead of TEA. The beginning pH was measured as approximately 10 and the reaction monitored over the course of a month.

While the reaction time course shows some indirect evidence of reaction by the appearance of a carbonate peak, glyoxylate consumption is still extremely slow at slightly basic pH value (Figure 4.11). Additionally, the appearance of sugar peaks is difficult to detect, especially at low conversions. Sugars have many different diastereomers causing their overall concentration to spread out over a wide region of the spectra, rather than concentrate in a single point as with the carbonate peak. This makes detection and analysis using  $^{13}\text{C}$ -NMR difficult unless many scans are taken.

As an alternative analytical technique, direct injection MS was used to track the starting 3C-adduct. This species carries a formal positive charge, and so can be easily detected due to high ionization efficiency. To determine whether reaction was taking place at low conversions would require a high sensitivity technique. If the 3C-adduct were reacting, then it should lose its unlabeled carbon adduct, and add a new labeled carbon adduct. The difference in molecular weight between these species is +3 m/z.

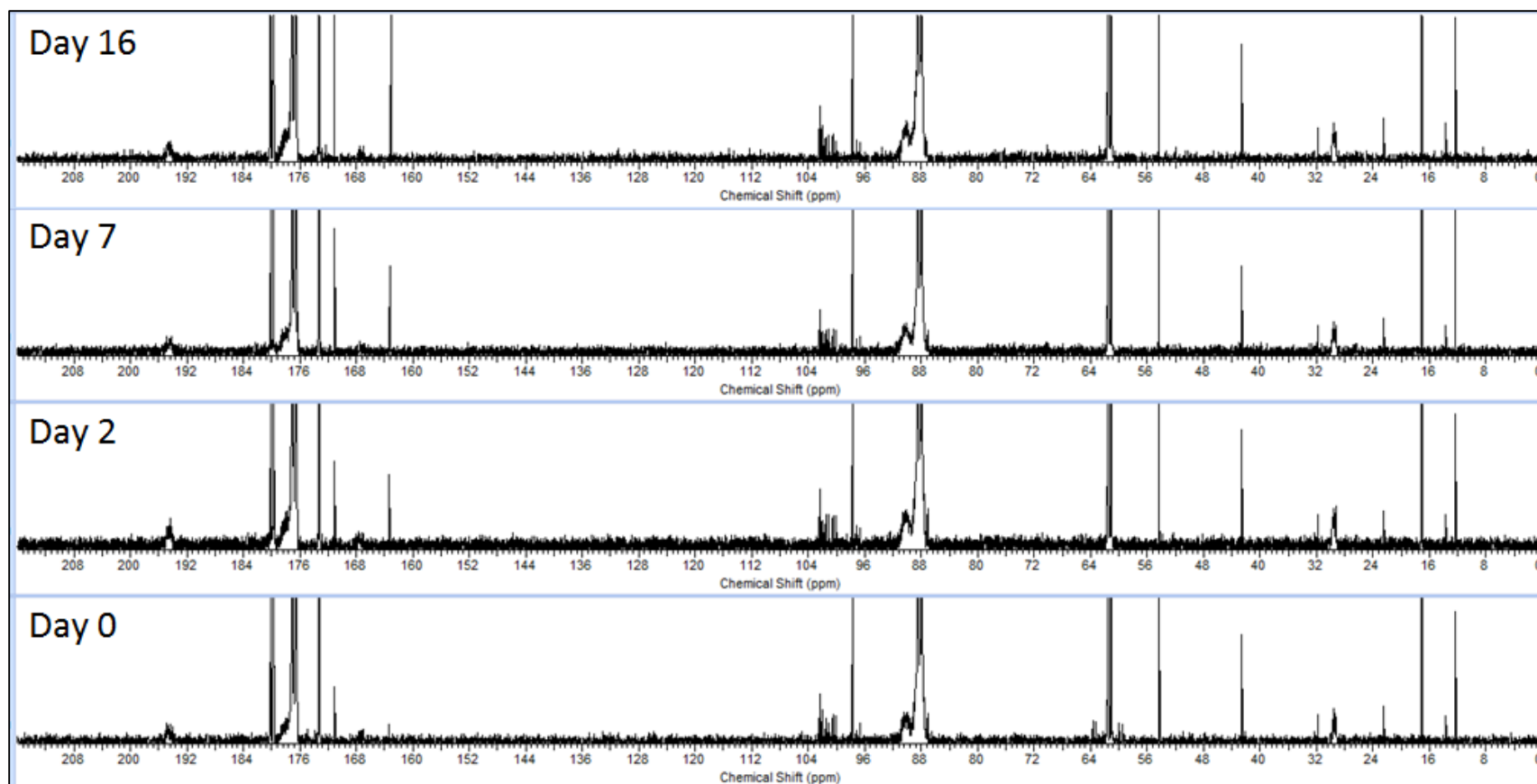


**Figure 4.11** Reaction time course monitoring the progress of reaction with 3C-adduct and Ga\* in borate buffer. Even after 16 days, the only major changes noted are in the carboxylate region. The peak for carbonate around 164 ppm increases with time, along with the carboxylate peak at 170 ppm. |

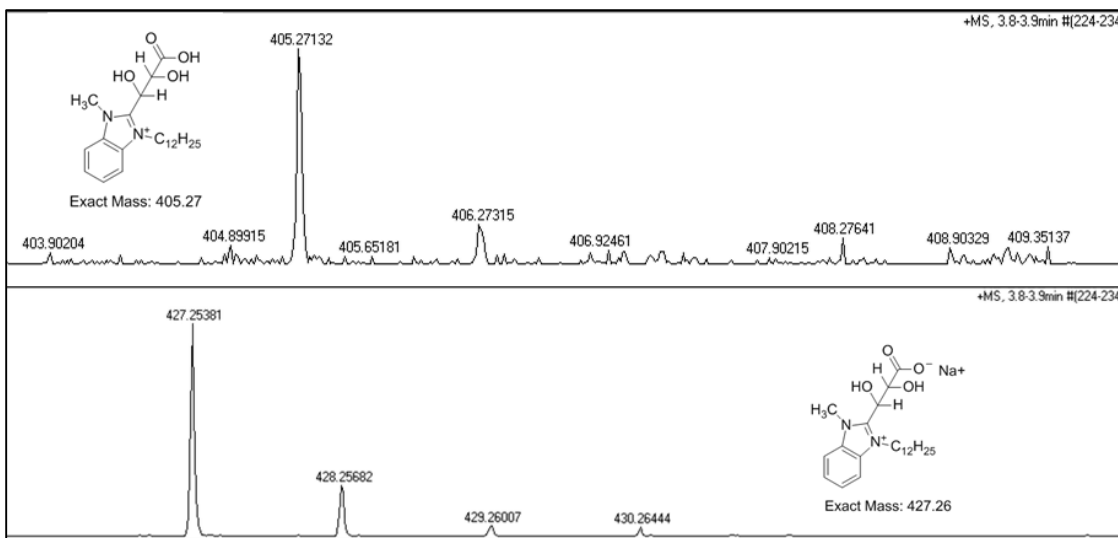


**Figure 4.12** Mass Spectra of 3C-adduct monitored by direct injection of sample. After 24 days reaction, the major peaks correspond to unlabeled starting materials.

Normally this would not be an issue; however, due to the high molecular weight of the starting ion, it was possible that isotopic effects could interfere with detection.

TOF MS was used to examine the 3C-adduct after 24 days reaction in borate buffer with labeled glyoxylate. Two species that correspond to the 3C-adduct were detected using electrospray ionization in positive mode: the molecular ion, and the molecular ion associated with sodium. These structures and the spectra are shown in Figure 4.12. The results appear to confirm the NMR findings since the major signal corresponds to the unlabeled 3C-adduct. If reaction were occurring, then all of the adduct carbons should be exchanged with the labeled glyoxylate carbons leading to a +3 m/z shift in the molecular ion.

The 3C-adduct is composed of 23 carbon atoms, which results in a relatively large isotope peak at 406 m/z and 428 m/z. Natural abundance of  $^{13}\text{C}$  isotope is ~1%, meaning that for every carbon in a structure, there is a 1% chance of being isotopically labeled. Statistically, this would mean that the incorporation of three  $^{13}\text{C}$  isotopes, is around one in one hundred molecules. This can be visualized by generating a predicted isotope

pattern spectrum to compare against the experimental results. Mass spectra are normalized to the largest peak, setting the value at 100%, thus allowing a visual, and possibly a quantitative approach. This methodology was applied to both the molecular ion and the sodium adduct, as the later displayed a better signal to noise ratio. These isotope patterns are shown in Figures 4.13 and 4.14.

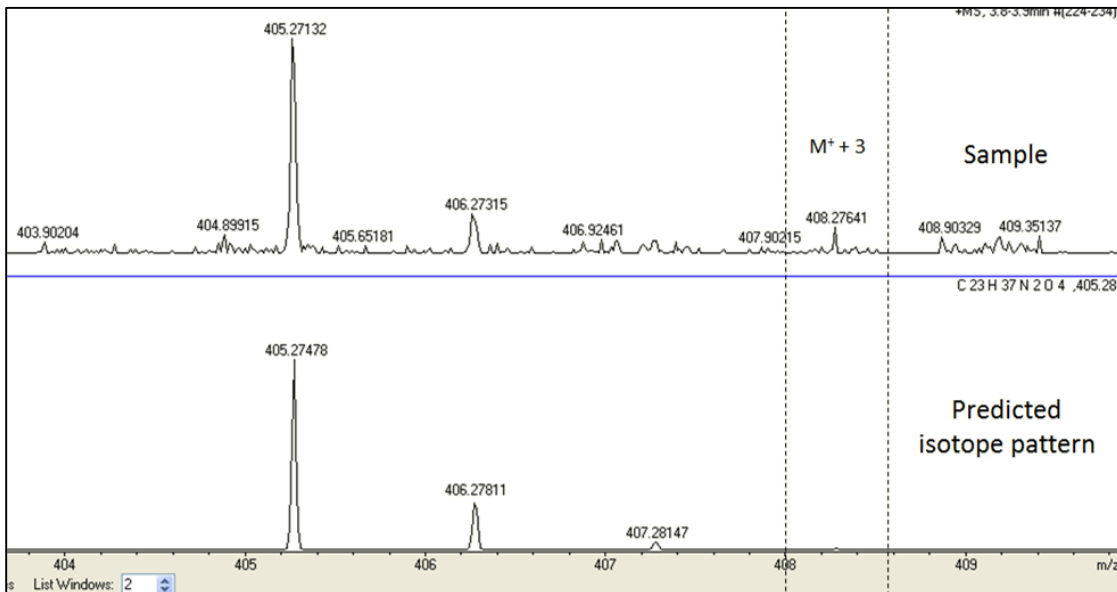


**Figure 4.13** Direct injection TOF MS of 3C-adduct molecular ion. Top: reaction after 24 days. Bottom the predicted isotope pattern.  $M^+ + 3$  isotope shown in dashed box.

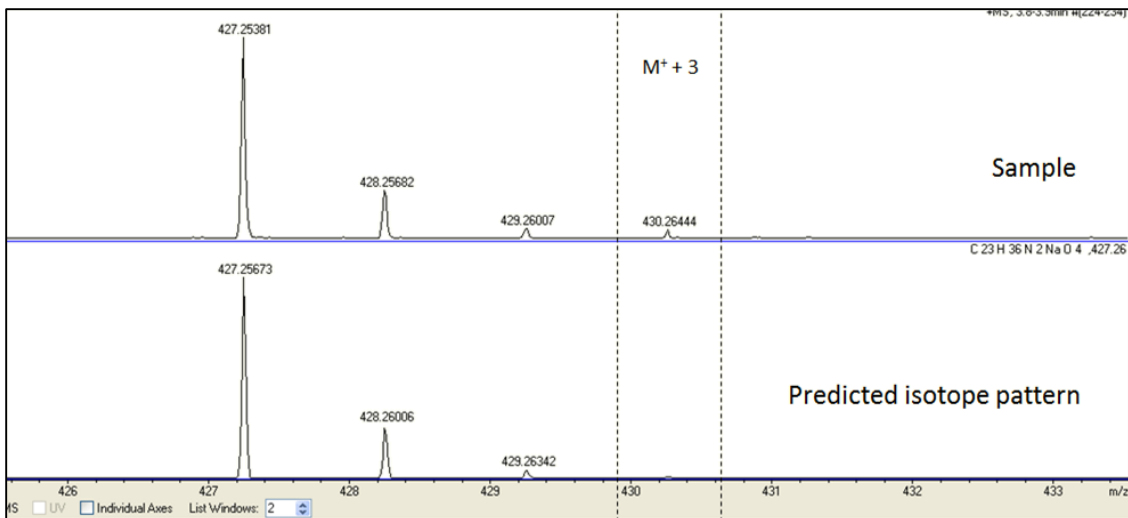


**Figure 4.14** Direct injection TOF MS of 3C-adduct sodium adduct. Top: reaction after 24 days. Bottom predicted isotope pattern.  $M^+ + 3$  isotope shown in dashed box.

#### 4.4 Discussion

Reactions with glyoxylate are initially limited by the formation of the carbene form of the catalyst. At low pH, free catalyst is detected in solution; however, no reactivity with GA is noted. However, after passing the transition pH, all mixtures of GA, BzIm, and TEA are homogenous and display formation of the C3-Adduct. While the formation of a catalyst adduct is spontaneous over a large range of pH values, further addition of glyoxylate is extremely slow, and there is evidence of side products.

However, azolium ions can be used to catalyze carbon-carbon bond formation using GA as a substrate. Thiazolium ions are known to be more active catalysts, compared to imidazolium ions. Reaction of thiamine with glyoxylate displayed full conversion of starting material, and indication of sugar products. It is likely that other thiazolium ions would also be capable of catalyzing this reaction.

While no studies were conducted, it would be of interest to examine the stability of thiazolium ions in aqueous solutions. They are known to be less stable than imidazolium ions, so determining the number of reaction cycles a thiazolium could complete before deactivating would improve the discussion of such a cycle persisting on early Earth. Additionally, a prebiotic synthesis of thiazolium ions is still needed; however, at some point these molecules must have arisen. The prevalence of thiamine in biology suggests that such catalysts could have played a very important role promoting carbohydrate chemistry on early Earth.

#### 4.5 Conclusions

Reaction of glyoxylate under aqueous conditions was monitored using a Benzimidazolium catalyst and thiamine. This work suggests that imidazolium catalysts

would have required strongly basic conditions or long time scales to achieve reaction. However, if thiazolium catalysts were present on early Earth, these would have quickly led to production of sugars and sugar acids, providing an alternative pathway to carbohydrates, instead of using formaldehyde.

#### 4.6 References

- Butch C, Cope ED, Pollet P, Gelbaum L, Krishnamurthy R, Liotta CL (2013) Production of tartrates by cyanide-mediated dimerization of glyoxylate: a potential abiotic pathway to the citric acid cycle. *JACS* 135:13440-45
- Castells J, Geijo F, Lopez-Calahorra F (1980) The “formoin reaction”: a promising entry to carbohydrates from formaldehyde. *Tetrahedron Lett* 21:4517–4520. doi:10.1016/S0040-4039(00)74538-2
- Teles H, Melder J, Ebel K, Schneider R, Gehrler E, Harder W, Brode S, Enders D, Breuer K, Raabe G (1996) The chemistry of stable carbenes. Part 2. Benzoin-type condensations of formaldehyde catalyzed by stable carbenes. *Helv Chim Acta* 79:61–83. doi:10.1002/hlca.19960790108
- Eschenmoser, A. (2007). The search for the chemistry of life's origin. *Tetrahedron*, 63(52), 12821-12844.
- Iwamoto, K. I., Hamaya, M., Hashimoto, N., Kimura, H., Suzuki, Y., & Sato, M. (2006). Benzoin reaction in water as an aqueous medium catalyzed by benzimidazolium salt. *Tetrahedron letters*, 47(40), 7175-7177.

## FUTURE DIRECTIONS

### 5.1 Continuing Project from Section 2

Section two focused on developing a proof of concept process for synthesizing imidazolium catalysts from a simple feedstock of formaldehyde, primary amine, and acid. This project could be extended by examining the effect of competition from different amine sources. Some initial reactions have already been explored to test this hypothesis. The first was to demonstrate that other amines could be substituted in place of aniline using the same reaction conditions. The primary amine 3-aminopyridine (3AP) was chosen as a close structural analog of aniline, since aromatic amines were believed to be necessary to achieve catalysis. These reactions used the same conditions for DHA + aniline reactions in section 2, but instead of 2 eq aniline, 2 eq 3-aminopyridine were used.

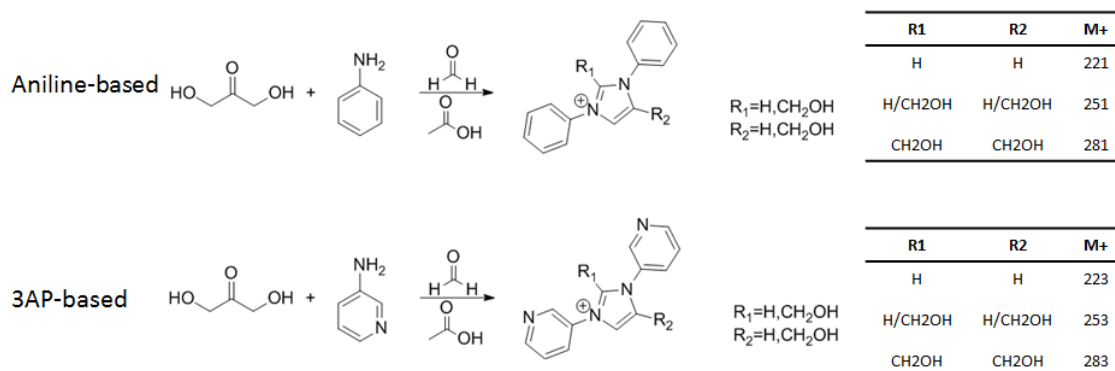


**Figure 5.1** Comparison of the reaction of DHA with aniline or 3-aminopyridine (3AP). Several expected imidazolium products and their masses are shown in the table on the right. The difference in molecular weight of the two substrates results in a +2 m/z shift.

Products from these reactions were identified using LCMS and MSMS fragmentation. Similar fragmentation patterns were identified compared to analogous

structures found when using aniline, thus indicating successful reaction using 3-amino pyridine as the starting amine.

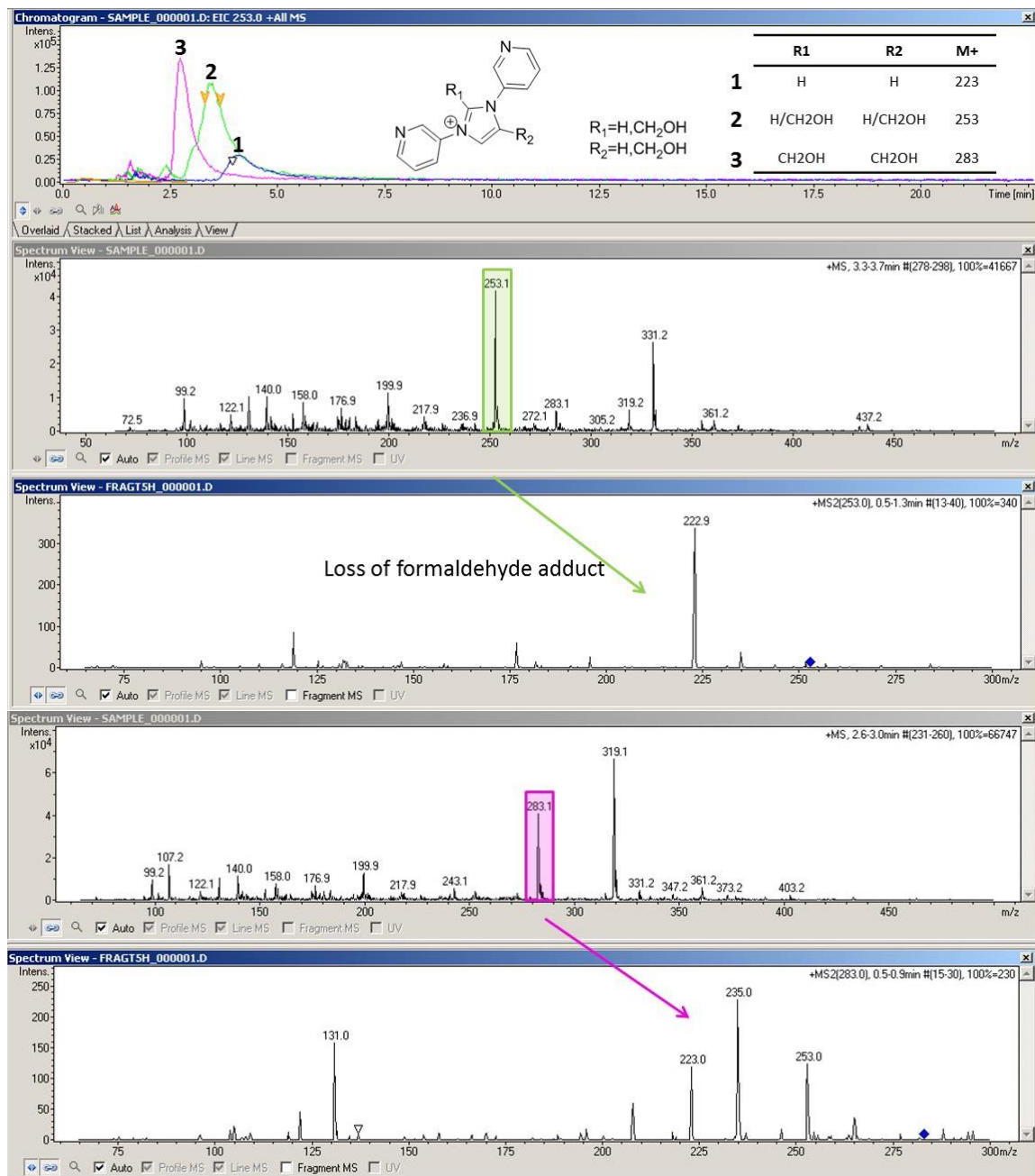


**Figure 5.2** EIC of the predicted reaction products are show at the top of the figure, along with the molecular ion, and chemical structure. The bottom spectra display the molecular ion corresponding to the chromatograph peak as well as the MSMS fragmentation pattern. The spectrum for 223 m/z was not included because fragmentation efficiency was too low.

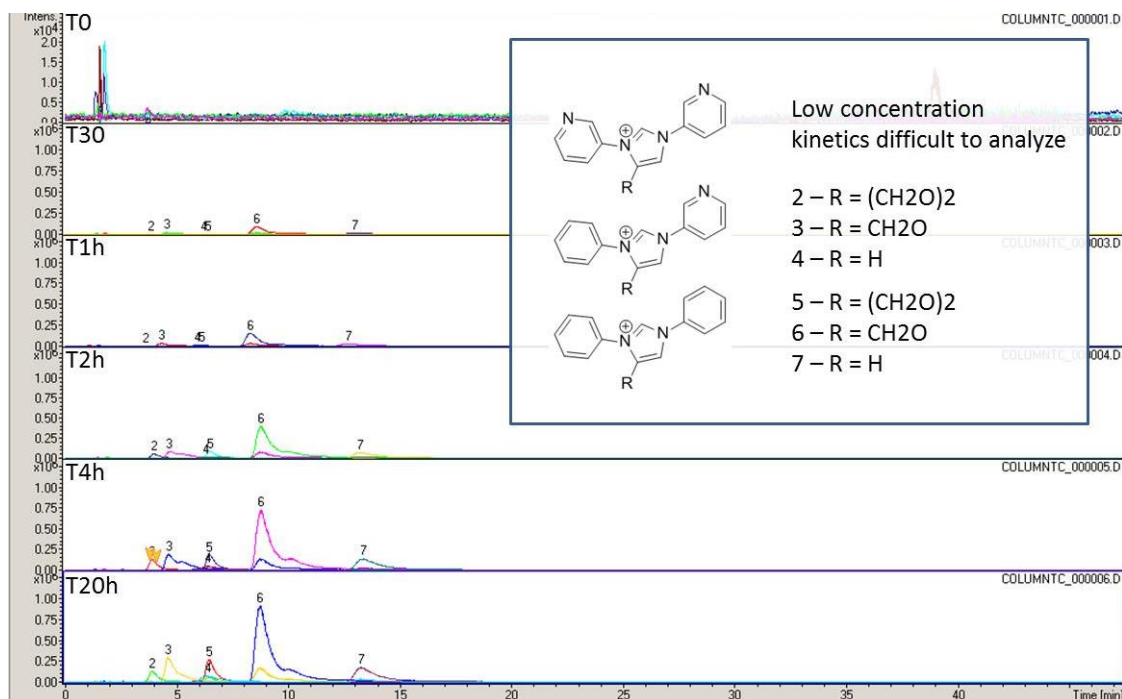


**Figure 5.3** EIC traces showing the kinetic time course of a reaction with DHA, aniline, and 3AP. Three products with varying substitutions at the 4(5) position were tracked as shown in the boxed insert.

Successful reaction and characterization of products using 3AP indicated that a mixed amine reaction could be conducted. Again the same procedure was used, except now a mixture of 1 eq aniline and 1 eq 3AP were used and the kinetics of imidazolium growth tracked over time. Product kinetics were tracked over the course of 20 hours to observe formation of 1,3-phenyl, 1,3-pyridyl, and the mixed imidazolium products. These chromatographs are shown in Figure 5.3.

One of the major observations was that a 1,3 dipyridylimidazoliums were almost undetectable due to their low concentrations. This spurred further analysis of the two observed populations of imidazolium structures, which confirmed that differences in the kinetics of formation are dependent on the amine used. Statistically, if an equal mixture of 3-aminopyridine and aniline reacted with DHA at the same rate, then a 1:2:1 product composition of imidazolium products would be detected. Instead the ratio is closer to

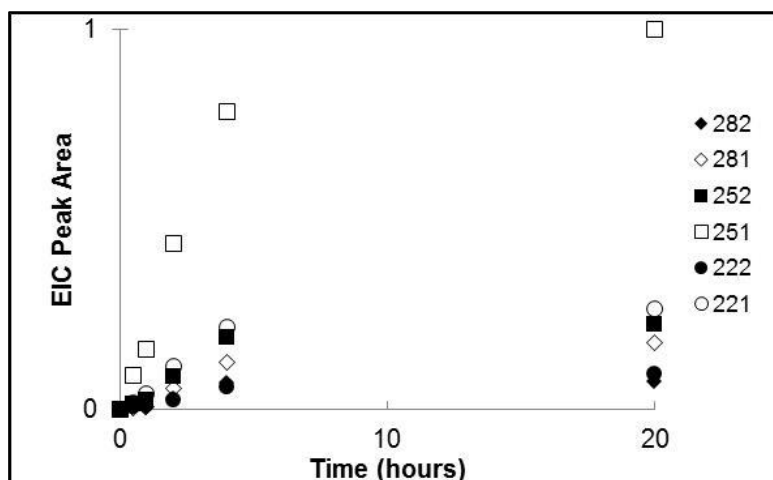


**Figure 5.4** Kinetics plot following the increase in peak area over time. Filled objects correspond to the mixed imidazolium ions; outlined objects correspond to the 1,3 diphenylimidazolium.

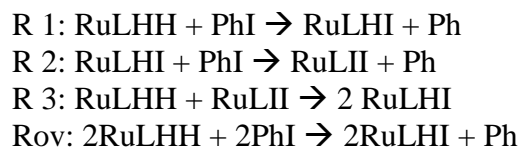
3.7:1 favoring the 1,3 diphenyl substitution as shown by the wide disparity in peak area shown in Figure 5.4.

As mentioned in section 4, developing a pathway for the simple synthesis of thiazolium ions would be incredibly interesting because of their wider substrate applications, and activity under aqueous conditions.

### 5.2 Continuing Project from Section 3

Section three is meant to stand on its own as a critique of the use of autocatalysis as a kinetic descriptor. This could be further developed through a critique of the IUPAC definition which states, “A chemical reaction in which a product (or a reaction intermediate) also functions as a catalyst. In such a reaction the observed rate of reaction is often found to increase with time from its initial value.” A catalyst that is a reaction intermediate should not be referred to as a catalyst. By definition a reaction intermediate is both produced and consumed in a reaction. However, a catalyst should not be consumed or modified at the end of a reaction. This confusion was evident in a recent paper by Milserdov et al. They characterized the reaction between haloaromatics and a

ruthenium centered metal. Over the course of reaction, the metal was oxidized, acting as a stoichiometric reactant, rather than a reaction catalyst. However, the authors noted a pathway for regeneration of the fully oxidized metal, which led to a stoichiometric pathway for autocatalysis as shown in the mechanism below:



The overall reaction shows that 2 equivalents of “catalyst” (RuLHI) are produced, when really RuLHI cannot be considered a catalyst. Compared to the starting oxidation state of the metal complex, RuLHI may display faster kinetics, but this does not make it a catalyst for the reaction. RuLHI simply provides a parallel pathway for the reaction to occur.

This confusion between autocatalysis and parallel reaction pathways may also be part of the reason why autocatalytic was adopted to describe polymer elongation kinetics. These authors note correctly, that there are two pathways for monomer addition: formation of a new strand, and elongation of a strand. Differences in these two parallel pathways can lead to non-linear kinetic profiles, which increase in rate as the reaction progresses. However, these reactions should not be described as autocatalytic.

### **5.3 Continuing Project from Section 4**

Section four was focused on transitioning azolium chemistry to more plausible prebiotic conditions by altering catalyst structure, and conducting reactions under aqueous conditions. Formaldehyde is still a plausible substrate for azolium catalyst, so characterizing its reactivity in water compared to DMF would provide a simple

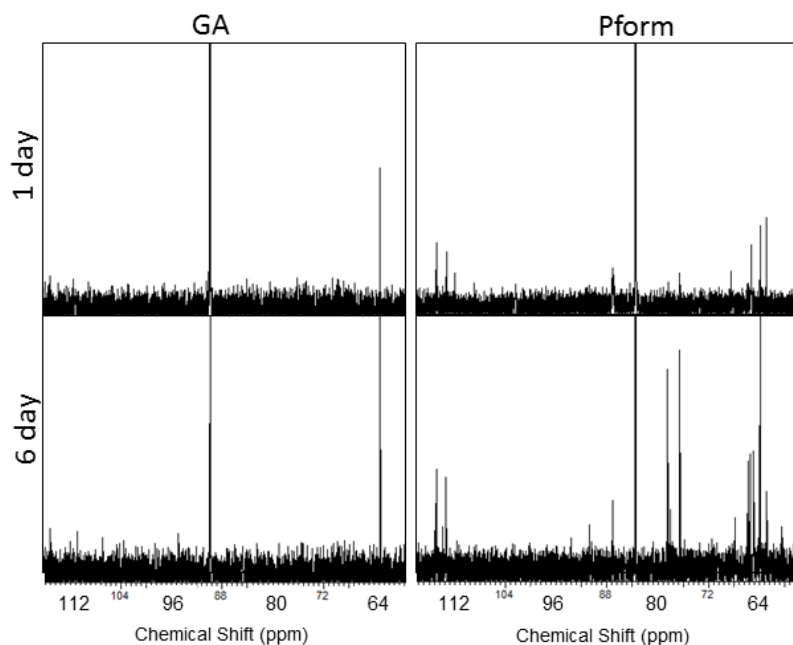


**Figure 5.5** Compares the kinetics of BzIm catalyzed carbon-carbon coupling reactions using two aldehyde substrates (GA and Pform). A single peak is noted in the GA reaction; however, this peak corresponds to glycolate, a side product.

extension. It would also allow for comparison of GA and formaldehyde to see if GA is truly a better substrate for producing sugars.

Initial reactions were conducted to examine if formaldehyde would yield sugars under the same conditions as GA. Two reactions, one with GA and one using paraformaldehyde, were prepared at the same solution pH to compare their reaction kinetics, using  $^{13}\text{C}$  NMR to track two regions specific to sugars. The region between 60-80 ppm is indicative of  $-\text{CH}_2\text{OH}$  carbons, and the region between 96-116 ppm is indicative of  $-\text{CH}(\text{OH})_2$  carbons (Figure 5.4). Comparing both reactions it is apparent that GA shows few carbon signals in this spectral region. The only peaks seen are starting material near 90 ppm, and glycolate side product near 64 ppm. In the case of paraformaldehyde a greater product complexity is noted. In both cases full consumption of starting material (GA – 90 ppm; Pform – 84 ppm) was not noted, even after 1 week.

# APPENDIX A

## SUPPORTING INFORMATION

### Outline

A1. Characterization & Synthesis of Imidazolium Standards: 1,3-Diphenyl imidazolium Cl<sup>-</sup> and 1,3-Diphenyl 2-hydroxymethyl imidazolium AcO<sup>-</sup>

A2. DHA+Aniline Reactions and Products

- a. Identification of standards
- b. Identification of Isomers
- c. Identification of other imidazolium structures

A3. Catalysis Using SPE Purified Imidazoliums

- a. LCMS tracking of Breslow Intermediates after Reaction with Formaldehyde
- b. MSMS Fragmentation of Imidazoliums after Reaction with Formaldehyde

A4. Process Control Experiment 1 – Effect of Separation Stage S1

A5. SPE Chromatography (S1)

A6. Experimental Stages and Characterization

- a. Process Initiation
- b. Influence of Dilution

## A1. Characterization & Synthesis of Imidazolium Standards: 1,3-Diphenyl Imidazolium Cl<sup>-</sup> and 1,3-Diphenyl 2-hydroxymethyl Imidazolium AcO<sup>-</sup>

### Synthesis of 1,3-Diphenyl Imidazolium Chloride

Product was synthesized using a procedure taken from Clavier, H. *et al. Eur. J. Inorg. Chem.* **2009** with minor changes. The procedure was followed up to the addition of a saturated solution of NaHCO<sub>3</sub>, which forms a two-phase mixture. The aqueous layer was removed, and, instead of adding HBF<sub>4</sub>, it was concentrated to about 30% of its initial volume. This layer was allowed to stand at room temperature then placed in a 4°C refrigerator overnight. Rod-like, white crystals were collected and washed with acetone. Analytical spectra of the dried product are below:

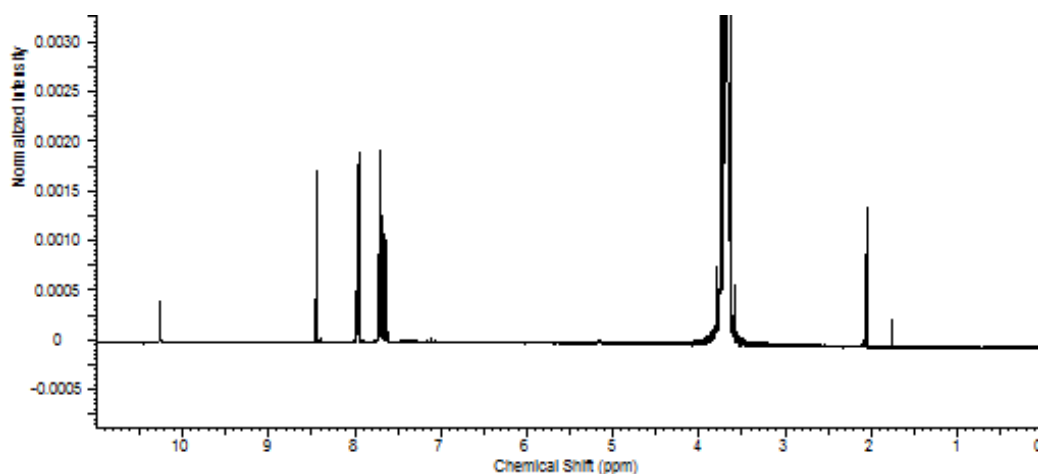


**Figure A.1** Proton <sup>1</sup>H NMR in d<sub>6</sub>-acetone + H<sub>2</sub>O: full Spectrum (water was added to improve solubility)

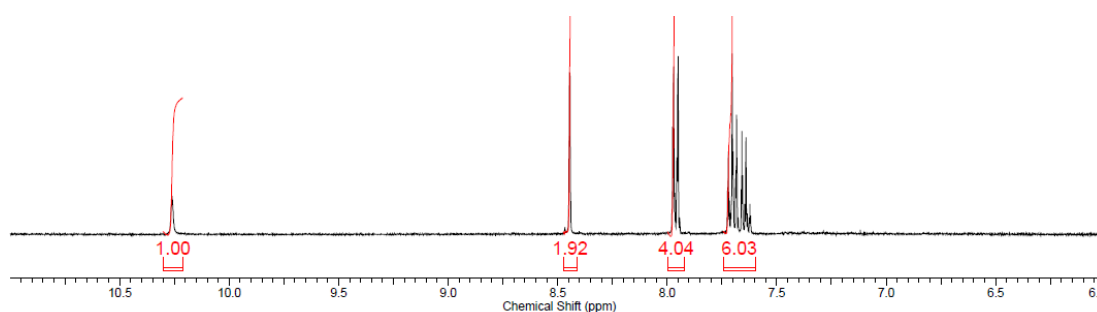


**Figure A.2** <sup>1</sup>H NMR zoom aromatic region displaying peak integration

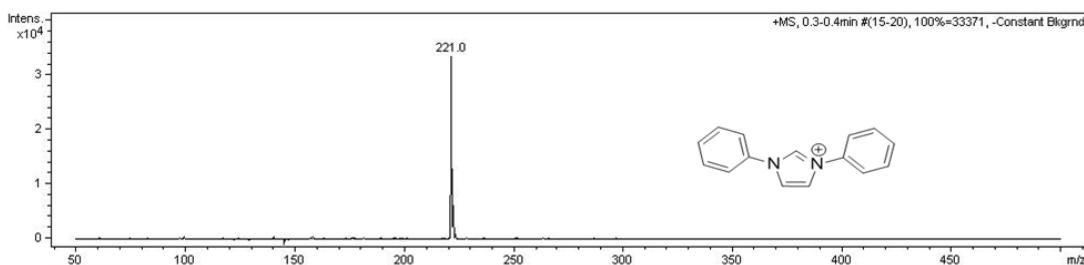


**Figure A.3** MS direct injection. Only a single significant peak is seen at 221 m/z.

### Synthesis of 1,3-Diphenyl 2-Hydroxymethyl Imidazolium Acetate (Adduct)

In dimethylformamide (DMF), a reaction of 50 mg (0.2 mmol) 1,3-diphenyl imidazolium chloride and 8 mg (0.24 mmol) paraformaldehyde was stirred at 80°C until clear then allowed to react for another 2 min. Purification was attempted by acetone precipitation, but this yielded poor results. The mixture was then left in the hood to evaporate. Conversion was quantitative based on analytic spectra below:

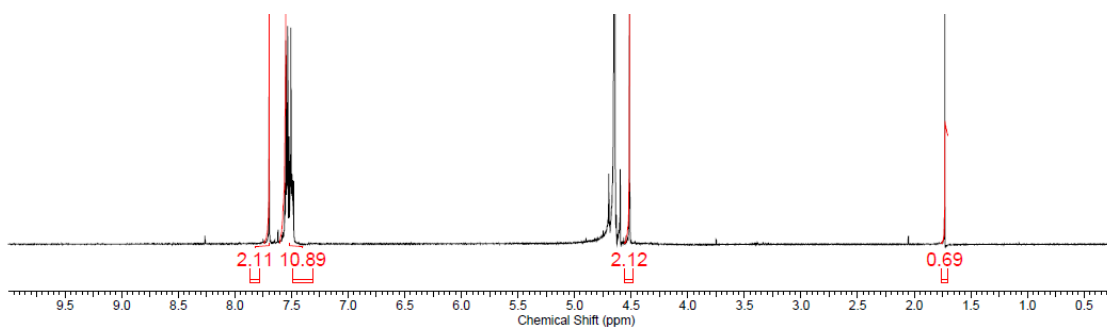


**Figure A.4** <sup>1</sup>H NMR in D<sub>2</sub>O with peak integrations

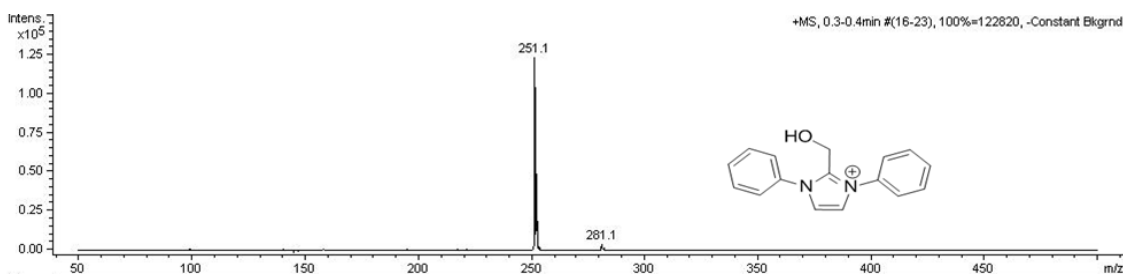


**Figure A.5** MS direct injection. One major peak appears at 251 m/z, the mass of a single formaldehyde adduct. A small peak at 281 m/z is also present which would correspond to addition of two formaldehyde molecules.

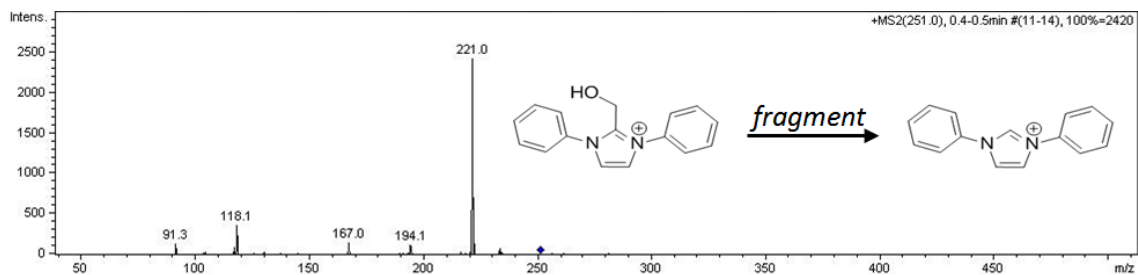


**Figure A.6** MSMS of the synthesized formaldehyde adduct (251 m/z) yields a major peak corresponding to the starting imidazolium indicating the loss of formaldehyde (-30 m/z).

## A2. DHA+Aniline Reactions and Products

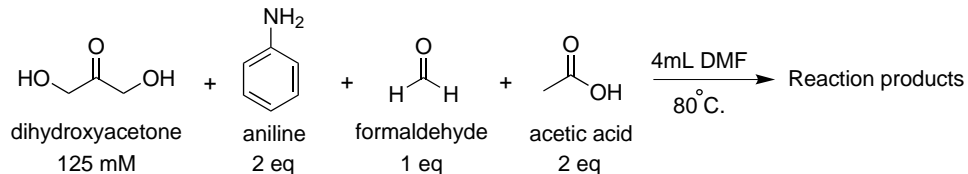


**Figure A.7** DHA+Aniline Reaction scheme

### Identification of Standards

A DHA+Aniline Reaction containing 125 mM DHA, 2 eq aniline, 1 eq H<sub>2</sub>CO (as paraformaldehyde), and 2 eq AcOH was analyzed by LCMS for comparison against the extracted ion chromatograph (EIC) of two Imidazolium standards. 1,3-diphenyl imidazolium ( $m/z=221$ ) was identified in the reaction mixture using only retention time; however, comparison of the  $m/z=251$  EIC peaks indicated the possible presence of a structural isomer for 1,3-diphenyl 2-hydroxymethyl imidazolium as shown in Figure A.8.

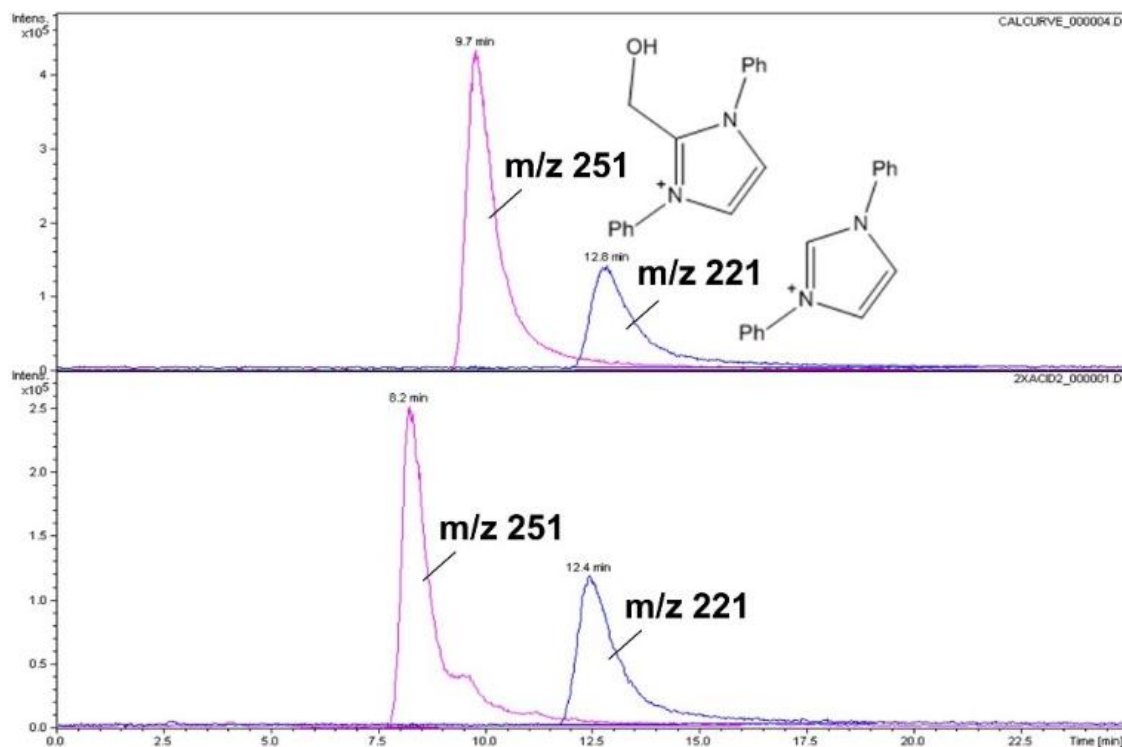


**Figure A.8** DHA+Aniline Reaction products (bottom EIC) were compared against synthesized imidazolium standards (top EIC) to illustrate that these structures can be produced from dihydroxyacetone.

## Identification of Isomers

The identity of this structural isomer was further investigated using two pieces of information: (1) the kinetic behavior of the 251 m/z isomers in Figure A.9, and (2) MSMS fragmentation of the two 251 m/z isomers in Figure A.10.

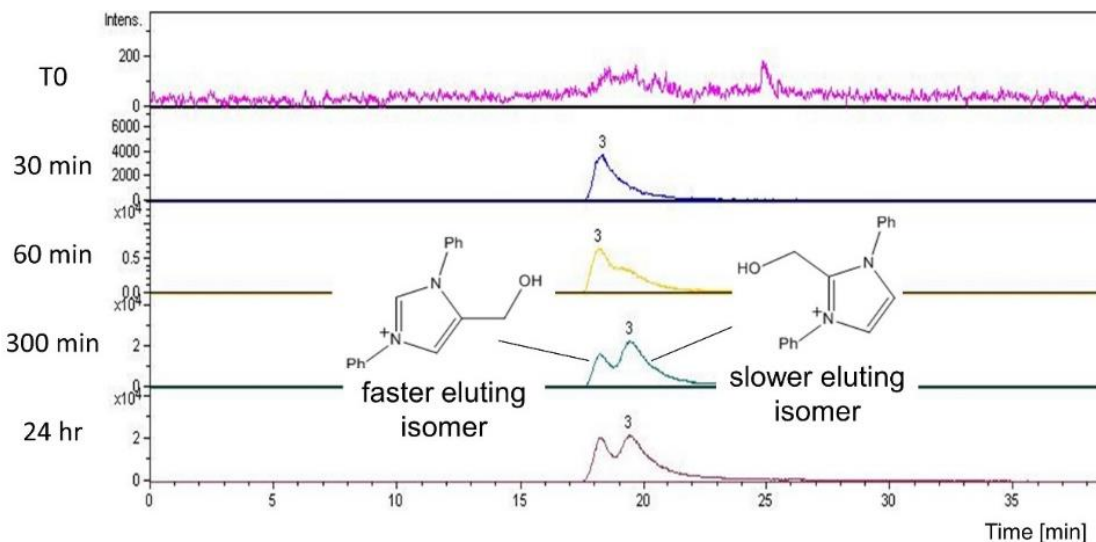


**Figure A.9** Kinetic time course showing the formation of two peaks with  $m/z=251$ . A faster eluting and slow eluting isomer are not completely resolved, but display different growth rates.

*Interpreting kinetic results:* The two isomers are produced by different mechanistic pathways. The isomer to appear first (faster eluting) should bear greater structural identity to starting materials. The isomer appearing later should bear lower identity or may require additional modifications to the structure after formation of the imidazolium ring.

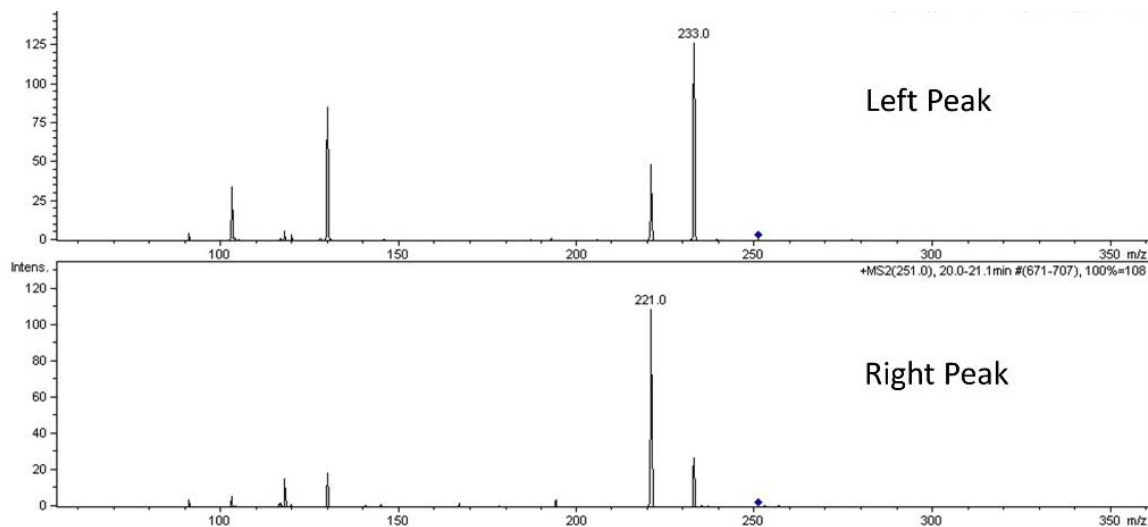


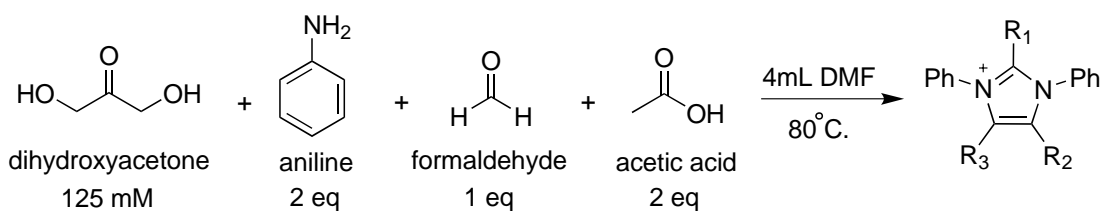
**Figure A.10** Even though the peaks were not completely resolved, a significant difference in fragmentation pattern could still be seen. The slower eluting isomer (right peak) matched the fragmentation pattern of the standard 1,3-diphenyl 2-hydroxymethylimidazolium, while the faster eluting isomer displayed a major fragmentation pathway associated with loss of water 251-->233 m/z (-18 m/z) not loss of formaldehyde 251-->221 (-30 m/z).

*Interpreting fragmentation results:* The right peak (slower eluting) displayed a major daughter ion at 221, a decrease of 30 m/z. This would occur from the loss of a neutral formaldehyde molecule and matched the fragmentation pattern of the standard 1,3-diphenyl 2-hydroxymethylimidazolium. The left peak (faster eluting) displayed a major daughter ion at 233, a decrease of 18 m/z. This would occur from the loss of a neutral water molecule. Some overlap was noted due to lack of baseline resolution between the two isomers. This is why only the major daughter ions are considered.

*Conclusion:* Using both the kinetic information and fragmentation, the structure of the left peak (faster eluting) isomer was assigned to 1,3-diphenyl 4-hydroxymethylimidazolium.

## Identification of Other Imidazolium Structures

The DHA+Aniline Reaction is not selective and produced a wide array of imidazolium substitution patterns. Based off the proposed mechanism, EICs were produced using  $m/z$  values corresponding to “alternative” imidazolium structures. The imidazolium chromatographs all show a distinct tailing behavior that is indicative of their structure. Additional confirmation of catalytic activity and MSMS structural information is provided in the next section (SI-3).



$m/z$	R1	R2	R3	Isomer detected?
281	H <sub>2</sub> COH	H <sub>2</sub> COH	H	No
251	H <sub>2</sub> COH/H	H/H <sub>2</sub> COH	H	Yes
221	H	H	H	No
235	H	CH <sub>3</sub>	H	No
326	CH <sub>2</sub> NH <sub>2</sub> Ph/H	H/CH <sub>3</sub>	H/NH <sub>2</sub> Ph	Yes

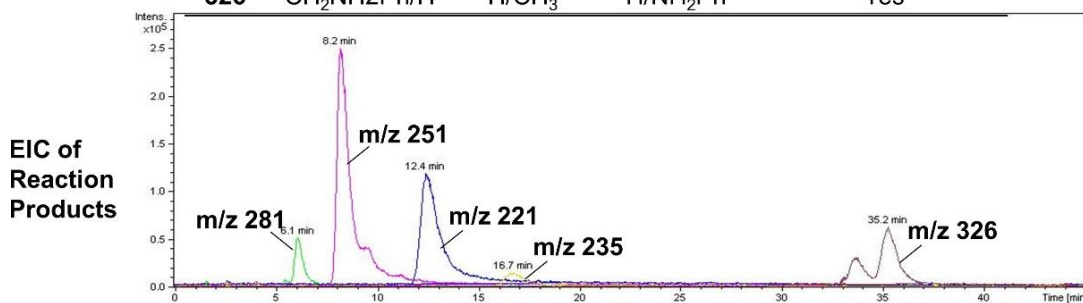


**Figure A.11** The DHA+Aniline reaction is shown at the very top of this image. Subsequently there is a table describing the imidazolium  $m/z$  values, and substitution patterns at 3 key positions on the imidazolium framework. The information in this table was used to construct the combined EIC shown at the very bottom.

### A3. Catalysis Using SPE Purified Imidazoliums



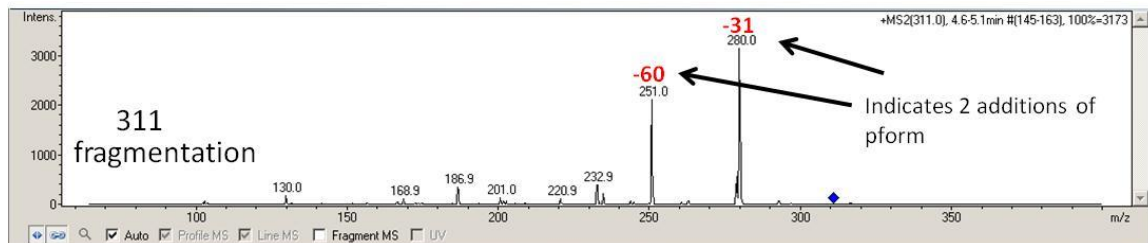


**Figure A.14** MSMS of 311 m/z ion indicated structure is likely a glycolaldehyde adduct (+60 m/z) of 1,3-diphenyl 4-hydroxymethylimidazolium (251 m/z).

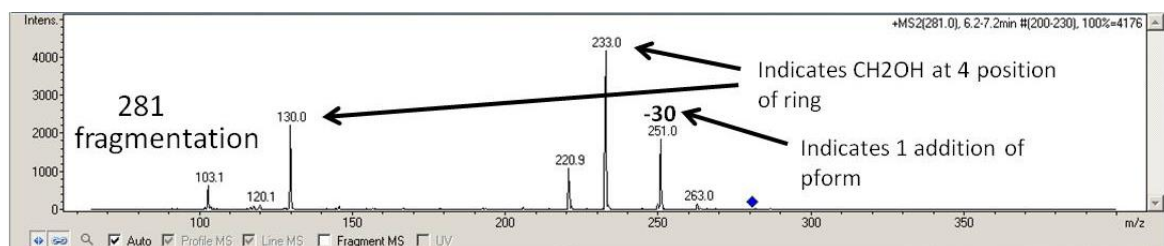


**Figure A.15** MSMS of 281 m/z ion indicated structure is likely a formaldehyde adduct (+30 m/z) of 1,3-diphenyl 4-hydroxymethylimidazolium (251 m/z).

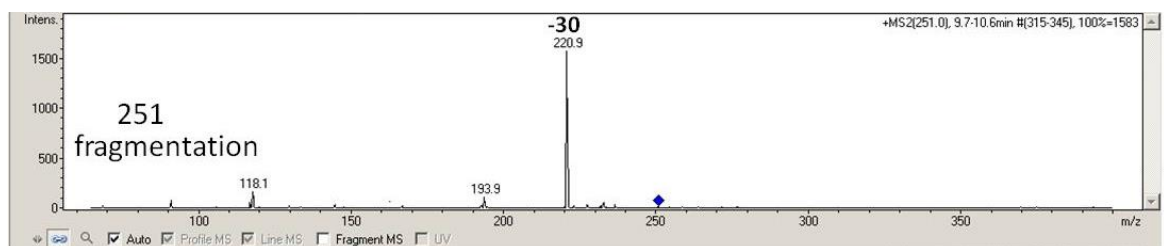


**Figure A.16** MSMS of 251 m/z ion indicated structure is likely a formaldehyde adduct (+30 m/z) of 1,3-diphenyl imidazolium (221 m/z)

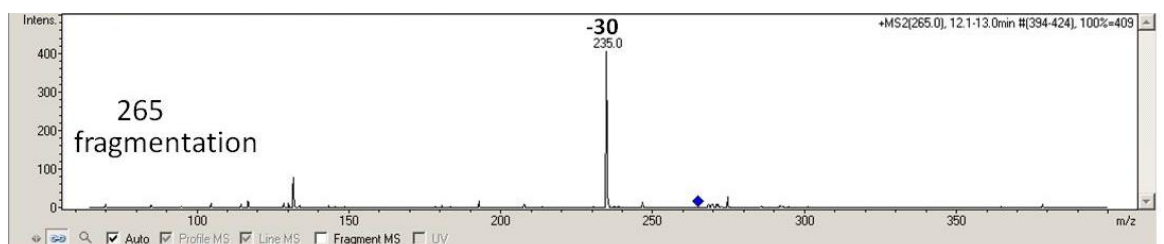


**Figure A.17** MSMS of 265 m/z ion indicated structure is likely a formaldehyde adduct (+30 m/z) of 1,3-diphenyl 4-methylimidazolium (235 m/z)

*Observations:* Neutral loss of a formaldehyde molecule (-30m/z) was common among many of the ions. However, in one case a loss of glycolaldehyde (-60m/z) was seen, along with a loss of -31m/z that could occur due to radical cleavage of CH<sub>2</sub>OH from the

glycolaldehyde adduct. A signal at 233m/z is indicative of hydroxymethyl substitution at the C4(5) position.

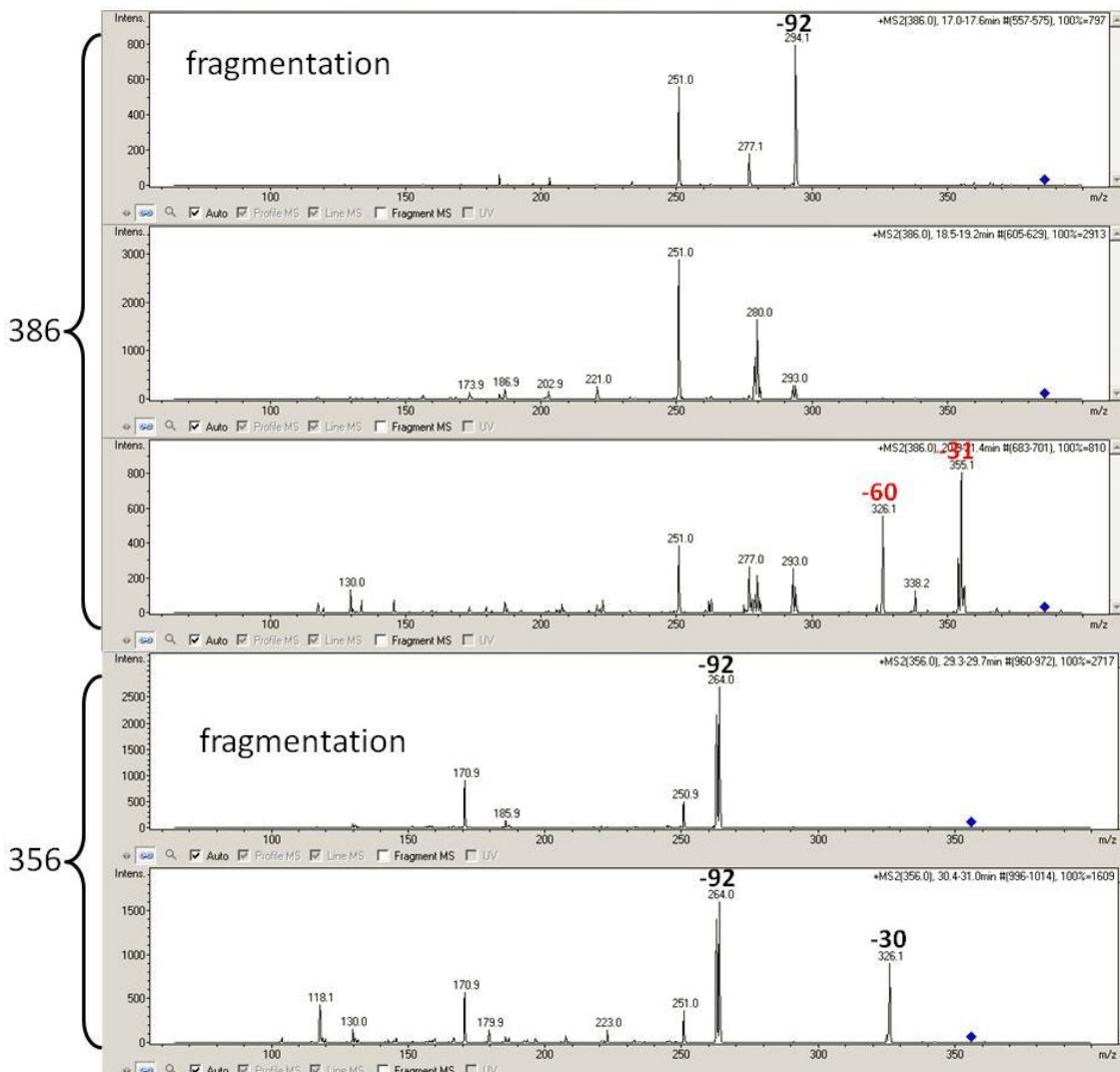


**Figure A.18** These high molecular weight imidazolium ions incorporated 3 equivalents of aniline and had a much larger number of possible isomer structures based on the fragmentation patterns generated. These peaks were also not well resolved.

*Observations:* It is unnecessary to determine all of the parent ion structures that correspond to these daughter peaks. Based on the observations discussed previously—loss of formaldehyde (-30 m/z) or loss of glycolaldehyde (-60 m/z)—there is evidence for the formation of an imidazolium structure with a 4-methyl 5-phenylamine substitution that would correspond to a starting mass of 326 m/z.

#### A4. Process Control Experiment 1: Effect of Separation Stage S1

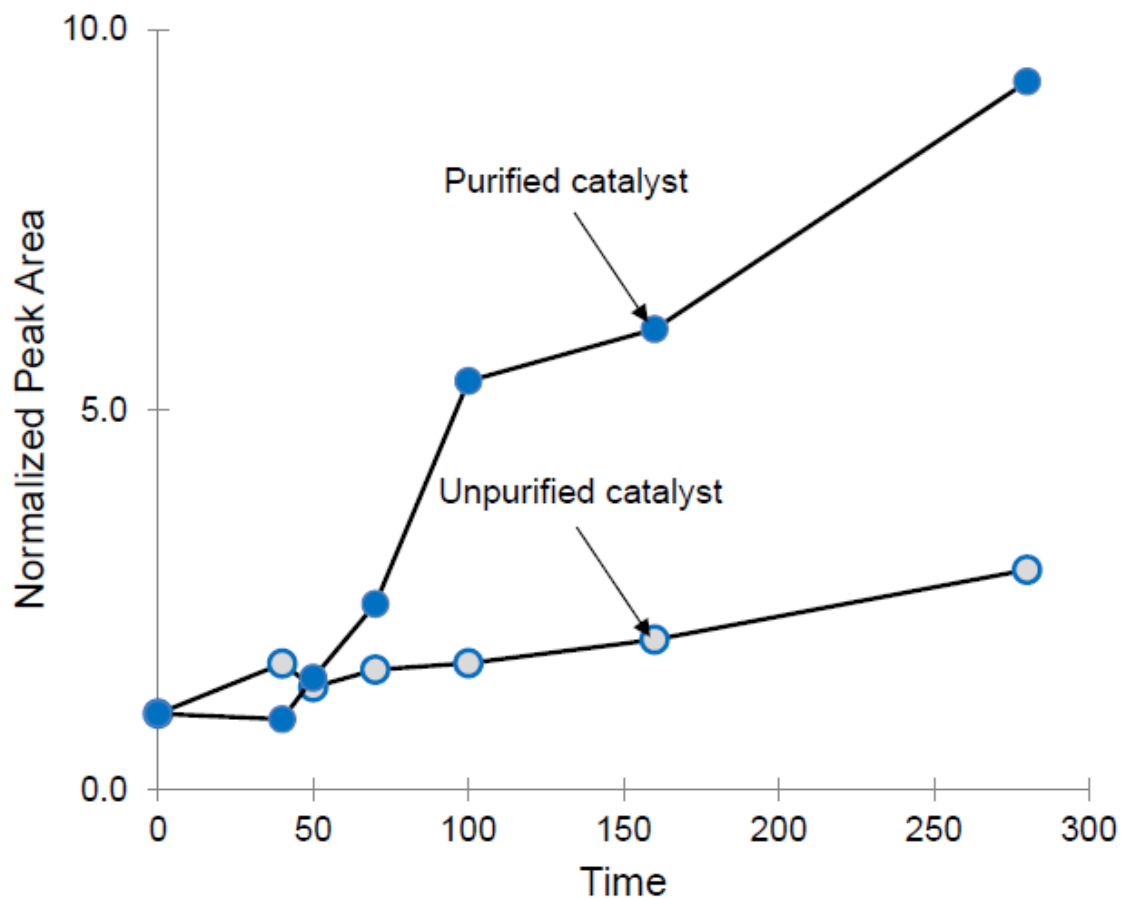


**Figure A.19** Effect of Separation Stage S1 on the formation of new imidazolium catalyst in Reaction Stages R1 and R2. A time course is plotted showing the normalized amount of new imidazolium catalyst so that each experiment would start with the same value. The unpurified catalyst did not go through Stage S1 and shows limited production of new catalyst. Purified catalyst did go through Stage S1 and shows the expected kinetic behavior: the initial time points are constant and after the start of R2 and significant increase in new catalyst signal occurs.

## A5. SPE Chromatography

Using the C18 solid phase extraction (SPE) method, fractions were collected and analyzed by direct injection MS after the addition of each new solvent. The overlaid chromatograms at the top of Figure 5.1 display the extracted ion chromatographs (EICs) of 251 m/z, a distinctive signal for imidazolium ions, for each fraction. The only significant peak occurs during the elution fraction - E1. Following the chromatogram are direct injection spectra for purification fractions. F1+F2 refers the DI H<sub>2</sub>O fraction which contained most of the solvent, DMF ([M+H]<sup>+</sup> 74, [M+Na]<sup>+</sup> 96, [2M+H]<sup>+</sup> 147). F3 refers to the acetone fraction which contained some residual DMF and other minor peaks. F4 (MS not shown) refers to the methanol fraction which had no significant peaks. Finally E1 refers to the elution fraction using methanol with 0.1 M ammonium acetate. This fraction included the imidazolium peaks 251, 281, 311, and 386 m/z.

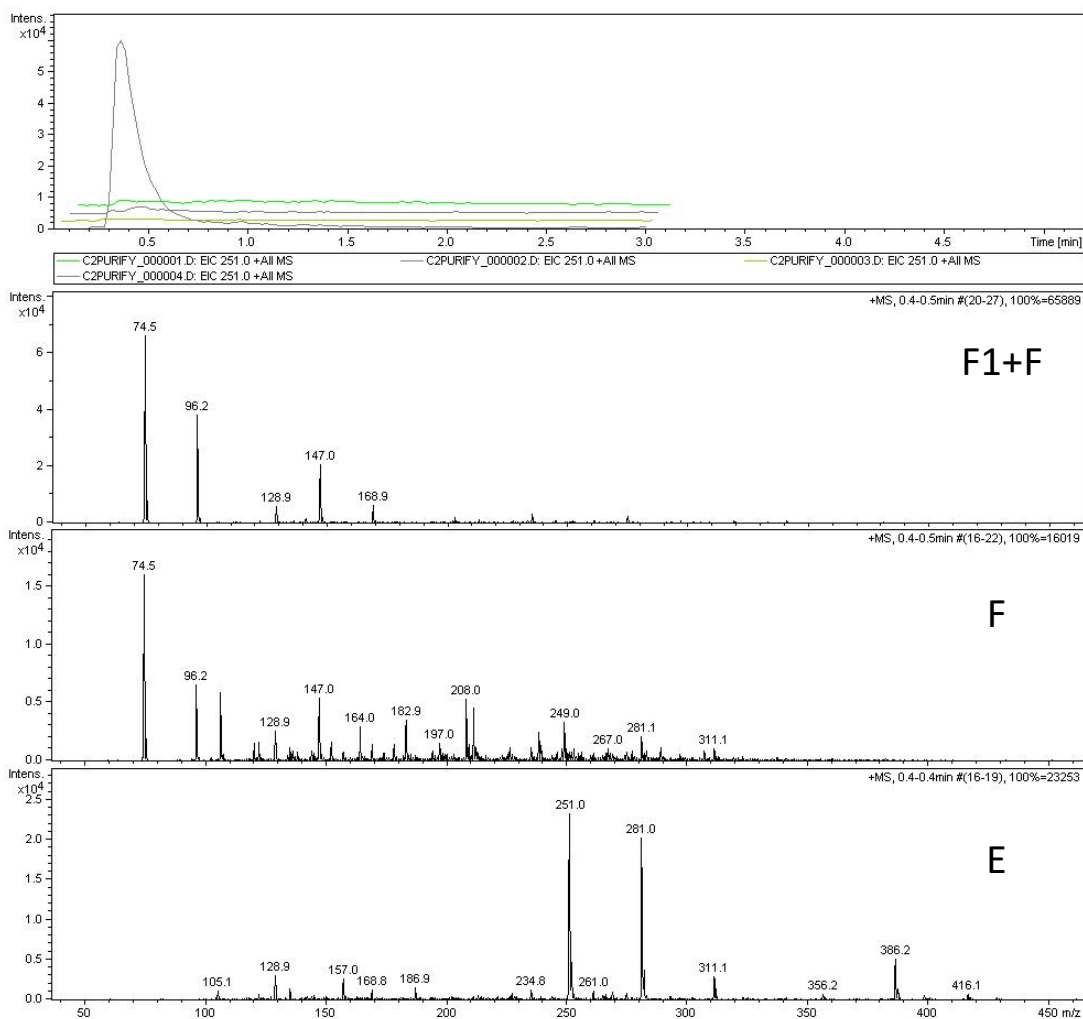


**Figure A.20** Results of the Process Separation Method on a DHA+Aniline Reaction. Each of the four different eluents were collected to determine the method selectivity for imidazolium ions: DI H<sub>2</sub>O (F1+F2), acetone (F3), methanol, and methanol with 0.1 M ammonium acetate.

## A6. Experimental Stages and Characterization

### Process Initiation

Process initiation was the generation of starting catalyst from a DHA+Aniline Reaction, also referred to as cycle 0. This reaction generated a large quantity of an imidazolium displaying 326 m/z, indicating the addition of 3 equivalents of aniline. This distinction was thought to make it an attractive primer for subsequent reaction cycles because of its unique mass and retention time.

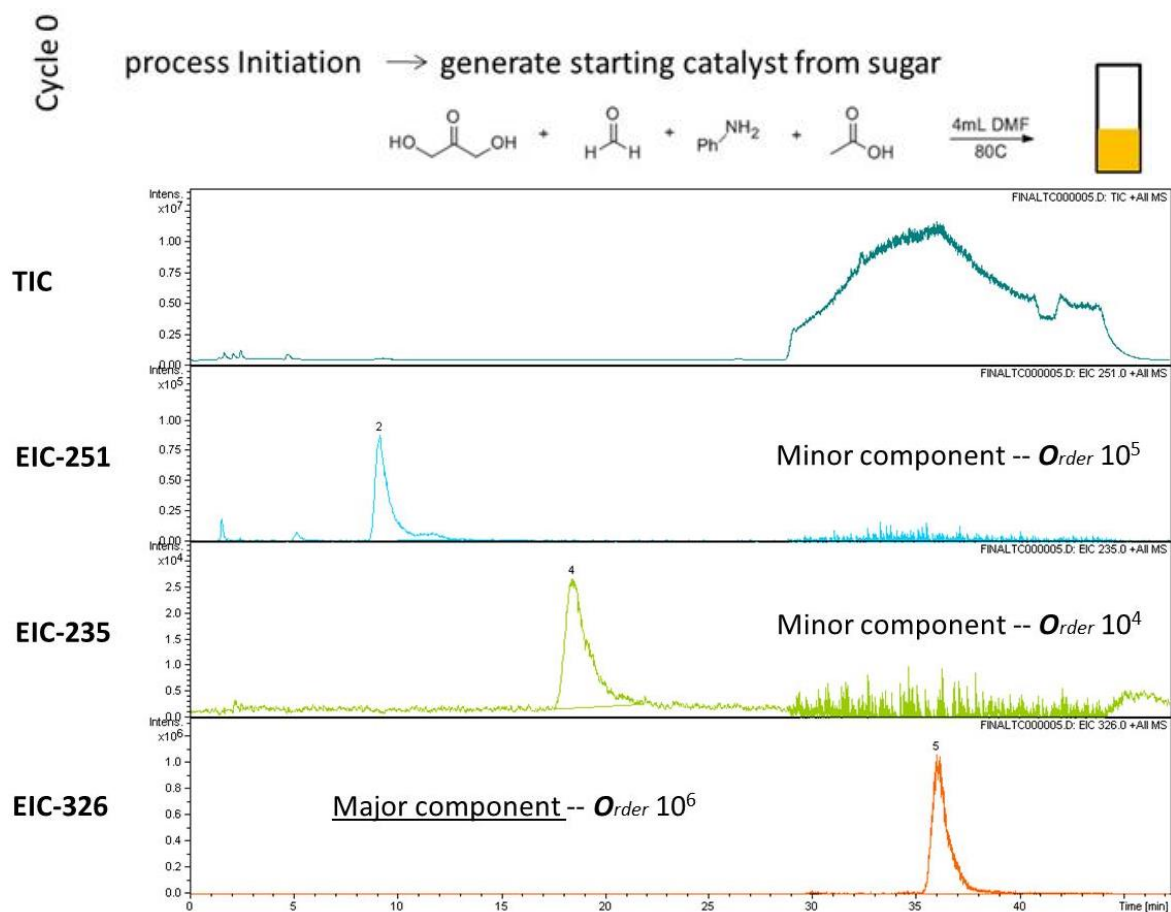


**Figure A.21** LCMS ion chromatographs of initiation mixture products (cycle 0). The total ion chromatograph (TIC) does not display any significant peaks. However, imidazolium structures could be identified by the extracted ion chromatographs (EICs)

### Influence of Dilution

Influence of dilution experiments varied the starting concentration of catalyst. This was accomplished by purifying a specified volume of the initiation mixture, then evaporating the imidazolium fraction to dryness. Reconstituting the imidazolium ions in a new volume of solvent provides the factor of concentration dilution as shown in Figure A.22. To demonstrate the purification was consistent between the two dilution experiments, the catalyst elution from Stage S1 was analyzed by direct injection MS as shown in Figure A.23.

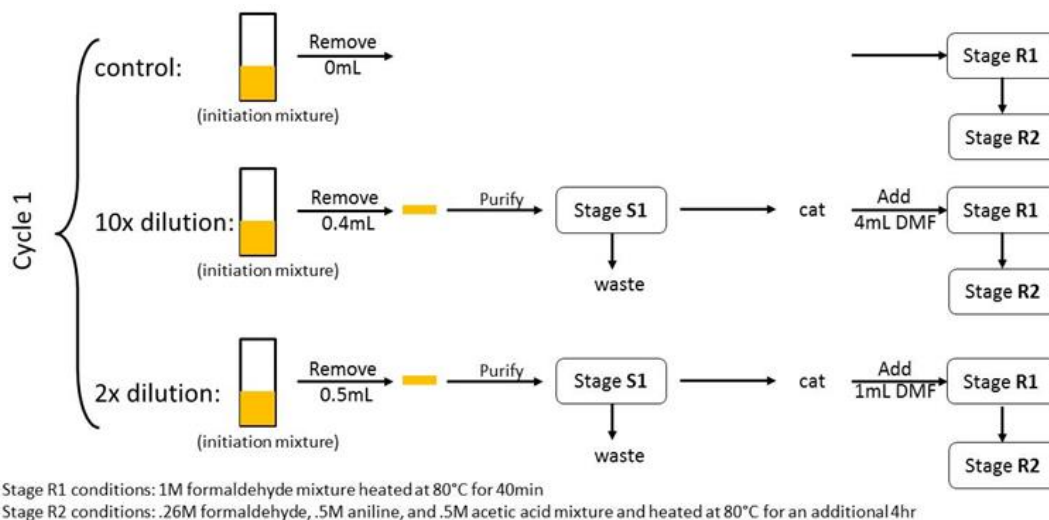


Figure A.22 Process flow diagram showing volumetric dilution quantities and conditions as conducted in Experiment 2.

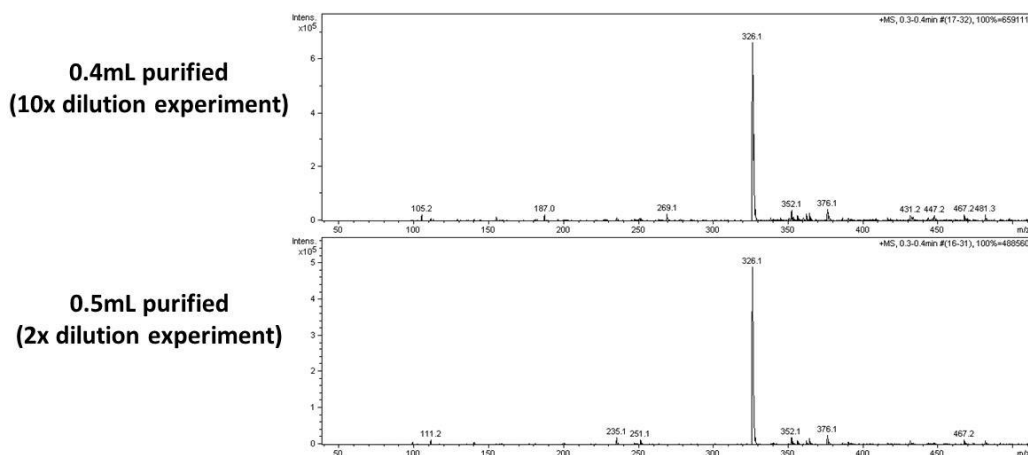
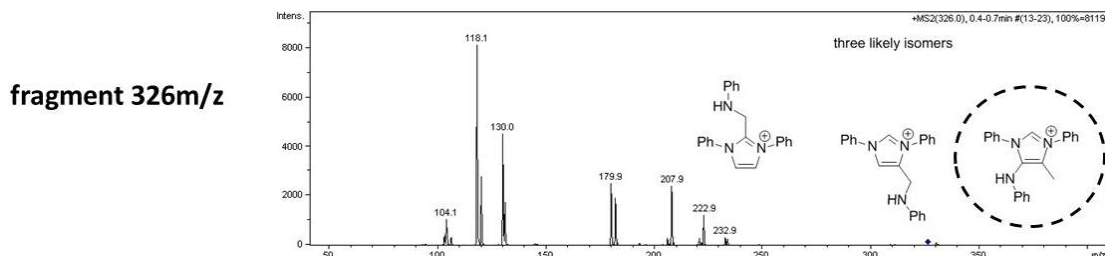


Figure A.23 Purified catalysts from both dilution experiments were analyzed using direct injection MS. Only one major peak displaying 326 m/z is present in both spectra.

### Characterization of 326 m/z Ion

Both of the purified imidazolium fractions displayed a major ion at 326 m/z. This ion was characterized using MSMS and NMR before applying the compound as a catalyst in the iterative process.



**Figure A.24** The structure of the 326 m/z ion was characterized by MSMS. However, the complex fragmentation pattern required that additional analytical techniques be applied such as NMR

SPE purified elutions were evaporated under reduced pressure then placed in a sand bath with an Argon stream blowing over it. The resultant residue was reconstituted in  $\text{CDCl}_3$  for  $^1\text{H}$  NMR. It was extremely dark in color.

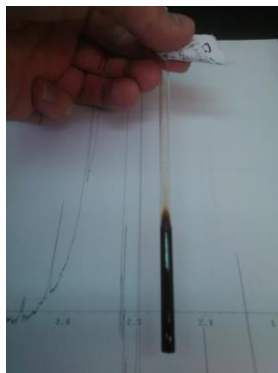


**Figure A.25** The 326m/z ion dissolved in  $\text{CDCl}_3$

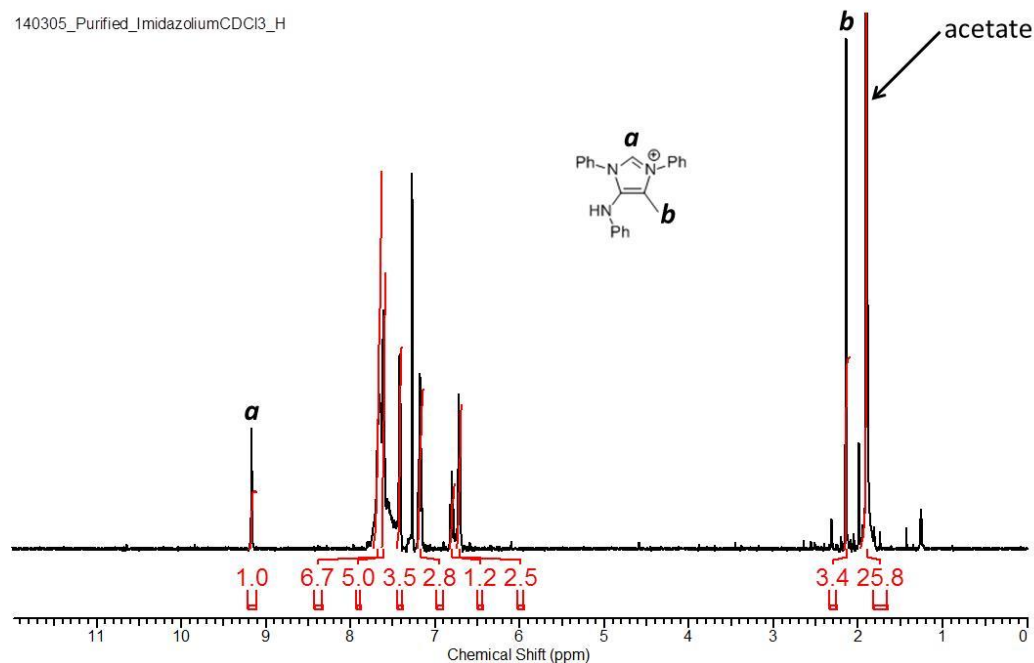


**Figure A.26**  $^1\text{H}$  NMR of the 326m/z ion. The aromatic region is difficult to analyze, but overall the spectra appears to agree with the above structure. It shows that it is the major imidazolium compound.

### Process Iterations

Process iteration experiments did not vary any experimental variable. The same procedure was applied in each stage for each process iteration. A volumetric dilution of 2x was conducted before the start of Stage R1 so that over time new imidazolium catalysts produced in stage R2 would increase in concentration, while primer imidazolium catalyst would be slowly diluted out of the process.

#### 2x Dilution iterations:

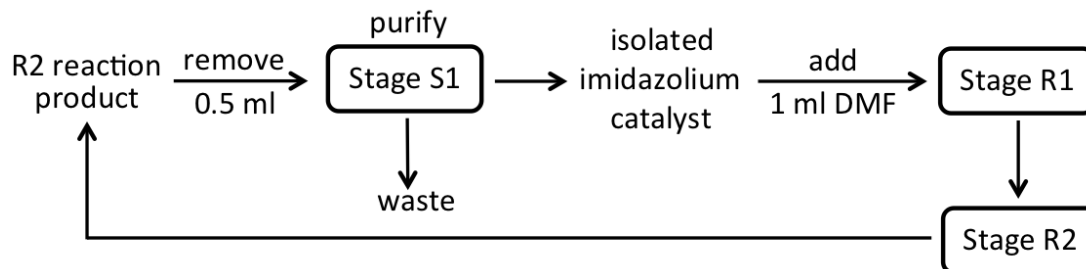


**Figure A.27.** Process flow diagram showing the iterative process as conducted for Experiment 3

## **APPENDIX B**

### **CASE STUDY PLASTIGON PROGRAM**

This case review is a critical assessment of the Plastigon program, “Campbell’s first production-scale attempt at a microwavable soup, a product area that was considered key to Campbell’s future success” (Gill, 1990, pg. 69). Gordon McGovern was CEO of Campbell’s Soup at the time. His push for a microwaveable soup product was based on increased competition in the marketplace from foreign sources and consumer demand for greater convenience. In 1983 a proposal was initiated to construct a Plastigon production line in Maxton, North Carolina. The company had been researching the technology before this time, but a working pilot line had not been developed. By 1988 the Plastigon line was still having technical issues, generally running for only 30 minutes and with inconsistent product quality. It is our team’s suggestion to discontinue work on the Plastigon line in Maxton. The following discussion provides an analysis of how the Plastigon line evolved to its current state and justifies our decision for the Plastigon line. We conclude by detailing several areas that Campbell’s Soup can learn from its experience developing a microwaveable soup.

The current status of the Plastigon line can be ascribed to a combination of internal and external factors. Internal factors include (1) lack of a working pilot process, (2) lack of dedicated staff to run the Plastigon line, and (3) competing research in other microwaveable products such as DRG. Without a working pilot, engineers had to travel extensively to the factory in Maxton to debug new equipment that was “first of a kind”. Once in Maxton, engineers also suffered from a lack of staff since employees were not willing to be involved with setting up the Plastigon line. Both of these issues slowed

development of the Plastigon line. Additionally, competing research in microwaveable soups, while resulting in alternative products, drew resources away from starting a new production line.

External factors are much harder for a company to control, but need to be accounted for when developing a new process/product. The Plastigon line wanted to use a new technology, but without fully understanding its limitations. These limitations included lower material tolerances to heating and sealing which greatly reduced production rates, cutting into the economics of using Plastigon. Beyond technical requirements, products require a consumer market. For Plastigon the existence of this market was unsure. Parallel research efforts within the company illustrate how developing a premium microwaveable soup (Plastigon) is at odds with the company's expertise.

Knowing these facts we now provide a response, taking into account the manufacturing costs and the progress so far of the Plastigon program, the summaries from Elsner's subordinates, and the management structure of the Campbell's Soup company, to present a plan of action for Jim Elsner.

The market research, critical for this decision process, is out of date. The most recent surveys of customers are from 1983, and while a willingness to pay \$0.99 for microwavable soup and a preference for the Plastigon package may have been favorable at the time, much has changed since then. Internally, the price of the Plastigon package has failed to drop as predicted and the operating costs have far exceeded original estimates. Externally, there have been breakthroughs leading to other forms of microwavable soup not previously available, and while the Plastigon concept still

represents a higher quality product, its competitive advantage—and perhaps the price consumers are willing to pay—has dropped considerably. There are several key questions in light of the developments over the past five years.

We recommend the immediate formation of a market survey designed to answer two main points: Given the existing option of \$0.70 for a microwavable DRG soup, how much would consumers pay for the same soup in a Plastigon container? How large is the market for a top-quality soup in a Plastigon container similar to the previous attempt at the “Cookbook Classics” line?

If the answer to the first question remains \$0.99 or drops even lower, the Plastigon program becomes untenable. Even taking into account the optimistic estimates of Gardner for doubling the line rate (despite the quality problems still present at the current rate) and a halving of packaging costs due to “learning curve effects” (despite the resolute fixture at \$0.28 seen over the last 5 years), the Plastigon line would still stand to lose \$11 million annually, and would lose \$162 million annually at current production costs (See Appendix A). Given the additional personnel and development requirements laid out by Gardner to attempt to increase the line rate and production quality, we recommend any consumer preference resulting in a wholesale price point lower than \$1.20 lead to a termination of the Plastigon program in its current form.

Another option would be to convert Plastigon to a higher quality product. Since the Plastigon package is a significant improvement over previous SFP products, a product similar to “Cookbook Classics” containing “top-quality ingredients” may be feasible since the packaging and operating costs would become a smaller fraction of the overall

production. This could allow for a profitable product—depending on the market size for top quality, microwavable soup.

However, we expect that the price point of a Plastigon product will not rise to \$1.20 and that the market size for top quality, microwavable soup will not be large enough to justify the continued development costs to bring the Plastigon program online. If a market survey is unattainable, we would therefore recommend termination of Plastigon. Campbell's has positioned itself well as a flow shop business with a good management structure to compete on quality at the secondary level with small improvements such as "low-salt recipes". By attempting to conquer an entire new problem in "one giant step", we believe Campbell's has strayed too far from its traditional strengths.

Problems with the Plastigon process reveal several key areas that Campbell's Soup could learn from or improve. We believe the company should reevaluate their practices in three areas, organizational structure, company culture/mentality, and management communication, to prevent further difficulties bringing new products to manufacture.

The Plastigon project was initiated at a time when the company was going through major organizational changes. Gordon McGovern's decentralization of Campbell's Soup into 5 regional areas was meant to strengthen community ties, but also resulted in greater autonomy for each of the business units. At Maxton there was little incentive for the workers to help initiate a new process that, while useful to the company, would draw resources away from more profitable operations. Executives at Campbell's soup must learn to maintain central authority over regional production lines. Though the

Plastigon process was not economically sound, further problems controlling decentralized operating units will slow bringing innovation to market and prove harmful to the company.

Company culture during the 1980s was greatly affected by Campbell's size and experience resulting in a complacent atmosphere. Systems were in place for producing high level research (CIRT and CCID), but engineering systems and research-based employees were not empowered to make necessary decisions. The Plastigon project suffered from employees not asking enough questions and management not providing the opportunity. A striking example of this occurred while developing a pilot line for Plastigon, the technology "differed significantly from [the technology] proposed by engineering for the actually production line...eventually [the pilot line] was discontinued" (Gill, 1990, p. 75). At this point the engineers should've stated the line isn't ready to be implemented for a full scale production; instead of such empowered action the company decided to rely on its experience manufacturing food products and neglected to develop a working pilot process. Executives must learn from this and give engineers greater decision making power and flexibility when developing new processes.

Management of the Plastigon process suffered on many levels due to lack of communication to employees. Management plays a huge role in communicating to employees both a company's organizational structure and culture, two areas that were not strongly defined for the Plastigon project (noted above). Additionally a business needs to understand their competitive priorities when developing new products. Campbell's soup has a flow shop organization that competes on price, not quality. As a flow shop, profit is affected by "economies of scale" so developing a large production scale would be

necessary to justify investment in a new process. Executives must learn to communicate these constraints to management so they can better inform engineers.

Campbell's difficulties with the Plastigon process offer great insight into a major US manufacturer that has withstood more than a century of business. Based on projected economic costs and the lack of a defined market for the Plastigon product we suggest Elsnor scrap the project. However, Campbell's Soup should learn from issues that have arisen during Plastigon to ensure continued innovation and improved timelines for bringing product to market.

#### References

1. Gill, G., & Wheelwright, S. (1990). *Campbell Soup Company*. HBS No. 9-690-051. Boston, MA: Harvard Business School Publishing

#### Appendix – Calculations

Yearly Profit on Chunky Soup – Based on figures in Exhibit 8

Assuming Campell's sells at the wholesale price of \$0.58 and it costs \$0.41 to manufacture.

$$\text{Units sold} = \$195 \text{ million} * \left( \frac{1 \text{ unit}}{\$0.57} \right) = 342 \text{ million}$$

$$\text{Total cost} = \text{Units Sold} * \text{Cost} = 342 \text{ million} * \$0.41 = \$140 \text{ million}$$

$$\text{Yearly Profit} = \$195 - \$140 = \$45 \text{ million}$$

Yearly Profit on DRG (using figures from Exhibit 8)

$$\text{Profit} = \$140 - \$140 / \$0.60 * \$0.64 = -\$9.3 \text{ million}$$

Yearly Profit on Platigon (using figures from Exhibit 8)

$$\text{Profit} = \$200 - \$200 / \$0.85 * \$1.54 = -\$162 \text{ million}$$

Yearly Profit on Plastigon (using increased output speed projected in Exhibit 10)

$$Profit = \$200 - \$200 / \$0.85 * (\$1.54 - \$0.50) = -\$45 \text{ million}$$

Yearly Profit on Plastigon (using theoretical maximum production speed from Exhibit 8)

$$Profit = \$200 - \$200 / \$0.85 * (\$1.54 - \$0.75) = \$14 \text{ million}$$

Yearly Profit on Plastigon (using theoretical maximum production speed and “learning curve” reduction in package costs)

$$Profit = \$200 - \$200 / \$0.85 * (\$1.54 - \$0.75 - \$0.14) = \$47 \text{ million}$$

Yearly Profit on Plastigon (using increased output speed projected in Exhibit 10 and “learning curve” reduction in package costs)

$$Profit = \$200 - \$200 / \$0.85 * (\$1.54 - \$0.50 - \$0.14) = -\$11 \text{ million}$$

## APPENDIX C

### CASE STUDY UNIVERSAL LUXURY GROUP

Universal Luxury Group (ULG) is an international group of companies that are working in production and sale of prestigious luxury goods under world-famous brand names. The company is active in a variety of markets such as food, beverages, fashion, leather goods, jewelry, perfumes and cosmetics. Perfume and cosmetic divisions manufacture and market products under 4 major brands: *Rio*, *Queen*, *Andanzy* and *Lienzo*. Product range includes fragrances and derivative-scented products, makeup and beauty (i.e. skincare) treatments.

The perfumes and cosmetics division has a decentralized organizational structure that gives each brand freedom to develop its own markets and products. *Rio* is the biggest, most profitable division among the group's brands and contributes 50% of total sales of the perfumes and cosmetics division. *Queen* contributes to 20% of sales in perfumes and cosmetics division. It aims to grow on a global scale while maintaining its exclusivity through quality and selectivity of its distribution channels. Moreover, *Queen* wants to extend its product range to skincare and makeup. *Andanzy* also contributes to 20% of sales in perfumes and cosmetics division. It is recognized for its perfume expertise; however it aims to expand in makeup products market.

Research and Development (R&D) at ULG is kept centralized to decrease cost of product development and improve share of innovation across its brands. In order to maintain ULG's reputation and continue growing its product line, ULG places great importance on new product development. Their R&D center employs 300 research and technical staff. Activities at R&D include pure research, product development, and an

advisory role on regulation. In order to meet demands from ULG's marketing department, R&D interacts with research institutions and suppliers in order to access new technologies.

Each of ULG's brands aims to grow with innovative solutions and expand their product range by increasing investment in R&D. However, differences in brand goals often result in conflict between individual brands and the centralized R&D. This conflict is further exacerbated by the research funding process, which requires individual funds to be pledged by a brand. *Rio*, as the largest and most profitable brand at ULG, is able to pledge the largest R&D budget and so their projects are given priority. Conflicts can also arise from brands making last minute changes to a product. The effect of these changes on formula stability and the additional testing required by R&D are not taken into account by the brands, causing development delays that could impact market entrance. These development delays need to be accounted for by the pilot department, which works on formula scale-up. Lack of communication between the pilot department and brands results in the hiring of temporary workers to ensure production timelines are not excessively delayed.

Increasing demand from each brand on R&D resources has resulted in growing tensions at ULG over the past 3 years. Going forward in this report, our goal is to analyze how resources are being allocated to help guide company executives to viable business solutions.

Analyzing R&D resource capacity at ULG, it is clear that the necessary capacity does not exist to accept all projects proposed by marketing for the three brands (year 2002). Skincare is at 146% utilization, Ancillaries is at 194%, Shade is at 64% (the only

department below capacity), and Texture is at 122%. The major assumptions in computing this were that “Development” as defined in Exhibit 5 is the fraction of time R&D employees spend devoted to conducting trials and that one employee each from both texture and shade must spend 1.5 days (the average of 1-2 days described in the text) to integrate a shade with a texture or a texture with a shade. To address the overutilization of resources for the current year, two alternate scenarios were developed.

The goal of alternate scenario #1 was to equalize the overutilization rate across the different R&D departments so that a “fair” request could be made to each marketing team to make equal cuts in their R&D requests. This assumed that no additional resources were available to R&D and that asking different departments to make cuts of different sizes would induce more harm through resentment than good from uneven profit gains. This scenario was optimized by shuffling R&D employees between departments to achieve a minimum difference between the utilization rates. This assumed that the “highly skilled chemists” in each department could readily transfer their skills without significant productivity loss. This scenario resulted in roughly 126% utilization rate in each department which would require a ~30% reduction in marketing requests to each department to bring utilization below 100%.

The goal of alternate scenario #2 was to increase R&D capacity until current demand could be met. This made the assumption that new hires were the only way to increase capacity because R&D employees could not readily transfer skills between departments. This scenario found that with 20 new hires to R&D, the marketing demand could be met .

These two scenarios account for current R&D capacity at ULG, but going forward the challenge for company executives will understand how to continually account for

R&D capacity issues. In the following year marketing demand on R&D is expected to again rise by 15.4%, to account for this and any future increases we suggest ULG rely on certain metrics that would help determine the best way to shift resources. Due to low R&D utilization fragrance remains the most profitable sector in terms of productivity, an easily determined metric that will be defined as percentage of sales divided by percentage of resource utilization (See **Exhibit I**). This number is indicative of the efficiency of a product line and can be related to net sales generated per company investment, thus the higher the number the more efficient the product line. This information indicates that improvements in R&D efficiency should focus on Makeup and Skincare product lines. Both these product lines also have great market growth potential (based on premium market sector trends) making them prime areas for either restructuring or increased investment.

There are three ways to account for increased demand from marketing on R&D: (1) improve R&D efficiency, (2) increase R&D budget, and (3) reduce marketing demand. The first two of these were already taking place at ULG through the implementation of synergy efforts and annual budget increases. If R&D budget increases remain constant, ULG must explore reducing the number of projects to not overburden R&D. Based on productivity analysis Skincare is the least efficient product line. We suggest that innovation projects in Skincare go through an initial screening effort to assess product risk. Innovation projects are specifically targeted due to their high resource demands and greater uncertainty. This screening would require an experienced team of Skincare chemists, toxicologists, and product managers to meet with a team from marketing. Each team would rank the innovation projects using different metrics (e.g.

team Skincare – ease of development, team marketing – product demand). These rankings would be combined to reduce the number of innovation projects based on R&D capacity.

Using this methodology we can directly address the 15.4% increase for the following year by assuming “harmonization efforts” reduce  $x\%$  of the increase, budget increases reduce  $y\%$ , and project screening reduces  $z\%$ . Inputting numbers for variables  $x$  and  $y$  based on data from previous years provides an estimate for the number of innovation projects ULG should reduce in the coming year. An example calculation is provided in (See **Exhibit J**); if “harmonization efforts” result in no productivity increase (worst case scenario) then 15 Skincare innovations will need to be cut, an approximately 50% reduction in Skincare innovations (INSEAD, 513). The same process can also be applied to Makeup innovations to further streamline R&D at ULG.

So far we have focused on addressing R&D capacity issues using a reductive system that decreases investment in low productivity products. Reductive systems help to streamline companies and require little or no change in organization structure, thus their implementation can proceed quickly. Further recommendations are additive, providing ways to promote communication between marketing departments and R&D. R&D is a centralized function of UL; however, marketing is broken into operational and central teams. This results in R&D receiving different (often conflicting) requirements from each of the marketing branches. To account for this marketing should alter its structure so that all new product ideas are sent to and organized by the central team. After this an iterative process will take place where operational marketing then receives the new product list and makes its own suggestions. Only when both of the marketing

teams reach consensus will the new product list be sent to R&D. Incorporating this additional step will increase the amount of time spent in predevelopment. However, it should also help marketing focus their requirements and reduce the number of changes after development begins.

ULG has been able to thrive in the fragrances and cosmetics market by continually being innovative. The ever changing nature of this marketplace requires a high investment in product development; however, ULG must be careful it does not overwork its R&D team. Employee burnout can lead to mistakes and, even more detrimental, loss of experienced workers. The conclusions in this report are meant as a guideline to help ULG continue to succeed in a complex market, while not overburdening their researchers.

**Exhibit I – Productivity Calculations**

$$Productivity = \%net\ sales/\%R\&D\ resource\ utilization$$

Fragrance	Makeup	Skincare
3.9	0.6	0.4

**Exhibit J – Model for Determining Project Cuts**

$$15.4\% \leq x + y + z$$

**x** = 22.33% per year (best case scenario) or 0% per year (worst case scenario)<sup>a</sup>

**y** = 1.67% per year<sup>b</sup>

$z = 0.94\%$  per year per project<sup>c</sup>

best case scenario:  $15.4\% \leq 22.33\% + 1.67\% + 0.94\%(N)$  **N=0 projects**

worst case scenario:  $15.4\% \leq 0\% + 1.67\% + 0.94\%(N)$  **N≥15 projects**

<sup>a</sup> Productivity improvements have been able to absorb yearly 24% project increases for the last 3 years. The best case scenario assumes productivity improvements continue at the same rate. The worst case scenario assumes that synergy projects reach saturation and no further productivity improvements are possible.

<sup>b</sup> Future R&D budget increases are taken as the average value for the previous 3 years (5% budget increase over this period). All monetary investment is then assumed to directly reduce R&D demand through staff increases.

<sup>c</sup> Each Skincare innovation requires 180 trials. The total yearly trial capacity of Skincare is 9622.8 trials (with the 55% of the time devoted to development assumption). So  $180/9622.8=1.87\%$  of the total Skincare R&D resources, 50% of total R&D resources is used for Skincare indicating a 0.94% reduction per innovation.

## VITA

Ryan Clairmont was born and grew up in northern Virginia. He attended University of Virginia where he graduated with a BS in Chemical Engineering. After graduation he traveled across the country before returning to pursue his PhD in Chemical Engineering at Georgia Institute of Technology. During his time in grad school, Ryan met his husband and life partner Anthony Thompson, who was pursuing a JD at Emory. Ryan's graduate work was funded by the Center for Chemical Evolution.